

**THE EMERGING ROLE OF THE INTERACTION BETWEEN
JUNCTOPHILIN-2 AND L-TYPE CALCIUM CHANNEL IN EXCITATION-
CONTRACTION COUPLING MICRO-SIGNALING DOMAINS DURING
CARDIAC PATHOLOGICAL REMODELING**

A Thesis
Submitted to
the Temple University Graduate Board

In Partial Fulfillment
of the Requirements for the Degree
DOCTOR OF PHILOSOPHY

by

Polina Gross

December 2019

Examining Committee Members:

Steven R. Houser, PhD.; Cardiovascular Research Center, Lewis Katz School of
Medicine, Temple University

Walter J. Koch, PhD.; Center for Translational Medicine, Lewis Katz School of
Medicine, Temple University

Rosario Scalia MD., PhD.; Cardiovascular Research Center, Lewis Katz School of
Medicine, Temple University

Abdel Karim Sabri, PhD.; Cardiovascular Research Center, Lewis Katz School of
Medicine, Temple University

Iliia Fishbein MD., PhD.; Department of Pediatrics, Division of Cardiology, The
Children's Hospital of Philadelphia

ABSTRACT

THE EMERGING ROLE OF THE INTERACTION BETWEEN JUNCTOPHILIN-2
AND L-TYPE CALCIUM CHANNEL IN EXCITATION-CONTRACTION
COUPLING MICRO-SIGNALING DOMAINS DURING CARDIAC
PATHOLOGICAL REMODELING

Polina Gross

Doctor of Philosophy

Lewis Katz School of Medicine, Temple University 2019

Doctoral Advisory Committee Chair: Steven R. Houser, PhD

Pathological cardiac remodeling is a set of cellular and molecular changes culminating in ventricular dysfunction, malignant arrhythmias and heart failure. Prominent effects of pathological cardiac remodeling include loss of transverse tubules (T-tubules) and disruption of cardiac dyads. The dyad composes the basic microstructural element in cardiomyocytes by forming a junctional complex, in which the T-tubular membrane and the junctional sarcoplasmic reticulum (jSR) membrane are brought into a close proximity. In this spatially restricted microdomain, the L-type Ca^{2+} channel (LTCC) in the T-tubules is closely located to the juxtaposed Ryanodine receptors (RyRs) in the jSR membrane. Ca^{2+} influx through LTCC triggers Ca^{2+} release from the RyRs, in a process known as Ca^{2+} induced Ca^{2+} release (CICR), which enables excitation-contraction coupling (EC coupling). Under physiological conditions, the majority of LTCCs reside in the T-tubules. However, upon disruption of the cardiac dyad complexes during pathological remodeling,

LTCCs are redistributed away from the T-tubules, leading to defective EC coupling and abnormal CICR. The molecular mechanism responsible for LTCCs recruitment to the T-tubules, or their redistribution away from the T-tubules under pathological remodeling in cardiac diseases, is not fully elucidated.

Junctophilin-2 (JPH2) is a crucial regulator of the dyad structure that provides a structural bridge of 12-15nm between the plasma membrane (PM) in the T-tubules and the jSR. By stabilizing the dyad structure, JPH2 enables the functional crosstalk between LTCCs and RyRs to ensure a proper CICR. While most of the JPH2 domains functions are well known, the role of the 'Joining region', which is located between two PM interacting domains in JPH2, remains unknown. Moreover, it remains unexplored if the Joining region in JPH2 directly interacts with LTCCs and contributes to LTCC recruitment to T-tubules.

The overarching theme of this dissertation is to determine the role of the Joining region in JPH2 in cardiomyocytes and to explore if the Joining region in JPH2 recruits LTCC to T-tubules via direct interaction that promotes order to enable efficient CICR.

We validated that pathological remodeling in *in vivo* feline model with progressive pressure overload involves alterations of JPH2 abundance and LTCC redistribution across the cardiomyocyte PM. Similar changes with JPH2 and LTCC expressions were observed in *in vitro* models of cultured adult feline ventricular myocytes (AFVMs). Adenovirus-mediated overexpression of mutated JPH2 in the Joining region (mut^{PG1}JPH2) in AFVMs induced severe T-tubules remodeling and dyad degradation. Protein-protein interaction studies showed that the Joining region in JPH2 interacts with the pore-forming subunit $\alpha 1C$ in LTCC. In addition, our data showed that JPH2 elicits LTCC distribution to dyads, where it colocalizes with the Ryanodine receptor. The interaction between LTCC and JPH2 was

crucial for T-tubule stabilization. Disruption of this interaction introduced asynchronous Ca^{2+} release with impaired EC coupling that could be detected after β -adrenergic stimulation. Overall, Ca^{2+} imbalance in mut^{PG1} JPH2 overexpressing AFVMs induced Ca^{2+} /calmodulin-dependent protein kinase II (CaMKII) activation and altered the myocyte bioenergetics.

Collectively, the data presented in this dissertation provides extensive evidence that the interaction between LTCC and the Joining region in JPH2 facilitates dyad assembly and regulates appropriate CIRC in cardiomyocytes.

DEDICATION

This dissertation is dedicated to the memory of Alexandra Gross, who inspired me to pursue my doctoral degree but was unable to see my graduation.

I also dedicate this thesis to my niece and nephews: Sharel, Mayan and Ofir, who are on their path to pursue self-empowerment, excellence and knowledge.

ACKNOWLEDGEMENTS

First, I would like to express my sincere appreciation to my advisor, Dr. Steven Houser, who provided his valuable guidance, knowledge and support throughout my doctoral training. I owe my scientific motivation and inspiration to Dr. Houser, who taught me a great deal about dedication to science, critical thinking and setting high standards for research reproducibility. I am most grateful to Dr. Houser for providing me the freedom to develop my project in various directions and pursue original, innovative paths.

Secondly, I would like to express my gratitude to my committee members: Dr. Walter Koch, Dr. Abdelkarim Sabri, Dr. Fabio Recchia and Dr. Rosario Scalia for providing constructive criticism, suggestions and invaluable professional assistance. Especially, I would like to acknowledge Dr. Sabri for dedicating extra time and providing essential input into my project. Dr. Sabri's guidance, precision and attentive approach significantly contributed to my professional progress and for this I am very grateful. Special acknowledgment also goes to Dr. Xiongwen Chen for his mentorship and support. Dr. Chen encouraged me to think independently and creatively when tackling scientific challenges. His enthusiasm towards science has been a great inspiration. I would like to thank Dr. Ilia Fishbein, who has generously agreed to serve as my external examiner on a short notice.

This project would not have been possible without the help of our outstanding collaborator Dr. Julia Gorelik and her team: Dr. Jose Sanchez-Alonso, Dr. Claire Poulet and Dr. Clara Lucarelli. Important recognition goes to Jean Ross, Jonathan Lambert, Erdem Varol, Jaslyn Johnson, Carlos Manuel, Dr. John Elrod and Dr. Victor Rizzo for their contribution, advice and scientific expertise. An important recognition is paid to my current

and previous colleagues in the Houser lab, as well as to my family and friends: Alexandra Gross, Nelly Weinberg, Aldo Calix, Polina Gonta, Zeinab Etwebi, Inna and Slava Rom, Lydia Svetlitsky, Winston Hamel and Shelly Cooper for their unconditional support all along.

TABLE OF CONTENTS

	Page
ABSTRACT	iii
DEDICATION	vi
ACKNOWLEDGMENTS	vii
LIST OF TABLES	xiii
LIST OF FIGURES	xiv
LIST OF ABBREVIATIONS.....	xvi
CHAPTER	
1. INTRODUCTION	1
Heart failure	1
Transverse tubules	2
Life cycle of T-tubules in the heart.....	4
Functional roles of T-tubules	6
T-tubules dysregulation in pathological remodeling	7
Cardiac dyad and EC coupling	9
Abnormal EC coupling in cardiac remodeling	12
LTCC modulation in the dyad	13
Triggered Arrhythmias.....	14
Delayed afterdepolarizations (DADs).....	16
Early afterdepolarizations (DADs)	17
Junctophilin-2	17
Loss and gain of JPH2 function in the heart	21

JPH2 in heart disease – a clinical perspective	22
Hypothesis and aims	23
2. MATERIAL AND METHODS	24
Left ventricular hypertrophy (LVH) animal model	24
Adenovirus cloning and transduction	24
Computational prediction of protein structure	25
Isolation of adult Feline ventricular myocytes (AFVMs), cell culture and transduction with Adenovirus	25
Isolation of adult Rat ventricular myocytes (ARVMs) and cell culture	26
Histology and immunofluorescence staining	27
Di-8-ANEPPS staining	28
Subcellular Protein Fractionation	29
Protein Isolation and Western Analysis	29
Sucrose Density Gradients	30
Transmission electron microscopy (TEM)	31
Co-immunoprecipitation (Co-IP)	31
Proximity ligation assay (PLA)	32
Distance-based co-localization analysis	32
Global Ca ²⁺ transients measurements and Caffeine assay	33
Ca ²⁺ waves detection via line scanning	34
I _{CaL} Measurement via patch clamping	35
Super resolution scanning patch clamp and SCIM	35
Mitochondrial morphological analysis	36

Oxygen consumption assays	36
TUNEL assay	37
Trypan blue – cell death staining	38
Statistical analysis	38
3. RESULTS	39
LVH decreases JPH2 expression on the plasma membrane and redistributes JPH2 and LTCC across the sarcolemma	39
Isolated adult cardiomyocytes in culture undergo T-tubule remodeling and exhibit JPH2 downregulation.....	42
Mutating the Joining region in JPH2 leads to exacerbation of T-tubules remodeling and reduced dyad frequency	48
The Joining region in JPH2 interacts with LTCC α 1C subunit and elicits LTCC distribution to dyad microdomains where it colocalizes with RyR	56
Disrupting the interaction between the Joining region in JPH2 and LTCC in cardiomyocytes impairs EC coupling and CICR.....	65
The effect of mutPG1JPH2 overexpression on EC coupling proteins and Ca ²⁺ handling proteins in cardiomyocytes	75
Cardiomyocyte overexpression of WT and mutPG1 JPH2 alter mitochondrial morphogenesis and bioenergetics	78
Cardiomyocyte overexpression of mutPG1 JPH2 does not exacerbate cell death after Iso stimulation.....	84

4. DISCUSSION AND FUTURE DIRECTIONS	86
Alteration of JPH2 abundance elicits LTCC disposition during cardiomyocyte remodeling Oxygen consumption assays	86
The role of the Joining region in JPH2	87
The Joining region in JPH2 interacts with LTCC.....	89
Interaction between The Joining region in JPH2 and LTCC is important for efficient EC coupling	91
JPH2 Joining region contributes to intracellular Ca ²⁺ stability and energy balance in cardiomyocyte	93
Future directions	95
 REFERENCES CITED	 98

LIST OF TABLES

Table	Page
1. Comparison of tertiary structure modeling of JPH2 constructs	51
2. Frequency of mitochondrial disposition and nanotunnel structure	83

LIST OF FIGURES

Figure	Page
1. T-tubules structure in ventricular cardiomyocyte	3
2. T-tubule plasticity during development.....	5
3. Dyad – the junctional membrane complex in cardiac muscle.....	9
4. Local Ca ²⁺ microdomain and major proteins concentrated in the dyadic junction.	10
5. Ca ²⁺ dynamics during EC coupling	11
6. Schematic structure of JPH2	19
7. LVH in Feline hearts induces downregulation of JPH2 expression in the PM and shifts the membrane localization of JPH2 and LTCC.....	39
8. Subcellular protein fractionation of Feline heart	41
9. Adenoviral overexpression of human WT-JPH2 and mut ^{PG1} JPH2 constructs in cultured	42
10. Localization of JPH2 in AFVMs overexpressing WT-JPH2 or mut ^{PG1} JPH2 and effect on the myofibrillar organization	46
11. JPH2 and LTCC redistribute across the PM during remodeling in culture.	47
12. Secondary protein structure predictions	49
13. Overexpression of mut ^{PG1} JPH2 averts the restoration of T-tubules in cultured ARVMs	53
14. Length analysis profile of dyads	55
15. The Joining region in JPH2 interacts with LTCC and regulates membrane microdomain distribution of LTCC.....	57
16. Co-localization of LTCC(α 1C)-JPH2-RyR molecular complex	60
17. LTCC (α 1C) knockdown in AFVMs	63
18. LTCC and JPH2 jointly stabilize T-tubules	64

19. Mutation of the Joining region in JPH2 alters Ca ²⁺ signaling in AFVMs after β-adrenergic stimulation.....	67
20. Representative line scan recordings of AVFMs	69
21. Abnormal LTCC localization to the crest with modified voltage dependence activation and reduced CICR in mut ^{PG1} JPH2 AFVMs.....	71
22. Voltage dependence of I _{Ca,L} activation	74
23. Global effect of WT-JPH2 and mut ^{PG1} JPH2 overexpression on Ca ²⁺ handling proteins	76
24. Effect of mut ^{PG1} JPH2 on expression of EC coupling proteins	77
25. Global effect of WT-JPH2 and mut ^{PG1} JPH2 overexpression on mitochondrial disposition, morphogenesis and bioenergetics in AFVMs.....	80
26. mut ^{PG1} JPH2 does not exacerbated cell death after Iso.....	84
27. Representative illustration of the LTCC-JPH2 interaction via the Joining region in cardiomyocyte	96

LIST OF ABBREVIATIONS

Ad	Adenovirus
AFVMs	Adult feline ventricular myocytes
AR	Adrenergic / Adrenoreceptor
ARVMs	Adult rat ventricular myocytes
ATP	Adenosine triphosphate
BIN1	Bridging Integrator 1
BSA	Bovine Serum Albumin
Ca ²⁺	Calcium
CaMKII	Ca ²⁺ /calmodulin-dependent protein kinase II
cAMP	Cyclic adenosine monophosphate
Cav1.2	Cardiac LTCC isoform
CICR	Ca ²⁺ induced Ca ²⁺ release
CKE	Cytoskeletal extract
Co-IP	Co-immunoprecipitation
CPVT	Catecholaminergic polymorphic ventricular tachycardia
CTE	Cytoplasmic extract
D0	Freshly isolated cardiomyocytes at day 0 in culture
D4C	Control cardiomyocytes in culture for 4 days
DAD	Delayed afterdepolarization
EAD	Early afterdepolarization
EC coupling	Excitation contraction coupling
ESC-CMs	Embryonic stem cell-derived cardiomyocytes

GAPDH	Glyceraldehyde 3-phosphate dehydrogenase
H	Homogenate
H3	Histone 3
HF	Heart failure
$I_{Ca,L}$	LTCC mediated Ca^{2+} current
Iso	Isoproterenol
JPH2	Junctophilin-2
JPH1	Junctophilin-1
JPH2	Junctophilin-2
JPH3	Junctophilin-3
JPH4	Junctophilin-4
jSR	Junctional sarcoplasmic reticulum
KHB	Krebs Henseleit Buffer
LTCC	L-type Ca^{2+} channel
LV	Left ventricle
LVH	Left ventricular hypertrophy
MORN	Membrane occupation and recognition nexus
mut ^{PG1} JPH2	Mutant Junctophilin-2 (in the Joining region)
NCX	Na^+ - Ca^{2+} exchanger
NE	Nuclear extract
OCR	Oxygen consumption rate
PKA	Protein kinase A
PKC	Protein kinase C

PLA	Proximity ligation assay
PLB	Phospholamban
PM	Plasma membrane
PME	Plasma membrane extract
PSG	Penicillin-Streptomycin-Glutamine
RFP	Red fluorescent protein
RyR	Ryanodine receptor
SCIM	Scanning ion conductance microscopy
SERCA2a	Sarco/endoplasmic reticulum Ca ²⁺ -ATPase
SR	Sarcoplasmic reticulum
STORM	Stochastic Optical Reconstruction Microscopy
TEM	Transmission electron microscopy
TM	Transmembrane
T-tubules	Transverse tubules
TUNEL	terminal deoxynucleotidyl transferase-mediated deoxyuridine triphosphate nick-end labeling
WT-JPH2	Wild-type Junctophilin-2

CHAPTER 1

INTRODUCTION

Heart Failure

Heart failure (HF) is a complex clinical syndrome originating from any structural or functional cardiac disorder that culminates in the cardiac inadequacy to fill or pump sufficient blood in response to the metabolizing tissues [1]. Within the clinical HF spectrum, common symptoms are fatigue and weakness, rapid or irregular heartbeat, dyspnea and edema. Traditional risk factors for HF include coronary heart disease associated with myocardial infarction and ischemia; valvular insufficiency, cardiomyopathies, hypertension, diabetes mellitus, obesity and smoking [2, 3].

Onset of HF is usually initiated by pathological structural or functional stimuli related to HF risk factors [2, 4, 5]. At first, these stimuli provoke a phase of compensated ventricular hypertrophy termed 'concentric hypertrophy' in order to preserve the cardiac output. As a result, the cardiomyocyte undergoes structural rearrangement and molecular adaptation that signify the beginning of pathologic cardiac remodeling. This compensatory phase allows cardiomyocytes to grow in length and width as part of the mechanism expanding the cardiac pump function and reducing the ventricular wall stress tension [4, 6]. However, persistent cardiac remodeling and increased ventricular wall stress over prolonged period promote the transition from compensated cardiac hypertrophy into cardiac dilation [4]. Inevitably, this stage leads to poor cardiac contractility, detrimental ventricular arrhythmias and sudden death [7] [6, 8].

HF is a major healthcare concern due to its rapidly growing prevalence, mortality rate and cost of healthcare support. It is estimated that 6.2 million Americans have HF and projections show that the prevalence will continue to increase by 46% in the following 11

years [2, 7]. Although survival after diagnosis of HF has improved in the past 30 years, the prognosis for HF patients still remains poor, estimating that ~50% of patients diagnosed with HF will die within 4 years [9]. Additionally, the overall costs for HF continue to increase. In 2012, the total cost of HF was estimated \$30.7 billion and by 2030, the projections forecast an increase of 127% to \$69.8 billion [2]. Current therapeutic approaches to treat HF focus on the alleviation of symptoms and are essentially limited to β -adrenoceptor antagonists, diuretics, vasodilators, renin–angiotensin–aldosterone axis inhibitors and Digitalis [9, 10]. Despite advances in patient symptoms management, HF is a chronic disease with progressive left ventricular remodeling resulting in a continuous loss of function and poor patient outcome [2, 9]. Consequently, there is a growing and unmet need to better understand the biological processes of heart disease underlying progressive pathological remodeling in order to identify novel therapeutic approaches.

Transverse Tubules

Transverse tubules (T-tubules) in ventricular cardiomyocytes are continuous plasma membrane (PM) invaginations formed from the cell surface down to the junctional sarcoplasmic reticulum (jSR). T-tubules are key structural features of large muscle cells that allow membrane excitation to be carried rapidly to the core of the cell, to induce coordinated contractions.

The existence of T-tubular structures was first proposed by *Gustaf Retzius* in 1881, while exploring the quick inward spread of action potentials penetrating into the muscle cells [11]. The first visual confirmation of T-tubules was provided in 1897 by Nystrom's study, in which the light microscope was used to track extracellular space after injection of India ink into a mammalian heart muscle [11]. However, it was not until the 1950s that

Huxley et al. reported the existence of tubular membrane structures in various muscle cells [12]. Remarkably, the architecture of T-tubules is polymorphic. It is composed of divergent transverse and longitudinal elements, with variable lumen diameters and subdomains, which altogether unite a dynamic network responsive to pathological stress (**Figure 1**) [13-15].

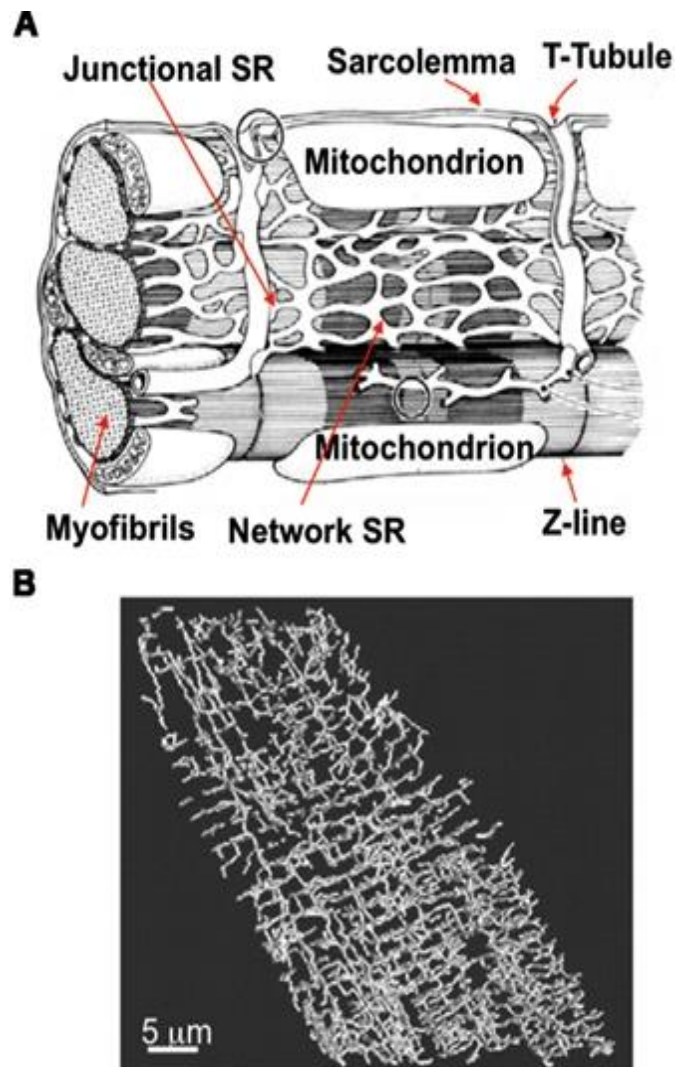


Figure 1: T-tubules structure in ventricular cardiomyocyte. (A) Illustration of intracellular structure in a cardiomyocyte [16]. (B) Two photon imaging of T-tubular network in a rat ventricular myocyte [17].

Highly organized t-tubular network is predominantly found in ventricular cardiomyocytes, whereas atrial cardiomyocytes have less developed T-tubules arranged in an irregular composition [15]. T-tubules are often localized close to the Z-line in the cardiac muscle and have estimated diameter of 100-400nm depending on the species. The morphology of T-tubules in ventricular cardiomyocytes is highly variable across studied mammal species (mouse, rat, rabbit, dog, sheep, human). The variations are most likely attributed to differences between the species heart rate [13, 15]. Considering that rodents have high heart rate at resting state (400-600 beats per minute), their T-tubular system appears denser, deeper and narrower than T-tubules from large mammals with resting heart rates of ~60-80 beats per minute. The complexity of the T-tubular structure goes hand in hand with the necessity to efficiently propagate action potential into the cell interior, such that synchronous Ca^{2+} release will be produced throughout the myocyte enabling synchronous contraction at the required heart rate.

Life cycle of T-tubules in the heart

Despite the organizational complexity of T-tubules, their life cycle and maintenance are incredibly well regulated [18]. During cardiac development, embryonic cardiomyocytes are lacking T-tubules. During the fetal stage, cardiomyocytes develop the sarcoplasmic reticulum (SR) system, but the biogenesis of T-tubules is not initiated until later – several days after birth, along with the increase of left ventricular (LV) pressure and stroke volume. Initially, the developing T-tubule network appears disorganized and predominantly aligned in a longitudinal axis of the cell. Full maturation of T-tubules is achieved by the end of the first month of life and as the T-tubule density increases, the network becomes transversely organized along the Z-lines (**Figure 2**) [19-21].

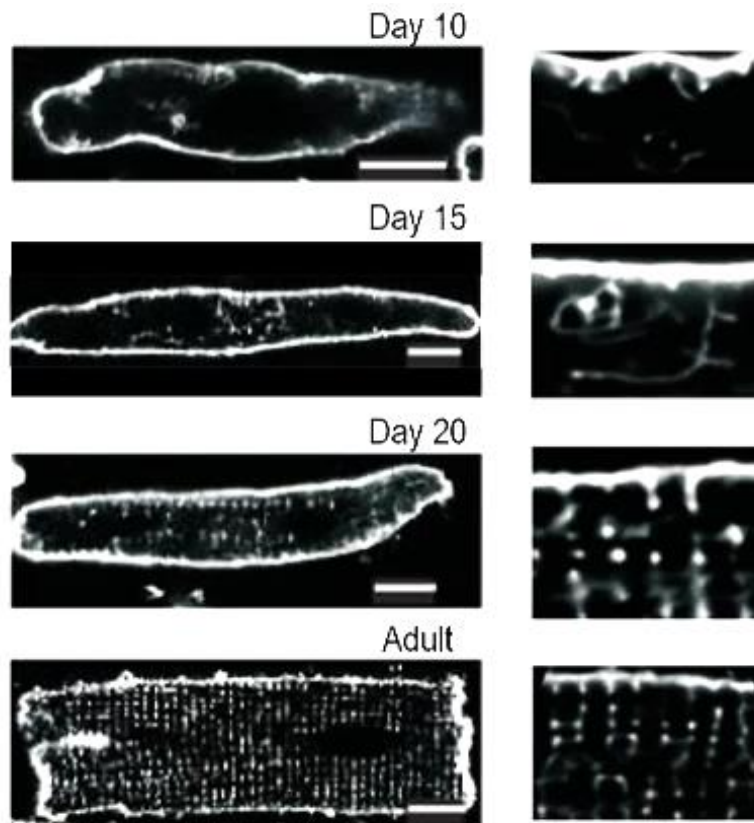


Figure 2: T-tubule plasticity during development. Confocal imaging of isolated rat cardiomyocyte at post-natal time points shows progressive T-tubule maturation. T-tubules initially appear as a scattered network which is largely oriented in the longitudinal orientation. The dense transverse network is established in adulthood. Scale 10 μ m [21].

The exact mechanism responsible for cardiac T-tubule development is not fully understood and it has been proposed that inward invagination of T-tubules is driven by membrane lipids and specific proteins [22]. Previous studies identified several molecules involved in T-tubules regulation. Among those molecules, Bridging Integrator 1 (BIN1) was shown to be involved in tubules formation. Mutations in BIN1 were linked to myopathies and regulation of excitation-contraction coupling (EC coupling) machinery [23-25]. A study exploring the lack of certain Tropomyosin isoforms showed consequences

of T-tubules disruption, suggesting that myofilaments may be involved in the conservation of T-tubules system [26]. Other studies identified Junctophilins as critical players in the stabilization of T-tubules and the accurate assembly of T-tubules with the jSR [27-29]. Overall, there were multiple components identified that contribute to T-tubular regulation, and each component might play an important role in the cardiac disease process.

During cardiac hypertrophy and HF, T-tubules undergo remodeling that can lead to their degradation [30-32]. Nevertheless, restoration of T-tubules may also happen during the functional recovery of the heart [32]. In addition to dynamic membrane turnover, mobilization of ion channels and receptors to the T-tubules is also highly dynamic. This flexible capacity of T-tubules regulation allows efficient adaptation to healthy and stressful environments.

Functional roles of T-tubules

One of the most important functions of cardiac t-tubules is related to their fundamental electrical properties. Essentially, T-tubules enable the homogenous spread of excitation inside the cardiomyocyte in order to generate synchronous contraction. For this reason, T-tubules are the most pivotal site for the EC coupling [15].

The architecture of cardiac T-tubules, which is composed of PM invaginations, enables the formation of local microdomains that serve as “hot spots” for the recruitment of receptors and ion channels (**Figure 4**). Essential Ca^{2+} handling proteins regulating EC coupling are enriched in T-tubules. The most famous “signature” protein localized in the T-tubules is the L-type Ca^{2+} channel (LTCC), also well known for its role as the Ca^{2+} transient initiator. Other sodium and potassium channels, as well as other handling proteins, such as Na^+ - Ca^{2+} exchanger (NCX), are also housed in the T-tubules but to a less degree

of enrichment [13]. Immunohistochemistry experiments demonstrated that LTCCs are concentrated at the T-tubules, and electrophysiological studies determined that 75-80% of the L-type current is originated in the T-tubules, indicating that the main source of Ca^{2+} trigger takes place in the T-tubules [15, 33, 34]. High concentration of LTCCs at the T-tubules is necessary to carry out appropriate Ca^{2+} induced Ca^{2+} release (CICR) and efficient EC coupling. In addition, increased concentration of LTCCs at the T-tubules also indicates that a targeting machinery is required to deliver LTCC to the appropriate localization spots. BIN1 has been shown to facilitate this process [35], however, the entire mechanism by which LTCCs are recruited to the T-tubules is not completely elucidated.

T-tubules also fulfill an important role in the compatibilization of β -adrenergic (AR) system. A distinct distribution pattern between β_1 -AR and β_2 -AR reveals that β_1 -ARs are homogenously distributed across the sarcolemma and the T-tubular system whereas β_2 -ARs are more selectively limited to t-tubules [36, 37]. The spatial localization of the β_2 -ARs depends on its co-localization with protein kinase A (PKA), which limits the spread of the cyclic adenosine monophosphate (cAMP) response and regulates the LTCC open probability. Localization of β_2 -AR in T-tubules also play an essential role in regulating survival pathways in cardiomyocytes, which are severely disrupted during pathological remodeling [36-38].

T-tubules dysregulation in pathological remodeling

Previous studies in humans and animal models have shown that hypertrophic and/or failing ventricular cardiomyocytes are associated with T-tubule remodeling, inhibition of *de novo* formation and a looser T-tubular network structure [14, 30, 38-40]. Historically, T-tubule remodeling was first observed in a failing heart using electron microscopy. Study

of a rat pressure overload hypertrophy model showed that hypertrophic cardiomyocytes had increased T-tubule membrane area [41]. Other studies that included biopsies from human patients with hypertrophic cardiomyopathies and end-stage HF identified irregular or dilated T-tubules in hypertrophic myocytes, and loss of T-tubules in degenerating myocytes [42-44]. Recent advances in this field were achieved via confocal laser scanning microscopy and application of fluorescent lipophilic membrane markers that detect T-tubules. These approaches allowed to quantify the decrease in density and regularity of T-tubules in hypertrophic and failing hearts [40, 45]. Collectively, these studies showed that T-tubule remodeling marks the transition from cardiac hypertrophy into HF [46]. Loss of T-tubule complexes in cardiac remodeling induces downregulation and/or redistribution of proteins and ion channels that normally reside within the T-tubules. For example, profound loss of T-tubules in HF in both humans and rats caused relocalization of LTCCs from the T-tubules to the crest. Only LTCCs localized to the crest demonstrated abnormal increased open channel probability, which contributed to HF pathogenesis through induced arrhythmogenesis [47]. A study conducted in ischemic hearts of a swine model has shown that post-ischemic cardiomyopathy was accompanied by severe T-tubule dysfunction. The downstream effects included reduced CICR synchronicity, lower amplitude of intracellular Ca^{2+} transient and prolonged time to peak of Ca^{2+} release [39]. In human studies, it has been shown that dilated cardiomyopathy and ischemic HF had profound T-tubule damage, followed by decreased T-tubular density and regularity [48, 49]. Interestingly, T-tubules remodeling in hypertrophic cardiomyocytes occurs independently of jSR organization or RyR distribution [39].

Further studies propose that the level of detubulation in cardiomyocytes interrelated to the degree of HF progression [32, 39, 50]. Interesting characteristics were identified in

isolated adult ventricular cardiomyocytes kept in culture. These myocytes undergo cellular remodeling that involves T-tubule degradation or detubulation similarly to HF [51, 52]. As a result, electrical stimulus causes increase in intracellular Ca^{2+} concentration at the cell periphery that later propagates into the cell interior via asynchronous CICR. Unlike myocytes with preserved T-tubular network and regulated CICR, myocytes lacking T-tubules show abnormal CICR followed by spontaneous Ca^{2+} release events (Ca^{2+} sparks) [52]. Studying cultured adult ventricular myocytes can be helpful to our understanding of the T-tubules function in healthy and diseased cardiomyocytes.

Cardiac dyad and EC coupling

The functional role T-tubules fulfill is to induce a synchronized cardiac muscle cell contraction. This occurs via dyads, which are highly organized junctional membrane complexes. In the dyads, the T-tubules come into close proximity with the jSR to set the platform where EC coupling takes place (**Figure 3**). Proper geometric dyad assembly enables close spatial proximity of LTCCs in the T-tubule to the juxtaposed Ryanodine receptors (RyRs) in the jSR (~1:10 ratio) [53], which is essential for efficient EC coupling (**Figure 4**) [54-56].

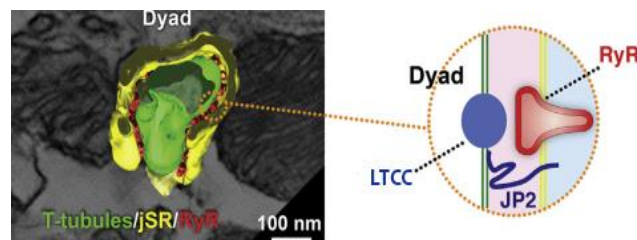


Figure 3: Dyad – the junctional membrane complex in cardiac muscle. Three-dimensional electron microscopy technology was used to demonstrate dyad in nano architectures in ventricular cardiac muscle obtained from adult mice [57].

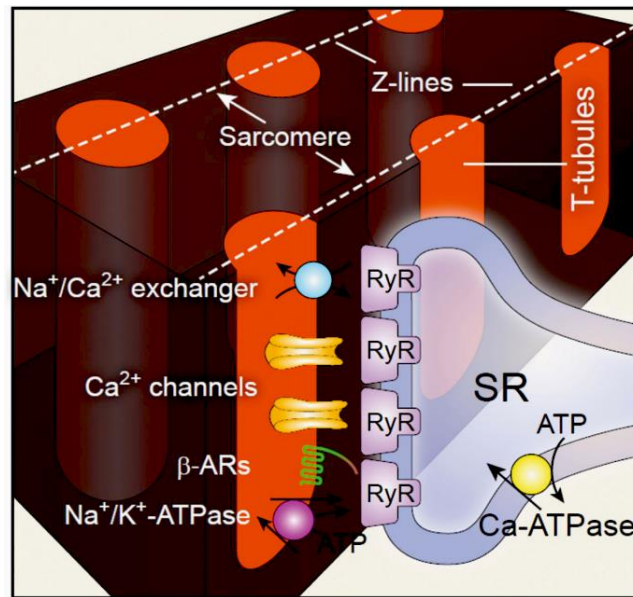


Figure 4: Local Ca^{2+} microdomain and major proteins concentrated in the dyadic junction. The local Ca^{2+} microdomain includes primarily LTCCs and opposing RyRs within a 12–15 nm distance between T-tubule and SR membrane, forming functional Ca^{2+} release units. Other important components such as NCX, Na^+/K^+ -ATPase, and β -adrenergic receptor (β -AR) are also condensed on the T-tubules [56].

At each heartbeat, cardiac contraction (systole) is a consequence of the interaction between the thick and thin myofilaments – myosin and actin, respectively. This interaction is Ca^{2+} dependent; therefore, it requires a rise in the cytoplasmic Ca^{2+} concentration [Ca^{2+}] through a triggered process of EC coupling (**Figure 5**). During the phase of PM depolarization, the cardiac action potential drives LTCCs activation to induce inward Ca^{2+} current. This local elevation of [Ca^{2+}] in the dyad activates juxtaposed RyRs located on the jSR membrane and induces a synchronous Ca^{2+} release from the SR store. In this emerging CICR, LTCC acts as an amplifying switch that gives rise to the global intracellular Ca^{2+} transient. Overall, effective EC coupling is highly dependent on efficient coupling between LTCC and RyR in the dyad that forms the elementary couplon unit – a Ca^{2+} release unit.

To induce cardiac muscle relaxation (diastole), the SR-adenosine triphosphate driven Ca^{2+} pump (SERCA2a) reduces the cytoplasmic $[\text{Ca}^{2+}]$ by returning Ca^{2+} into the SR store against the concentration gradient. Activation of SERCA2a is regulated via the phosphorylation of regulatory protein – Phospholamban (PLB) that is also located on the SR membrane. Although SERCA2a clears most of the cytosolic Ca^{2+} during the relaxation phase, NCX contributes to the mechanism of Ca^{2+} efflux by clearing Ca^{2+} into the extracellular matrix of the cardiomyocyte. In addition, mitochondria participate in the cytosolic Ca^{2+} buffering through mitochondrial Ca^{2+} uptake machinery. Mitochondria utilize the Ca^{2+} to activate its key enzymes responsible for oxidative phosphorylation and adenosine triphosphate (ATP) production [53, 54, 58].

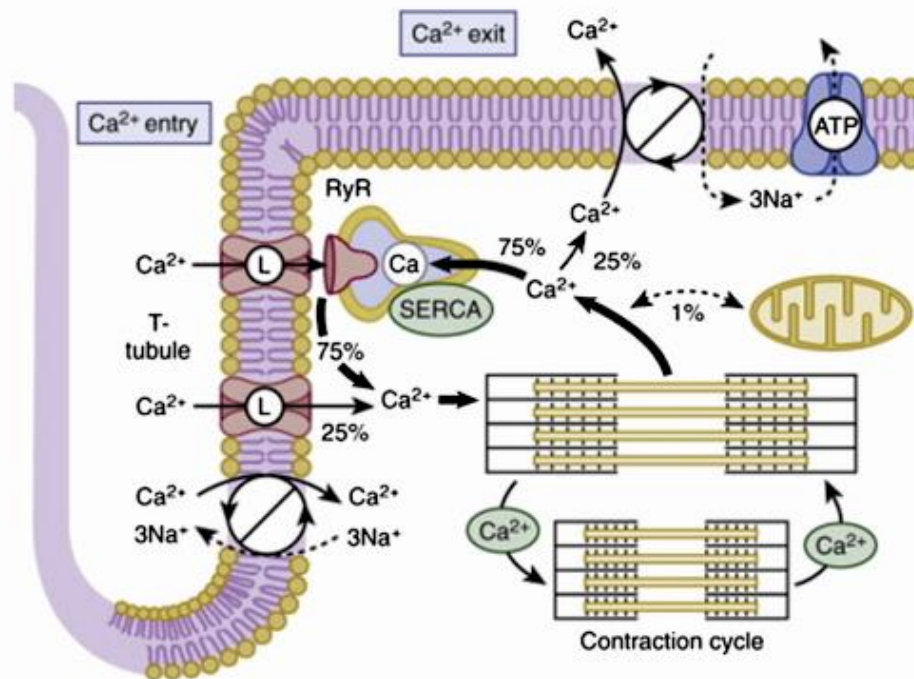


Figure 5: Ca^{2+} dynamics during EC coupling. Ca^{2+} enters the cell through LTCC, which triggers the release of Ca^{2+} from the SR via RyR to initiate contraction. Ca^{2+} leaves the myocyte via the NCX and returns to the SR via SERCA2a. Cytosolic Ca^{2+} is also buffered by the mitochondria [1].

Abnormal EC coupling in cardiac remodeling

Defective EC coupling has been observed in hypertrophy and HF [59], indicated by a reduction in Ca^{2+} transient amplitude, decreased SR content, asynchronous Ca^{2+} release, upregulation in Calcium/calmodulin-dependent kinase II (CaMKII) activity, which is a known Ca^{2+} modulator in cardiac pathologies, and mitochondrial bioenergetic decline [34, 39, 59-63].

Density and organization of the dyads have substantial functional implications. Cardiomyocytes abundant with dyads ensure that Ca^{2+} release occurs swiftly and evenly across the cell, producing a coordinated rise in intracellular Ca^{2+} concentration and rapid contraction. The underlying mechanism is explained by the stoichiometry that each couplon consists of 10-25 LTCCs clustered with 100-200 RyRs [53]. When LTCC opens, the local $[\text{Ca}^{2+}]$ rises within $<1\text{msec}$ to $10\text{-}20\mu\text{M}$ in the junctional cleft. The well-synchronized CICR will activate RyRs and raise the $[\text{Ca}^{2+}]$ in the dyad to $200\text{-}400\mu\text{M}$. Under physiological conditions, Ca^{2+} release from one couplon does not activate the neighboring couplon (which is approximately $1\mu\text{m}$ away) because $[\text{Ca}^{2+}]$ declines over the distance. The autonomous function of each couplon means that for synchronous EC coupling, all couplons in the cardiomyocyte must be simultaneously activated [53].

In cardiomyocytes with pathological remodeling, there is degradation of T-tubules and redistribution of LTCCs from T-tubules to the sarcolemma. This leads to reduced dyad frequency across the myocyte. Subsequently, LTCCs uncouple from RyRs, leaving behind “orphaned” or non-junctional RyRs that do not colocalize with T-tubules [39, 50, 64]. Orphaned RyRs are dependent on diffusion of Ca^{2+} released from neighboring RyRs; thus, their Ca^{2+} release is slow and dyssynchronous [39, 64]. As a consequence of these defects

in cardiac dyads, myocytes display reduced ability to trigger SR Ca^{2+} release, leading to fundamental changes in Ca^{2+} signaling, reduced contractility and arrhythmias [64, 65].

Irregular Ca^{2+} dynamics in cardiomyocytes has also been linked to elevated SR Ca^{2+} content, which makes RyR more sensitive to $[\text{Ca}^{2+}]$ [53]. During systole, this may cause greater SR fractional release for a given Ca^{2+} trigger originated from LTCC [66]. During diastole, this can lead to increased SR leak [67], spontaneous SR Ca^{2+} releases (Ca^{2+} sparks from individual couplons) [68, 69], and spontaneous Ca^{2+} waves, in which one couplon activates neighboring couplons and generates arrhythmogenic waves through the cell. Diastolic Ca^{2+} leak may occur because of dysregulated RyR. Over time, Ca^{2+} leak from the SR lowers the SR Ca^{2+} content, which leads to reduced SR Ca^{2+} release upon activation and weak contraction [70]. The molecular cause for “leaky” RyR remains to be speculative. However, several studies attributed this effect to hyperphosphorylation of RyR at serine 2814 by CaMKII [71-73].

Additional mechanism involved in abnormal EC coupling fluxes during HF is the loss of SERCA2a function. Downregulation of SERCA2a abundance has been associated with reduced SR Ca^{2+} content and systolic dysfunction [74]. However, abnormal SERCA2a function is not within the scope of the current dissertation theme.

LTCC modulation in the dyad

The cardiac LTCC isoform ($\text{Ca}_v1.2$) is a heterotetramer composed of a pore forming subunit $\alpha_1\text{C}$, β subunit, which determines where in the plasmalemma the $\alpha_1\text{C}$ subunit is targeted, an extracellular $\alpha_2\delta$ subunit and γ subunit [75]. Under physiological conditions, approximately 75% of LTCC reside in the cardiac dyads [76], whereas the majority of the dyad coupling occurs within the T-tubular network [54, 77]. The remaining 25% of the

dyads are found at the surface sarcolemma in ventricular myocytes [54, 78]. Therefore, it is assumed that although the majority of LTCC reside in the T-tubules, surface PM LTCCs may also play a particular role in the SR Ca^{2+} load, perhaps under pathological conditions [79]. Interestingly, LTCCs outside of T-tubules demonstrate slower inactivation kinetics, indicating that surface PM LTCCs are less sensitive to SR Ca^{2+} release [80, 81].

The role of LTCC in the aberrant Ca^{2+} transients in hypertrophied/failing cardiomyocytes is still unclear. Previous reports showed either no substantial changes in the magnitude of the LTCC current ($I_{\text{Ca,L}}$) in HF [82, 83], or decreased LTCC density with preserved basal $I_{\text{Ca,L}}$ along with increased adrenergic regulation [40, 84]. We speculate that T-tubular remodeling is associated with disruption of LTCC targeting to dyads to disrupt EC coupling. The short life span of functional LTCC [85, 86] requires that cardiomyocytes maintain a well-regulated dynamic process of LTCC synthesis, trafficking, recycling and degradation. Moreover, the necessity to preserve a functional pool of LTCCs in the dyads, at any given time, suggests intracellular LTCC reservoirs that can be mobilized in and out of distinct PM subdomains [13]. Notably, HF leads to redistribution of LTCC away from the T-tubules, resulting in decreased $I_{\text{Ca,L}}$ density at the T-tubules and increased $I_{\text{Ca,L}}$ density at the cell surface [87]. The mechanism by which the LTCC is targeted to the T-tubules is not fully understood. Previous studies suggested that LTCC $\beta 2\text{a}$ subunit [88] and scaffolding protein BIN1 [35] play a role in this LTCC $\alpha 1\text{C}$ trafficking. Nevertheless, the complete paradigm of LTCC trafficking, anchoring and stabilization in T-tubules is yet to be fully elucidated.

Triggered arrhythmias

Pathological remodeling and progression of HF predispose the myocardial tissue to arrhythmias and their prevalence increases. The HF research field has a general consensus

that ventricular cardiomyocytes from a failing heart have prolonged action potential duration. This can be linked either to alterations in ion channels activities, or to alterations in intracellular Ca^{2+} handling. The latter includes prolongation of intracellular Ca^{2+} transients, reduction of systolic Ca^{2+} and elevation of diastolic Ca^{2+} [89]. Therefore, electrophysiological changes are associated with the progression of systolic and diastolic cardiac dysfunction.

Ca^{2+} alternans and cardiac arrhythmias are interrelated. The phenomenon of beat to beat oscillations under constant heart rate was first diagnosed in 1872 as ‘pulsus alternans’. With the invention of the electrocardiogram, pulsus alternans were recorded in animal models and humans, and were classified for the first time as pathological conditions associated with severe cardiac diseases and poor prognosis [90, 91]. At the cellular level, alternans are defined as beat-to-beat alterations in cardiomyocyte contraction, action potential and magnitude of Ca^{2+} transient. The interplay between membrane voltage and intracellular Ca^{2+} handling is pivotal for the development of Ca^{2+} alternans [92]. In other words, the contributing mechanisms to Ca^{2+} alternans are composed of changes in the SR Ca^{2+} load and modulation of LTCC mediated Ca^{2+} currents. Several electrophysiological phenomena involve imbalanced intracellular Ca^{2+} dynamics in cardiomyocytes that can lead to the following clinically important arrhythmias [92]:

1. The delayed afterdepolarization (DAD) that occurs in conditions of intracellular Ca^{2+} overload.
2. The early afterdepolarization (EAD) that occurs when action potential duration is prolonged.

Delayed afterdepolarizations (DADs)

DADs occur after full repolarization of an action potential in cardiomyocytes overloaded with Ca^{2+} . Augmentation of intracellular Ca^{2+} is usually related to digitalis toxicity or catecholamine action, where a premature release of Ca^{2+} occurs during the diastolic phase. Initially, DADs were considered to be contained in a specific myocardial cell or group of cells that all have been exposed to the Ca^{2+} overload conditions. However, recent studies have shown that Ca^{2+} spreads across gap junction between cardiomyocytes leading to the propagation of spontaneous Ca^{2+} release – Ca^{2+} waves [53, 92]. DADs manifest in cardiac hypertrophy and HF and are always induced at increased heart rates [93, 94].

An example of DAD-induced arrhythmia is the catecholaminergic polymorphic ventricular tachycardia (CPVT) that is caused by a mutation on RyR or calsequestrin [95]. Usually, CPVT is caused by a “leaky” RyR, which is aggravated during catecholamine stimulation. The prevalence of CPVT is not definitively known but has been estimated at ~1:5000 to 1:10000. Approximately 62% of patients with CPVT (N=101) for at least 8 years experienced cardiac symptoms and 13%-31% had near-fatal events [2]. Previously, an *in vivo* mouse model was generated with heterozygous mutation of FKBP12.6, leading to leaky RyR and mimicking CPVT upon physical exercise [96]. RyR stabilization with a derivative of 1,4- benzothiazepine (JTV519) increased the affinity of calstabin2 to RyR. As a result, RyR was tightly regulated to maintain a closed state, and Ca^{2+} leak triggering arrhythmias was prevented [96].

Early afterdepolarizations (EADs)

EADs are depolarizations that take place during the action potential plateau or phase 3 repolarization. EADs are more likely to occur during prolonged action potential duration or bradycardia [53]. EADs are typically detected in cardiac tissue post-injury, ischemia, acidosis and catecholamines exposure. Moreover, ventricular hypertrophy and HF also stimulate the development of EADs [97].

Multiple ionic mechanisms were identified to be responsible for EADs. These include a reduction of repolarizing K^+ currents, an increase in the availability of Ca^{2+} current, an increase in the Na^+-Ca^{2+} exchange current attributed to upregulation of NCX activity and increase in the late Na^+ current. Combinations of these pathophysiological sources may facilitate the incidence of EADs [53, 97, 98].

Junctophilin-2

The maintenance of the cardiac dyad structure is regulated by multiple scaffolding proteins [38], among which Junctophilin-2 (JPH2) is a central one [99-101]. The junctophilin protein family is composed of four members (JPH1-4). JPH1 and JPH2 isoforms are expressed in the skeletal muscle. JPH3 and JPH4 are expressed in neuronal tissues [102]. JPH2 is the exclusive isoform expressed in the heart. Its role was defined to physically stabilize the cardiac dyads by maintaining the precise space of 12-15nm between T-tubule and jSR membranes [34, 102] (**Figure 3**).

The human JPH2 gene contains five coding exons that encode 696 amino acids. Analysis from over 40 species identified that the Junctophilin family contains highly conserved protein domains [99]. On the N-terminus, JPH2 consists of eight membrane occupation and recognition nexus (MORN) motifs, which mediate attachment to PM. All

eight MORN motifs have a consensus sequence of YxGxWxxGxRHGYG that is characterized by increased affinity for membrane phospholipids [103]. The MORN motifs (I-VI) and (VII-VIII) are interrupted by the Joining region. To date, the particular function of the Joining region remains unknown [100, 103]. Comparison of the Joining region amino acids sequence across all four Junctophilin isoforms in humans, mice and rats revealed that the Joining region in JPH2 shares 99.3% similarity with JPH3, 98.7% similarity with JPH4 and 87.3% similarity with JPH1 [103]. Collectively, the increased level of conservation in the Joining region of junctophilins highlights the potential function this domain may have. Clearly, more studies are required to explore the role of the Joining region in the cardiac JPH2.

The critical distance between the PM (in T-tubules) and jSR is determined by the JPH2 spanning element – α -helical domain. The length of this domain is approximately 70-100 amino acids, which correlates to ~10.5nm in length. This prediction was compared to the electron microscopy data that showed a distance of ~12nm between the PM and jSR membrane. Since this distance significantly decreased in the absence of JPH2 expression in cardiomyocytes, the overall conclusion was that the α -helical domain determines the proper distance between the T-tubule and jSR in the dyadic cleft. The divergent region is also highly conserved domain across species, but its specific role has not been identified yet. One assumption is that the divergent region hosts sites for post-translational modifications. Lastly, the transmembrane (TM) domain on the C-terminus is an additional highly conserved region between species. This domain is responsible for anchoring JPH2 into the jSR membrane [99, 100] (**Figure 6**).

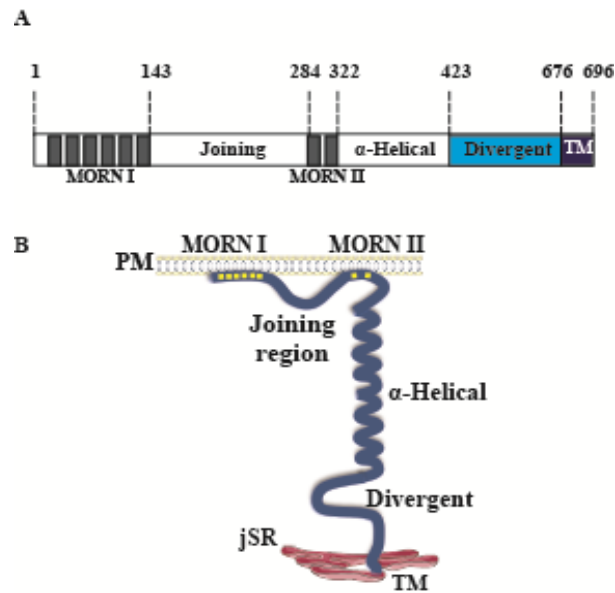


Figure 6: Schematic structure of JPH2. (A) Schematic representation of JPH2 amino acid sequence corresponding to structural domains. (B) The 3D illustration represents structural domains in JPH2 including two regions of MORN motifs (6 repeated regions and 2 additional regions), interrupted by the Joining region, followed by α -helical domain, divergent and TM domains.

Mass spectrometry screening and protein structure predictions (based on hidden Markov models) have identified 35 possible phosphorylation sites in JPH2, which are potential targets for PKA and protein kinase C (PKC). Among these sites, S469, S486 and T490 in the divergent domain of a human JPH2 isoform were diagnosed as the most appealing sites for phosphorylation [103, 104]. These sites could potentially regulate JPH2 binding, or act as a structural switch modifying the distance between the PM and the jSR.

Recent studies gained insight into Junctophilin's protein-protein interactions. JPH1 has been shown to physically interact with RyR in the skeletal muscle through their hyperactive Thiols groups [105]. Three Cysteine residues (101, 402 and 627) in JPH1 were potentially implicated to support this interaction. Follow-up studies utilized advanced

imaging techniques, such as Stochastic Optical Reconstruction Microscopy (STORM) to study JPH2 and RyR colocalization in rat ventricular myocytes [106, 107]. Sub-population of JPH2 was reported to colocalize in heterogeneous clusters with RyR at an approximate distance of 30-40nm. Additional sub-population of JPH2 was present in gaps between the RyR clusters, suggesting that these JPH2 molecules reside in the peripheral junctions; or alternatively, they are available to interact with other molecules in the dyad. In another study, it was reported that JPH2 co-immunoprecipitated with caveolin-3 [108], suggesting that JPH2 can be recruited to the caveolae microdomain, in the sarcolemma or to the T-tubular system, where sub-group of caveolae structures exist [109]. Recently, protein-protein interactions between LTCC-JPH1 and LTCC-JPH2 were identified in the triads of skeletal muscle. The region in JPH2 that was suspected to interact with LTCC was identified using the approach of protein-truncation mutations and co-immunoprecipitation experiments. This study concluded that amino acids sequence 216-399 in JPH2, which also contains the Joining region, is responsible for the protein-protein interaction with LTCC in the skeletal muscle [110]. Compelling evidence for the LTCC interaction with JPH1 and JPH2 in the skeletal muscle came from an additional study that used the approach of selective knock down of JPH1 and then JPH2 to evaluate the clustering of LTCC with the Junctophilins. The data from these studies concluded that LTCC interaction with the Junctophilins occurs on the C-terminus of the ion-channel – a region that contains LTCC's $\alpha 1C$ pore forming subunit. Moreover, this study reported that the interaction between JPH1 and LTCC facilitated LTCC recruitment to the triad junctional membrane in order to ensure efficient muscle contraction [111].

Loss and gain of JPH2 function in the heart

The physiological role of JPH2 in the heart was uncovered in studies that used JPH2 null mice that exhibited embryonic lethality. During embryonic development, these mice hearts failed to show rhythmic contractility and embryos died by day E10.5. Ventricular myocytes were isolated from these mice at E9.5 for structural and functional evaluation. Electron microscopy depicted severe reduction in the number of cardiac dyads. Ca^{2+} transients in these myocytes had reduced amplitude and were randomly evoked by PM depolarization. It was concluded that JPH2 expression in the heart was crucial for normal SR Ca^{2+} release [112]. Compelling evidence from JPH2 knock-down in cardiomyocytes *in vitro* [113] and cardiac-specific knock-down of JPH2 *in vivo* [27] showed that JPH2 downregulation resulted in abnormal CICR with reduced Ca^{2+} transients amplitude, increased Ca^{2+} sparks and cellular hypertrophy, which rapidly deteriorated into HF. These findings in adult mouse heart and adult ventricular cardiomyocytes were supported by studies conducted in embryonic stem cell-derived cardiomyocytes (ESC-CMs). Knock-down of JPH2 in ESC-CMs induced irregular, sporadic and reduced Ca^{2+} transients. These cells failed to differentiate into spontaneously contracting myocytes and demonstrated disordered myofilament arrangement [114].

The role of JPH2 in the heart was emphasized in additional study with cardiac-specific JPH2 overexpression in mice [115]. Cardiac-specific JPH2 transgenic mice showed no difference in cardiac function at baseline. However, once these mice were exposed to cardiac pressure overload, they displayed protective cardiac function that resulted in attenuated progression from hypertrophy to HF. This was also accompanied by decreased mortality rate and preservation of T-tubule network along with conserved dyad frequency.

JPH2 in heart disease – a clinical perspective

Immunohistological evaluation of failing human heart samples with ischemic heart disease or dilated cardiomyopathy demonstrated disorganization and redistribution of JPH2. This phenotype was accompanied by disruption of T-tubule integrity and severe myocardial dysfunction [116]. A possible mechanism explaining downregulation of JPH2 in failing hearts has been attributed to cleavage by calpain [117], a protease that is activated in the presence of increased intracellular Ca^{2+} concentrations during pathological cardiac stress [118, 119]. A recent study suggested that calpain proteolysis of JPH2 induces translocation of JPH2 N-terminal fragment into the nucleus, where it represses transcriptional reprogramming and antagonizes maladaptive cardiac remodeling [120].

Mutations in the JPH2 coding region have been associated with familial hypertrophic cardiomyopathies. Seven distinct mutations have been identified in patients with hypertrophic cardiomyopathy, among which two point mutations were found in the MORN motifs (S101R, Y141H), two mutations in the Joining region (S165F, E169K), one mutation in the α -helical domain (A405S), and two mutations in the divergent domain (R436C and G505S) [121-123]. Patients with the JPH2 mutation E169K also exhibited atrial fibrillation [121]. In order to understand the pathogenesis underlying these mutations, HL-1 cardiac muscle cells were treated with the adenovirus-mediated expression of JPH2 mutants (S101R, Y141H or S165F). These mutants induced a marked reduction in the frequency and amplitude of spontaneous Ca^{2+} release [123]. In skeletal myotubes, overexpression of JPH2 mutants (Y141H, S165F) similarly lowered peak amplitude of Ca^{2+} transients and significantly increased the resting cytosolic Ca^{2+} concentration [124, 125]. In conclusion, mutations in JPH2 led to altered EC coupling and disrupted cytosolic Ca^{2+} dynamics that induced hypertrophy and arrhythmia.

Hypothesis and aims

The present gaps of knowledge include the unknown functions of the Joining region in JPH2 and the unknown mechanisms by which LTCC is targeted to T-tubules in the cardiac dyads. It also remains speculative whether LTCC and JPH2 have a physical interaction in the dyad, and if this interaction supports efficient EC coupling.

Hypothesis: We hypothesize that under physiological conditions, the Joining region in JPH2 recruits LTCC to T-tubules, and during hypertrophic remodeling, this interaction promotes LTCC displacement and redistribution away from T-tubules. Specifically, we assume that the JPH2-LTCC interaction induces alteration of EC coupling and modifies the uniformity of Ca^{2+} release during pathological remodeling.

Aims:

- 1) To explore the roles of the Joining region in JPH2.
- 2) To examine if the Joining region in JPH2 region interacts with LTCC.
- 3) To evaluate how JPH2-LTCC interaction affects EC coupling and Ca^{2+} dynamics in adult ventricular cardiomyocytes.

CHAPTER 2

MATERIAL AND METHODS

Left ventricular hypertrophy (LVH) animal model

All animal procedures were approved by the Temple University Lewis Katz School of Medicine Institutional Animal Care and Use Committee and all experiments were performed in accordance with relevant guidelines and regulations. LVH was induced in Felines as previously described [126-128]. Briefly, 2 months old cats (~1.0 kg) underwent either aortic constriction (N=4), with customized pre-shaped bands, or a sham procedure (N=4). The animals developed concentric compensated hypertrophy after 4 months. A non-invasive transthoracic echocardiography was performed at baseline and at 4 months post-surgery using Vivid q Vet Premium BT12 using a 12S-RS sector probe. Left ventricular (LV) wall thickness was measured at end-diastole by calculating the mean of LV anterior ventricular septum and posterior wall diameter. LV fractional shortening (FS) were measured in B-mode from a right parasternal short-axis view. A cardioectomy was performed after 4 months, then the heart was rinsed and weighed.

Adenovirus cloning and transduction

For generation of WT-JPH2 adenoviral constructs, Human JPH2 cDNA was modified to contain N terminal HA peptide sequence downstream of the multiple cloning site. For mut^{PG1}JPH2 construct, Human JPH2 cDNA was mutated at the Joining region to introduce seven-point mutations (E209A, Q222A, R223A, E234A, S235A, D252A, D259A) and tagged with HA sequence on the N terminus. These constructs were PCR amplified to contain a 5' BamHI sequence and altered stop codon with 3' BamHI sequence, which were then cloned into the pUC57 vector (Bio Basic Inc., Ontario, Canada). pUC57 vector with

either WT-JPH2 or mut^{PG1}JPH2 construct was used for Adenoviral cloning (Vector BioLabs, Malvern, PA). To generate shRNA adenoviruses, human LTCC α 1C subunit (Human CACNA1C) clone was individually RT-PCR'd. PCR product was TA-cloned into the pCR4-TOPO vector. Clone was oriented with the 5' end nearest the NotI site and the 3' end nearest the PmeI site (Dharmacon, Cambridge, UK). Library constructed and then the clone sequenced by the BCCA Genome Sciences Centre (Vancouver, Canada). Four adenoviruses for hCACNA1C silencing containing hairpin loop sequence (CTCGAG) were generated under U6 promoter and tagged with RFP under CMV promoter. The scrambled shRNA was driven by U6 promoter and containing RFP tag (Vector BioLabs, Malvern, PA). Silencing screening was performed on cultured AFVMs via immunoblotting and immunofluorescence staining. The Adenoviruses were tittered with Adeno-XTM Rapid Titer Kit (Clontech).

Computational prediction of protein structure

The prediction of human WT-JPH2 and mut^{PG1}JPH2 protein structures containing HA-tag was performed using deep learning statistical software RaptorX[129, 130]. RaptorX generated protein secondary structure prediction and protein 3D prediction. P-values for the global quality of the 3D model and for each predicted protein domain were provided. RaptorX web server: <http://raptorx.uchicago.edu/>.

Isolation of adult Feline ventricular myocytes (AFVMs), cell culture and transduction with Adenovirus

Felines were anesethetized using 50 mg/kg sodium pentobarbital and hearts were excised and washed in with Krebs Henseleit Buffer (KHB) (12.5 mmol/L glucose, 5.4mmol/L KCl, 1 mmol/L lactic acid, 1.2mmol/L MgSO₄, 130 mmol/L NaCl, 1.2 mmol/L NaH₂PO₄, 25 mmol/L NaHCO₃, and 2 mmol/L Na-pyruvate, and aerated with 95% oxygen and 5% CO₂,

pH 7.35-7.4, and warmed to 37°C). Following aortic cannulation, retrograde perfusion on a Langendorff apparatus was performed with KHB, followed by digestion buffer (KHB with 180 U/mL collagenase and 50 μ mol/L CaCl₂). The ventricles were isolated and minced. Cardiomyocytes were filtered, equilibrated in KHB supplemented with 200 μ mol/L CaCl₂ and 1% bovine serum albumin (BSA) at room temperature, washed with Medium 199 (Sigma) plus penicillin-streptomycin-glutamine (PSG) (Gibco), and plated on laminin (BD Bioscience)-coated culture plates or glass cover slips. After 2 hours, medium was changed to Medium 199 supplemented with PSG, 5 mmol/L taurine (Sigma), 5 mmol/L creatinine (Sigma), and 2 mmol/L carnitine (Sigma).

Myocytes were infected with adenovirus expressing either Ad-RFP, Ad-WT-JPH2, Ad-mut^{PG1}JPH2 or Ad-shRNA LTCC(α 1C)-RFP for 12-hours at a multiplicity of infection (MOI) of 100 virus particles per cell (Ad-shRNA LTCC(α 1C)-RFP was used at MOI of 500 virus particles per cell). Then the media was changed to long-term culture media. During the experimental period, culture media was changed once per day. Infection efficiency was determined 36-48 hours after infection by RFP fluorescence intensity or HA immunofluorescence staining and was typically assessed to be 85%.

Isolation of adult Rat ventricular myocytes (ARVMs) and cell culture

Sprague-Dawley rats were anesthetized with 5% isoflurane-95% O₂ and euthanized by cervical dislocation. Hearts were fast extracted and placed in Tyrode solution containing in: 140 mmol/L NaCl, 6 mmol/L KCl, 1 mmol/L MgCl₂, 1 mmol/L CaCl₂, 10 mmol/L glucose and 10 mmol/L HEPES, adjusted to pH 7.4. Using aortic cannulation with the Langendorff setting, the hearts were perfused with Tyrode solution for 5 min, then with low Ca²⁺ solution containing in: 120 mmol/L NaCl, 5.4 mmol/L KCl, 5 mmol/L MgSO₄,

5 mmol/L sodium pyruvate, 20 mmol/L glucose, 20 mmol/L taurine, 10 mmol/L HEPES, 5 mmol/L nitrilotriacetic acid, and 0.04 mmol/L CaCl₂, adjusted to pH 6.96 for 5 min, and finally for 10 min with enzyme solution containing in: 120 mmol/L NaCl, 5.4 mmol/L KCl, 5 mmol/L MgSO₄, 5 mmol/L sodium pyruvate, 20 mmol/L glucose, 20 mmol/L taurine, 10 mmol/L HEPES, and 0.2 mmol/L CaCl₂, pH 7.4 with collagenase (1 mg/ml; Worthington) and hyaluronidase (0.6 mg/ml). The ventricles were cut into small pieces, resuspended in enzyme solution containing only collagenase (1 mg/ml; Worthington) and shaken in a water bath at 37°C for 20 minutes. The cell suspension was then filtered through a 200- μ m nylon mesh and washed twice before plating. Myocytes were plated on laminin-coated coverslips or glass-bottom dishes (MatTek) in modified M199 (Invitrogen, UK) culture medium containing bovine serum albumin (0.5 g/L), creatine (5 mmol/L), taurine (5 mmol/L), L-ascorbic acid (100 μ mol/L), carnitine (2 mmol/L), and penicillin/streptomycin (100 mmol/L).

Histology and immunofluorescence staining

Heart tissue: The hearts were rinsed with cold Krebs-Henseleit Buffer after cannulation of the Aorta. The hearts were then gravity perfused with 10% formalin at mean arterial pressure (100mmHg). Fixed hearts were immersed overnight in 10% formalin and stored in 70% ethanol for up to 1 week before being processed. The hearts were cut on a short axis plane and divided to lateral and septal walls, followed by embedding in paraffin wax blocks. 5 μ m tissue sections from 6 different levels from each sample were slide-mounted (AML Laboratories, Florida, USA). To determine myocyte cross-sectional area, LV tissue sections were stained for wheat germ agglutinin (WGA; Life Technologies; Eugene, OR) and nuclei were labeled with 4',6- diamidino-2-phenylindole (DAPI, Millipore; Billerica,

MA). Images were obtained using Nikon Eclipse T1 confocal microscope (Nikon Inc.; Mellville, NY). Myocyte cross sectional area was measured using NIH Image J software.

AFVMs/ARVMs: cardiomyocytes that were plated on laminin coated glass coverslips were washed 1X with PBS and fixed with cold 4% paraformaldehyde for 20 minutes. Cells were permeabilized with PBS containing 0.25% Triton X-100 and blocked with 10% donkey serum (Jackson ImmunoResearch Laboratories) in PBS for 30 minutes. Cells were then incubated overnight at 4° C with the following primary antibodies: LTCC (1:50, Alamone Labs), JPH2 (1:50, Santa Cruz), RyR (1:50, Abcam), α -sarcomeric actinin (1:100, Abcam). Then, cells were incubated with the secondary antibodies for 1 hour at 37° C. FITC donkey anti-rabbit IgG, rhodamine red-X donkey anti-mouse IgG, Alexa-647 donkey anti-goat IgG secondaries were used (Jackson ImmunoResearch Laboratories). Nuclei were stained with 4',6-diamidino-2phenylindole (DAPI, Millipore). Coverslips were mounted on glass slides with VECTA SHIELD HardSet Mounting Medium (Vector Labs). Images were obtained using Nikon Eclipse T1 confocal microscope or Zeiss LSM-780 inverted confocal microscope. Images were obtained via Z-stack scanning. Density and regularity index of JPH2 and LTCC were analyzed from mid cell sections using AutoTT[131], after selecting the entire cardiomyocyte surface area as the region of interest with the exclusion of the nuclei. The images were analyzed for global staining density and staining integrity (integrity index = global density \times global regularity). To review co-localization of LTCC-RyR-JPH2, Z-stack images were reconstructed into 3D model using NIS elements software.

Di-8-ANEPPS staining

Viable cultured cardiomyocytes were washed with PBS and incubated with 10 μ M Di-8-ANEPPS (Invitrogen) in PBS for 1 minute at room temperature. The stain was washed

twice with PBS and Z-stack images were obtained at dual excitation 450 and 510nm with detected emission at >570nm using Nikon Eclipse T1 confocal microscope or Zeiss LSM-780 inverted confocal microscope. T-tubular density and T-tubular integrity (TT_{int}) were analyzed from mid cell section images using AutoTT[131], after selecting the entire cardiomyocyte surface area as the region of interest. T-tubular density was calculated for transverse elements and longitudinal elements separately. TT_{int} index took into account both regularity and density using the following equation: TT_{int} = global T-tubule density × global T-tubule regularity.

Subcellular Protein Fractionation

Subcellular protein fractionations from snap-frozen LV septal wall tissue and from cultured AFVMs were prepared using commercially available kits (Thermo Fisher Scientific, #87790 and #78840, respectively) following the manufacturing protocols.

Protein Isolation and Western Analysis

Tissue homogenates and whole cell lysates, or plasma membrane preparations were prepared from isolated AFVMs. Protein concentration was measured as previously described [132, 133]. The following primary antibodies were used for detection: HA-tag (Cell signaling), JPH2 (Santa Cruz Biotechnology), LTCC- α 1C (Alamone Labs), LTCC- β 2a (Alamone Labs), H3 (Abcam), Sarcomeric actinin (Abcam), SERCA2a (Sigma), Bin1 (Sigma), total Ryanodine Receptor (RyR2, ThermoFisher), phosph-RyR2 (S2808 and S2814, Badrilla Ltd.), total phospholamban (Millipore), phospho-phospholamban (PS16 and PT17, Badrilla Ltd.), total CaMKII and phospho-CaMKII (Bardilla), Glyceraldehyde 3-phosphate dehydrogenase (GAPDH, AbD Serotec), Mouse IgG (Abcam). Where applicable, Western blot band intensities were quantified using Licor Image Studio computer software.

Sucrose Density Gradients

Membrane rafts were prepared from snap-frozen LV septal wall tissue or isolated AFVMs in culture as previously described [73, 134, 135]. Briefly, 50mg of LV tissue or $2-3 \times 10^6$ cultured AFVMs were homogenized with a dounce homogenizer in ice-cold, detergent-free Tricine buffer (250 mmol/L sucrose, 1 mmol/L EDTA, 20 mmol/L Tricine, pH 7.4) supplemented with protease inhibitor (Mammalian Cocktail, Sigma-Aldrich), phosphatase inhibitor cocktail 2 and 3 (Sigma-Aldrich). Homogenates were then centrifuged at 1,000g for 10 min at 4°C and the supernatant was collected. Homogenization and centrifugation were repeated on the cell pellets. An aliquot of pooled supernatant (30µl) was set aside as the homogenate (H) sample. The pooled supernatant was then mixed with 30 % Percoll (Sigma) in Tricine buffer and subjected to ultracentrifugation for 25 minutes (Beckman MLS50 rotor, 31,000 rpm, 4°C). The separated plasma membrane (PM) was collected, mixed with ice-cold MBS buffer (20 mmol/L 2 N-morpholinoethane-sulfonic acid, 20 mmol/L KCl, 135 mmol/L NaCl supplemented with protease and phosphatase cocktails) and centrifuged to pellet the membrane. The membrane pellet was resuspended in MBS buffer and sonicated. An aliquot (60µl) was set aside as the PM sample and protein concentration was measured. Then, the PM was mixed with 60% (w/w) sucrose to a final concentration of 40% sucrose. This mixture was overlaid with a 30-5% step sucrose gradient and subjected to ultracentrifugation (Beckman MLS50 rotor, 33,000 rpm, 4°C, 18 hours). Fractions were collected every 0.4 mL from the top sucrose layer, and proteins were precipitated using a solution of 0.1% wt/vol deoxycholic acid in 100% wt/vol trichloroacetic acid. Samples were then subjected to SDS-PAGE and immunoblotted using the indicated antibodies.

Transmission electron microscopy (TEM)

AFVMs were cultured in Permax cell culture dishes and fixed with 2% glutaraldehyde, 2% paraformaldehyde in 0.1M sodium cacodylate buffer, pH 7.4. The cells were then secondarily fixed in 1% Osmium tetroxide, en-bloc stained with 2% uranyl acetate, dehydrated through increasing concentrations of ethanol, then infiltrated and embedded with EMBed-812 epoxy resin. Small groups of AFVMs were located and mounted in both transverse and longitudinal orientations. Sections were cut at 65nm on a Reichert-Jung Ultracut E ultramicrotome and then post stained in uranyl acetate and Reynold's lead citrate. Transverse sections were collected at 2-4 intervals along the length of the cells and the longitudinal sections were collected at approximately midway through the cells. The images were acquired on a Zeiss Libra 120 transmission electron microscope (Delaware INBRE Grant #P20 GM103446). Morphometric analysis of randomly collected images was performed using Image J (NIH). Dyad frequency was assessed in longitudinal images (X5,000 magnification) and determined by relating the number of dyads to the number of intermyofibrillar spaces at the Z line where dyads are usually located [115, 136]. Dyads length was measured in cross sectional images (X10,000 magnification) as previously described [136].

Co-immunoprecipitation (Co-IP)

Plasma membranes (PMs) were prepared from either WT-JPH2 or mut^{PG1}JPH2 overexpressing AFVMs after 4 days in culture (as detailed above in the Sucrose Density Gradients section). PMs were resuspended in lysis buffer (0.25% Triton) supplemented with protease inhibitor (Mammalian Cocktail, Sigma-Aldrich), phosphatase inhibitor cocktail 2 and 3 (Sigma-Aldrich). PMs (~150µg protein) were then added to Pierce™ Anti-HA-Magnetic Beads (High-affinity mouse IgG1 monoclonal antibody covalently coupled

to a blocked magnetic bead surface, ThermoFisher) for 1 hr at 4⁰C. HA-bound material was separated magnetically from unbound material, subjected to SDS-PAGE and immunoblotted using the indicated antibodies. For negative control, only lysis buffer was applied on HA-Magnetic beads with PM prep. For positive control, Escherchia coli extract containing HA tagged GST-PI3K-SH2 domain (ThermoFisher) was used.

Proximity ligation assay (PLA)

ARVMs on coverslips were fixed with ice-cold methanol for 5 min at -20°C and blocked with 10% FCS in PBS for 30 min at room temperature. Incubation with primary antibodies was done in blocking buffer overnight at 4°C. Proximity ligation assay was then performed using the Duolink system (Sigma-Aldrich). Images were taken with a Zeiss LSM-780 inverted confocal microscope. Staining density was calculated by normalizing the area covered by the signal to the area of the cell.

Distance-based co-localization analysis

This method of co-localization is independent of confocal microscope intensity scanning and was performed similarly to previous custom made algorithms [106, 137]. To estimate the amount of colocalization between molecules detected by fluorophores expressed in different channels (i.e. green vs. red, green vs. blue), images were separated to individual color channels, which were treated as separate grayscale images. The first step in image pre-processing was to manually crop the images to exclude nuclei and other unwanted adjacent cells. Then, the remaining regions were segmented into foreground and background using Otsu's method [138]. The foreground was subsequently denoised using connected components algorithm, removing pixel clusters that were smaller than 5 pixels. In the denoised foreground image, given a source channel (i.e. the green channel), iso-

contours that denoted pixels that were equidistant to the nearest target cluster were determined for pixels with positive distance (which indicate regions outside the source fluorophore areas) as well as pixels with negative distance (which indicate regions inside the source fluorophore areas). The iso-contours were used as bins to construct a histogram that counted the number of active target fluorophore pixels that resided within and without the source fluorophore areas. The histogram was normalized by the total number of target fluorophore pixels to denote percentages rather than total counts in order to normalize for possible variations in the area of colocalization. The overall co-localization percentage was determined by computing the ratio of the histogram bins that count the pixels that fell inside the negative distance contours. The software tool was written in Matlab and is available for public use at <https://github.com/evanol/colocalization>.

Global Ca²⁺ transients measurements and Caffeine assay

AFVMs were loaded with 5 $\mu\text{mol/L}$ Fluo-4 AM (Molecular Probes) and placed in a heated chamber on the stage of an inverted microscope and perfused with a normal physiological Tyrode's solution containing: 150mmol/L NaCl, 5.4mmol/L KCl, 1.2mmol/L MgCl₂mmol/L, 10mmol/L glucose, 2mmol/L Na-pyruvate, 1mmol/L CaCl₂ and 5mmol/L HEPES, pH 7.4 for 5 minutes. Myocytes were then paced at 0.5Hz and intracellular Ca²⁺ transients were recorded using Clampex10 software (Molecular Devices). After 2-3 minutes of baseline recording, 100nM Isoproterenol (Iso, Sigma) was applied through the perfusion solution. Once a stable effect of Iso had been achieved, at least 15 continuous contractions and Ca²⁺ transients were recorded and averaged for analysis. The F₀ (or F unstimulated) was measured as the average fluorescence of the cell 50msec prior to stimulation. The maximal Fluo-4 fluorescence (F) was measured at peak amplitude. Background fluorescence was subtracted from each parameter before representing the peak

Ca²⁺ transient as F/F₀ [72, 139] Time to 50% and 90% recovery was measured as the decay rate of the average Ca²⁺ transient trace. To measure SR Ca²⁺ content, as previously described [72] myocytes were paced at 0.5 Hz for 10 consecutive contractions, and 10 mM caffeine was then rapidly applied via a glass pipette close to the myocyte with a Pico spritzer 6-7. Since caffeine cannot be repetitively applied on the same cell, the SR Ca²⁺ content after 100nM Iso was measured by a caffeine spritz after stable effects of Iso on myocyte contraction and Ca²⁺ transients had been observed.

Ca²⁺ waves detection via line scanning

Myocytes were loaded with 5μM Fluo-4 AM (Molecular Probes) and then placed in a chamber containing Normal Tyrode's solution on the stage of a Nikon Eclipse T1 confocal microscope. Myocytes were perfused with Normal Tyrode's solution with 2mM Ca²⁺ containing vehicle or Iso 100nM, while paced at either 1Hz or 0.5Hz using field stimulation. Line-scan images were obtained to measure intracellular Ca²⁺ signals with 488nm excitation and emission from 500-580 nm. Only myocytes with uniform shortening and clear striations were used to record fluorescence signal. Myocytes were stimulated for 10sec and then field stimulation was stopped to detect spontaneous Ca²⁺ releases. Data analysis was performed similarly to previous protocol [127]. Spatial Fluo-4 fluorescence profiles were analyzed at specific times after the stimulus. The percentage of the line scan fluorescence (F) signal was normalized to maximal fluorescence signal (4095) at selected time points (every 10msec up to 210msec). For 3D plots of line scanning, the RGB values of the line scan image was converted to HSV (hue, saturation, value) scale and the value at each pixel location was extracted to denote the intensity. The intensity was plotted as a surface that is a function of time and length.

ICaL Measurement via patch clamping

ICaL was measured in a sodium-free and potassium-free solution. Isolated myocytes were placed in a chamber mounted on an inverted microscope (Nikon Diaphot) and perfused with 1mmol/L calcium-containing Tyrode solution. Both the inflow solution and the chamber were water-heated to maintain the temperature at $36\pm 1^\circ\text{C}$. A 4-5 M Ω pipette filled with a Cs⁺-containing solution composed of: Cs-aspartate 130 mmol/L, N-methyl-Dglucamine (NMDG) 10 mmol/L, tetraethylammonium chloride 20 mmol/L, HEPES 10 mmol/L, Tris-ATP 2.5 mmol/L, MgCl₂ 1 mmol/L, and EGTA 10 mmol/L, pH 7.2, was used to obtain gigaseals. Once a gigaseal was formed, the patch was ruptured, and the cell was dialyzed for 10 min. The extracellular bath was then changed to a 2mmol/L calcium - containing Cs⁺ substitution bath solution (composition: 4-aminopyridine 2 mmol/L, CaCl₂ 2 mmol/L, CsCl 5.4 mmol/L, glucose 10 mmol/L, HEPES 5 mmol/L, MgCl₂ 1.2 mmol/L, and NMDG 150 mmol/L, pH 7.4 with CsOH). Membrane voltage was controlled by an Axopatch 2A voltage-clamp amplifier and digitized by Digidata 1322 using pClamp8 software (Molecular Devices). Once the signal was converted to digital format, it was stored on a personal computer for off-line analysis with Clampfit 10 (Axon Instruments). The flow of the bathing solution was 2–3 ml/min [72, 140].

Super resolution scanning patch clamp and SCIM

Scanning ion conductance microscopy (SICM) was used to generate high resolution 3D images of the surface of live cells using nanopipettes as scanning probes and to record single LTCC activity as described before [141]. Briefly, after a 3D image was generated by SICM using a sharp pipette (~ 100 nm inner diameter, 100M Ω resistance) the pipette was moved to a cell-free area and clipped by a controlled impact on the bottom of the dish to increase the size of the pipette tip (ranging from 281 to 711 nm inner diameter), thereby

decreasing the pipette resistance (ranging from 15 to 38 M Ω). The inner diameter of the pipette tip was calculated as described before[142], using the following equation $R_{\text{pipette}} = (\pi \cdot d/2 \cdot \tan(\phi/2) \cdot \rho)^{-1}$ where R_{pipette} is the pipette resistance, d the pipette tip inner diameter, ϕ the tip cone angle ($\sim 3.8^\circ$) and ρ the conductivity of the pipette solution (~ 1.8 S/m). After moving the pipette back to a position of choice on the 3D scan, it was lowered to touch the cell and gentle suction was applied to form a gigaseal. Cell-attached patch-clamp recordings of single LTCCs were then performed with an Axopatch 200A amplifier (Axon Instruments, Foster City, CA, USA) and pClamp software version 10 (Axon Instruments). Experiments were done at room temperature with the following bath solution: 120 mmol/L K-gluconate, 25 mmol/L KCl, 2 mmol/L MgCl₂, 1 mmol/L CaCl₂, 2 mmol/L EGTA, 10 mmol/L Glucose, 10 mmol/L HEPES, pH 7.4 with NaOH. The pipette solution consisted of: 90 mmol/L BaCl₂, 10 mmol/L HEPES, 10 mmol/L Sucrose, pH 7.4 with TEA-OH. Data were corrected for a liquid junction potential of -16.7 mV. Channel density per μm^2 was calculated by normalizing the total number of channels recorded to the total area of pipette openings. Channel open probability was calculated using Clampfit 10.7 software (Axon Instruments) and averaged from 10-20 traces per cell.

Mitochondrial morphological analysis

Quantification of mitochondrial number, area, circularity and aspect ratio were performed on TEM images using Image J software.

Oxygen consumption assays

A Seahorse Bioscience XF96 extracellular flux analyzer was employed to measure AFVMs oxygen consumption rates (OCR). A utility plate was incubated for 24 hours in XF media (a day prior the experiment) in non-CO₂, 37⁰C incubator to calibrate the probe. 2,400 AFVMs per well were plated in M199 media. On the day of the experiment M199 media

was changed to XF media pH 7.4 supplemented with 1 mM pyruvate, 0.2mM palmitate, 0.2mM carnitine, and 4mM glutamine (180uL). The cells were kept for 1hr in non-CO₂, 37°C incubator. Then, drugs were added to each well (20μL). Basal OCR was measured, then 3μM oligomycin was injected to inhibit ATP-linked respiration, followed by 1.5μM FCCP to measure maximal respiration, and finally to completely inhibit all mitochondrial respiration, 2μM rotenone/antimycin-A was injected. Detailed methodology has been previously reported [143].

TUNEL assay

Immunostaining with terminal deoxynucleotidyl transferase-mediated deoxyuridine triphosphate nick-end labeling (TUNEL) was performed on AFVMs overexpressing RFP/WT-JPH2/mut^{PG1}JPH2 and treated with 10μM Iso for 48 hours. These myocytes were fixed with 4% formaldehyde in PBS. The DeadEnd Fluorometric TUNEL system was used to label apoptotic nuclei (Promega #G3250; Madison, WI). For positive control slides were treated with DNASE I (10U/l) prior to TUNEL staining. Images were obtained using confocal microscopy. The identification of cardiomyocytes and quantification of TUNEL positive/negative myocytes was done semi-automatically using Nuquantus, a Matlab toolbox for machine learning based detection and quantification of cells of interest in complex fluorescent tissue images [144] The patterns needed to detect cardiomyocytes were trained in Nuquantus using a reference dataset of mouse and swine cardiomyocytes labeled by an expert histopathologist. These patterns were then used to automatically detect valid cardiomyocytes in the TUNEL study dataset. The automatic detection was then checked for quality control by the histopathologist analyst to remove false positive detection errors.

Trypan blue – cell death staining

Cells were cultured in 24 well dishes coated with laminin, and infected with adenovirus as described above. After 24 hours the media was replaced. After four days in culture and treatment with 10 μ M Iso for 48 hours, Trypan blue was added to the media and cells that took up the dye were counted as dead. Data is displayed as (blue positive cells)/Total cells, averaged from three separate culture experiments.

Statistical analysis

All values are expressed as mean \pm SEM. Non-parametric Mann-Whitney test and parametric unpaired t-test, paired t-test, and one-way ANOVA were performed to detect significance using GraphPad Prism6 software.

CHAPTER 3

RESULTS

LVH decreases JPH2 expression on the plasma membrane and redistributes JPH2 and LTCC across the sarcolemma

As expected, progressive pressure overload via aortic constriction in Feline hearts led to compensated hypertrophy (Figure 7A-C) with preserved fractional shortening (Figure 7D). Because compensated hypertrophy precedes development of HF, and since an impairment of T-tubule integrity begins before LV systolic dysfunction [46], we examined the early effect of hypertrophic cardiac remodeling *in vivo* on JPH2 protein expression and localization.

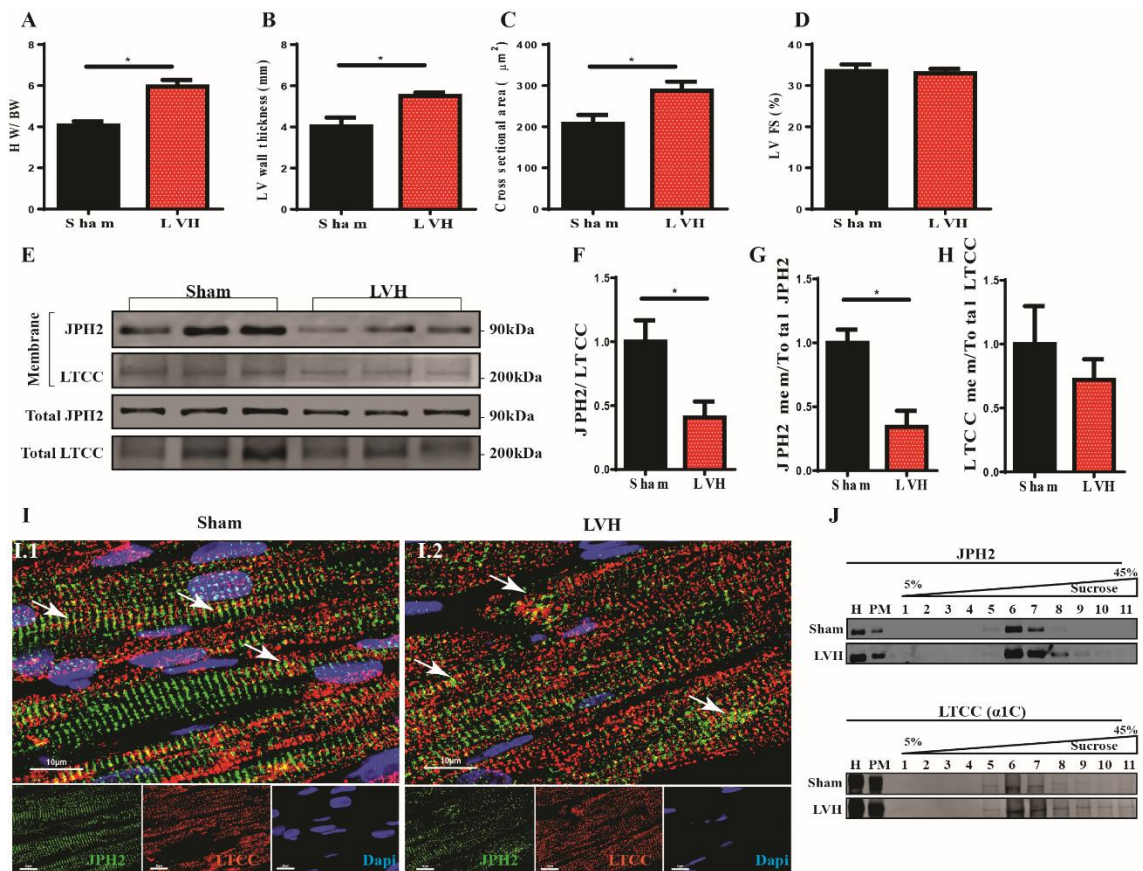


Figure 7. LVH in Feline hearts induces downregulation of JPH2 expression in the PM and shifts the membrane localization of JPH2 and LTCC. LV hypertrophic phenotype in

banded Felines was determined by **(A)** increased heart weight to body weight ratio (HW/BW), **(B)** enlarged LV wall thickness, **(C)** increased cardiomyocyte cross sectional area and **(D)** preserved LV fractional shortening (FS). **(E)** Representative immunoblotting of PM fractions extracted from Feline heart tissues and whole tissue lysates. **(F)** Summary densitometry analysis of JPH2 expression in the PM normalized to LTCC (α 1C) expression in the PM; **(G)** JPH2 expression in the PM normalized to total JPH2 and **(H)** LTCC (α 1C) expression in the PM normalized to total LTCC (α 1C). N=4 animals per group; P<0.05. **(I)** Representative immunofluorescence images of JPH2 and LTCC (α 1C) labeling in sham **(I.1)** and LVH **(I.2)** Feline hearts. Arrows indicate the difference in JPH2 organization and colocalization with LTCC. Scale 10 μ m. **(J)** Representative Western blots of JPH2 and LTCC (α 1C) across sucrose density gradient fractions (F1–F11) of sham and LVH Feline hearts.

The cardiac tissue was fractionated into subcellular fractions (Figure 8A) to examine the membrane fraction, as an indication for the T-tubular component. In PM fraction, LVH induced significant downregulation of JPH2 protein abundance (Figure 7E and 7G) and ~2-fold decrease in the ratio of JPH2 to LTCC pore-forming subunit α 1C (Figure 7F). These changes were compatible with the molecular rearrangement of JPH2 across the PM (Figure 7I and 7J). While, sham hearts displayed organized JPH2 staining patterns colocalized with LTCC (Figure 7I.1 – indicated by arrows), the LVH heart showed disorganized aggregate JPH2 staining colocalized with LTCC (Figure 7I.2 – indicated by arrows). The distribution of JPH2 and LTCC in myocardial membrane domains was examined by isopycnic ultracentrifugation. JPH2 was detected within PM fractions F6-F7

in sham hearts. In LVH, a broader redistribution of JPH2 was detected within PM fractions F6-F9, indicating a shift of the membrane domains where JPH2 resides (Figure 7J). Similarly, cardiac remodeling associated with LVH provoked redistribution of LTCC α 1C subunit (Figure 7J) and LTCC β 2a subunit (Figure 8B) across the membrane microdomains.

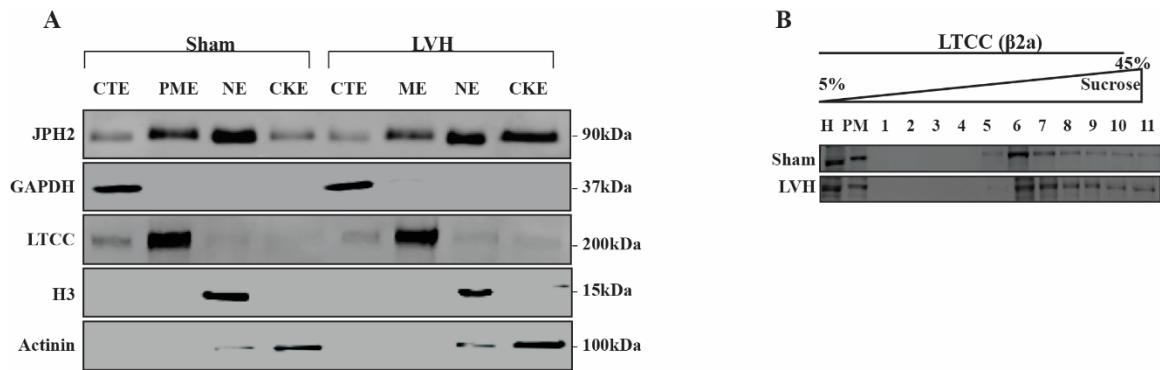
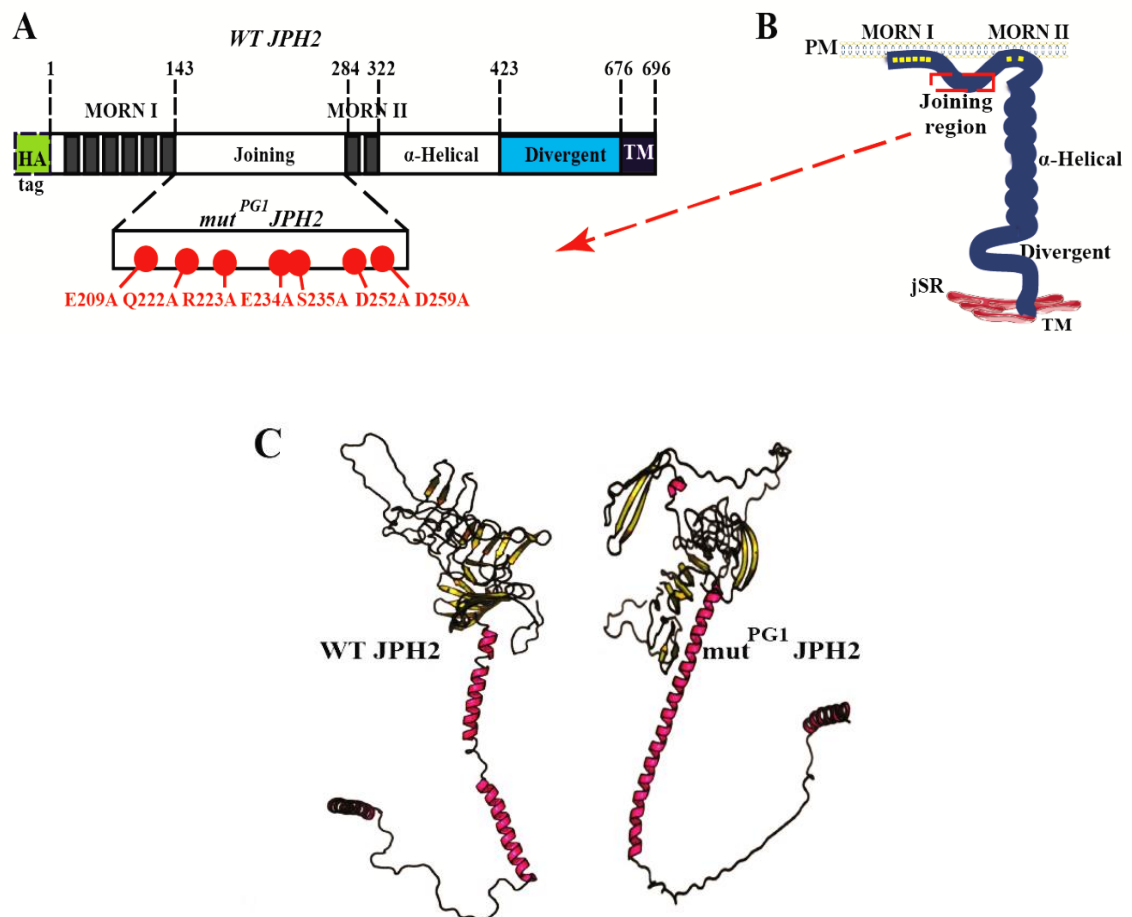


Figure 8. Subcellular protein fractionation of Feline heart tissue (A) Representative immunoblotting of Feline heart tissue samples that were effectively fractionated to cytoplasmic extract (CTE) using GAPDH as a specific marker, plasma membrane extract (PME) with LTCC (α 1C subunit) as a marker, nuclear extract (NE) with histone 3 (H3) as a marker and cytoskeletal extract (CKE) with actinin as a marker. (B) Representative Western blots of LTCC (β 2a) across sucrose density gradient fractions (F1–F11) of sham and LVH Feline hearts.

Isolated adult cardiomyocytes in culture undergo T-tubule remodeling and exhibit JPH2 downregulation

To study *in vitro* T-tubule and JPH2 remodeling that approximates that seen in *in vivo* LVH, we used cultured AFVMs. AFVMs resemble human cardiomyocyte electrophysiological and Ca^{2+} handling properties[145-147], and they are tolerant to Ca^{2+} , which enables their continuous stability in culture [146, 148]. Concurrently, after a few days in culture, AFVMs begin to display myofibrillar disorganization with increased contractile duration and prolongation of action potential[146]. These phenotypic shifts in myocyte structure and function are seen *in vivo* LVH and HF humans and animal models [126, 127, 146, 149].



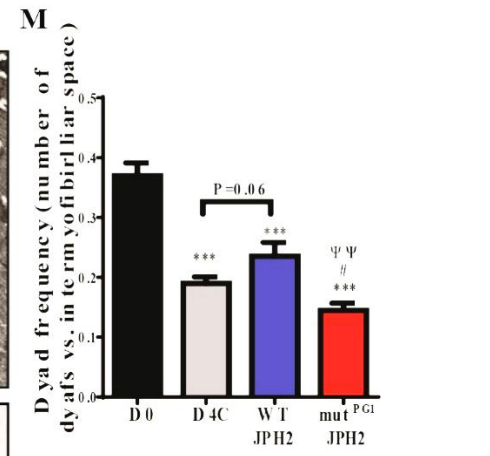
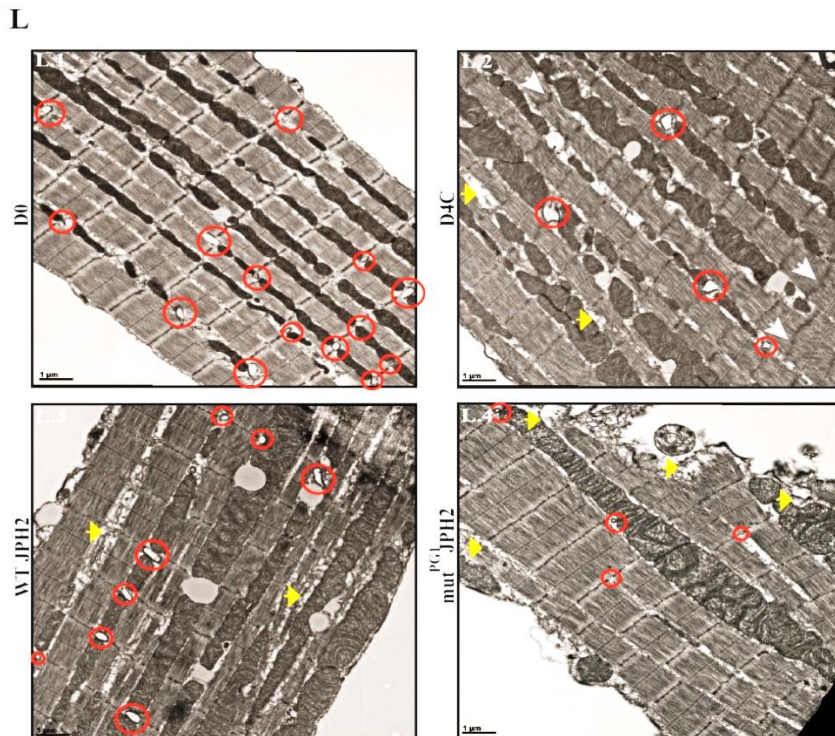
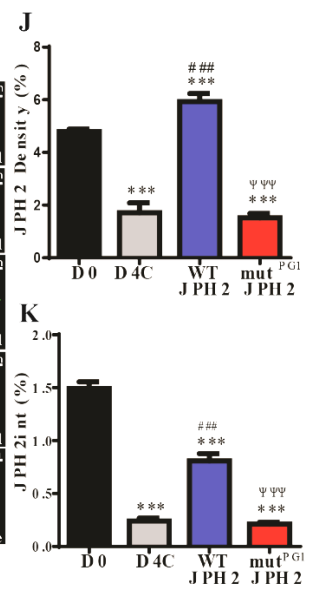
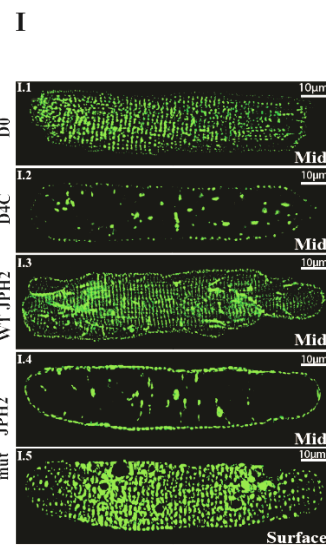
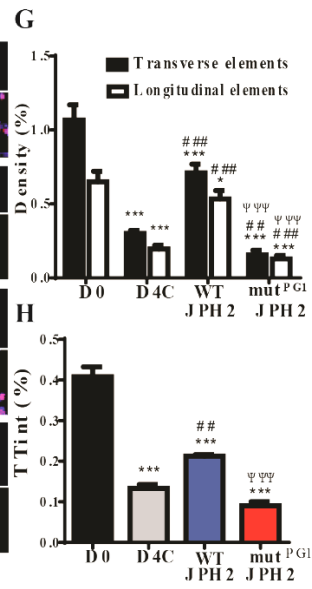
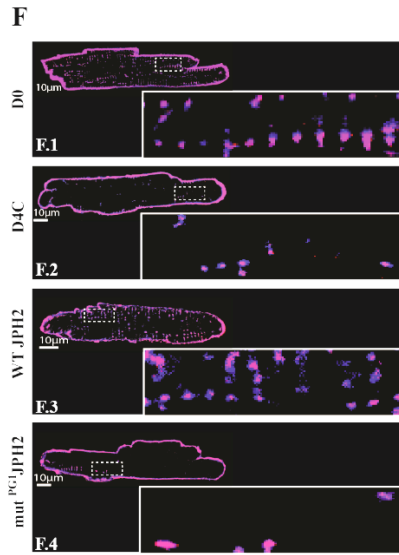
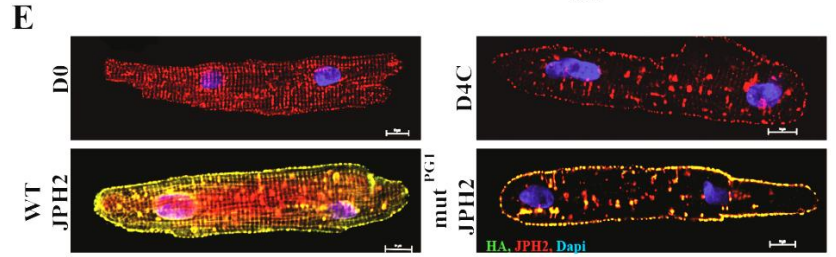
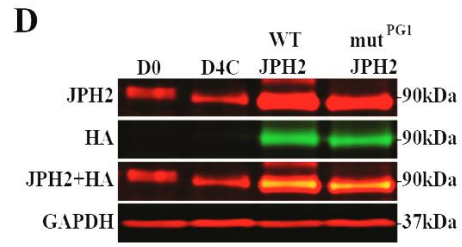


Figure 9. Adenoviral overexpression of human WT-JPH2 and mut^{PG1}JPH2 constructs in cultured AFVMs. (A) Protein topology of human JPH2 isoform (1-696 amino acids) that was cloned into Adenovirus WT-JPH2 is containing HA tag on N-terminus, MORN motifs, joining region, α -helical domain, divergent and transmembranal (TM) domains. The zoomed joining region shows the seven-point mutations that were modified in Adenovirus mut^{PG1}JPH2. (B) Overview of human JPH2 localized in the dyad of cardiomyocyte. The illustration depicts the structure of JPH2 domains. The region highlighted in red box is the joining region that was mutated in Ad-mut^{PG1}JPH2. (C) Template-based tertiary structure modeling of HA tagged WT-JPH2 (P-value 1.37×10^{-05}) and mut^{PG1}JPH2 (P-value 2.29×10^{-05}) proteins via RaptorX. (D) Representative Western blot and (E) Immunofluorescence staining of JPH2 and HA in freshly (D0) isolated AFVMs, control cultured AFVMs for 4 days (D4C), Ad-WT-JPH2 with HA tag transduced AFVMs and Ad-mut^{PG1}JPH2 with HA tag transduced AFVMs. Scale 10 μ m. (F) Distribution of T-tubules detected by Di-8-ANEPPS staining in freshly isolated AFVMs at day 0 (D0), after 4 days of culture in control AFVMs (D4C), in AFVMs after 4 days in culture overexpressing Ad-WT-JPH2 (WT-JPH2) and in AFVMs after 4 days in culture overexpressing Ad-mut^{PG1}JPH2 (mut^{PG1}JPH2). WT-JPH2 overexpression preserved T-tubules while overexpression of mut^{PG1}JPH2 averted the preservation of T-tubules in cultured AFVMs. Scale 10 μ m. The entire area of the cell was selected to measure (G) both T-tubular transverse and longitudinal densities and (H) the global T-tubular integrity. (I) Representative images of JPH2 staining in AFVMs at D0, control cells at D4, and AFVMs overexpressed with either Ad-WT-JPH2 or Ad-mut^{PG1}JPH2. I.1 – I.4 images represent mid-section of the cells obtained via Z-stack confocal scanning. D.5 image represents the surface of the cell. Scale 10 μ m. (J) Calculated JPH2 global density and (K) JPH2 global

integrity in the mid-section of the cell. N=4 isolations, n=15-20 cells. ***/***P<0.05/0.01/0.001 vs. D0, ###/### P<0.05/0.01/0.001 vs. D4C and $\Psi/\Psi\Psi/\Psi\Psi\Psi$ P<0.05/0.01/0.001 vs. WT-JPH2. (L) mut^{PG1}JPH2 overexpression induces downregulation of dyad distribution. Z-line organization and distribution of the dyads were evaluated in D0/D4C/WT-JPH2/mut^{PG1}JPH2 AFVMs. Dyads are indicated in red circles. Z-line streaming is indicated via white arrows. Myofilament degradation is indicated via yellow arrows. Scale 1 μ m. (M) Frequency of dyads quantified as the number of dyads per number of intermyofibrillar spaces. n= 6-7 randomly analyzed cells per group. ***/*** P< 0.05/0.01/0.001 relative to D0, ###/### P< 0.05/0.01/0.001 relative to D4C, $\Psi/\Psi\Psi/\Psi\Psi\Psi$ P< 0.05/0.01/0.001 relative to WT-JPH2.

We further assessed T-tubular remodeling in viable AFVMs by staining T-tubules with voltage sensitive dye. Cultured AFVMs for 4 days (D4C) showed reduced T-tubular density and integrity compared to freshly isolated AFVMs (D0) (Figure 9F.1 vs. 9F.2 and Figures 9G and 9H comparing D0 vs. D4C). JPH2 protein expression was downregulated in cultured cardiomyocytes compared to fresh cells (Figure 9D comparing D0 and D4C). Immunofluorescence staining of JPH2 and Z-stack confocal scanning (Figure 10.A) detected downregulation of JPH2 density and integrity in D4C AFVMs (Figure 9E – D0 vs. D4C, Figure 9I.1 vs. 9DI.2 and Figures 9J and 9K – D0 vs. D4C). D4C AFVMs showed PM redistribution of JPH2, LTCC α 1C and β 2a subunits (Figure 11). Moreover, decrease in myofilament organization (Figure 10B.1 and 10B.2), disruption of Z-lines ultrastructure and reduced number of dyads (Figure 9L.1 and 9L.2) were observed in cultured AFVMs.

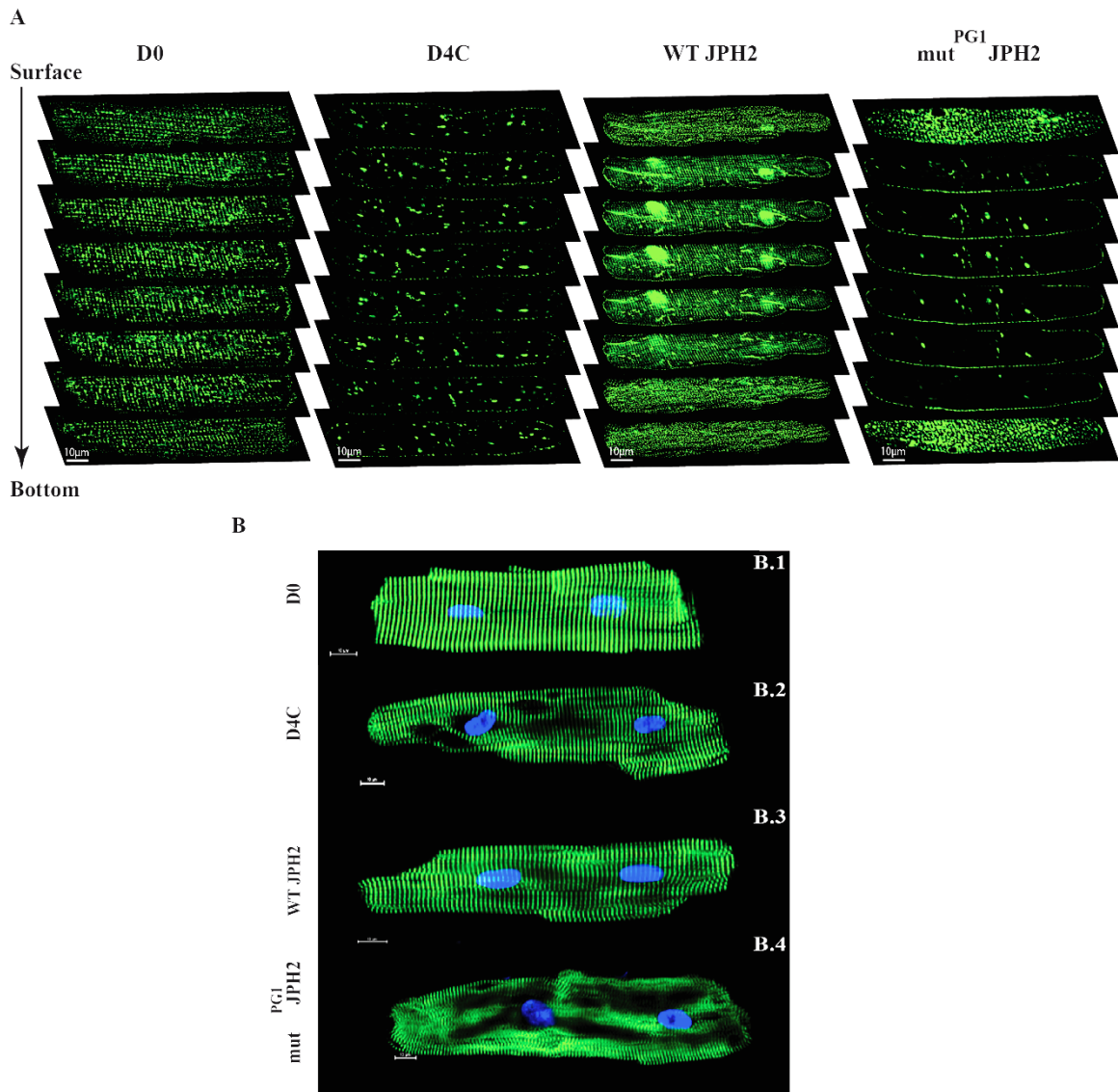


Figure 10. Localization of JPH2 in AFVMs overexpressing WT-JPH2 or mut^{PG1}JPH2 and effect on the myofibrillar organization. (A) Representative Z-stack images obtained via confocal microscopy of AFVMs stained for JPH2 in D0, D4C, WT-JPH2 and mut^{PG1}JPH2 overexpressed myocytes. Arrow indicates direction of scanning from the surface to the bottom of the cell. (B) AFVMs immunofluorescently stained for α-sarcomeric actinin in D0, D4 as a control, D4 after transduction with Ad-WT-JPH2 or Ad-

mutPG1JPH2. mut^{PG1}JPH2 overexpression induces downregulation of myofilament organization. Scale bar 10 μ m.

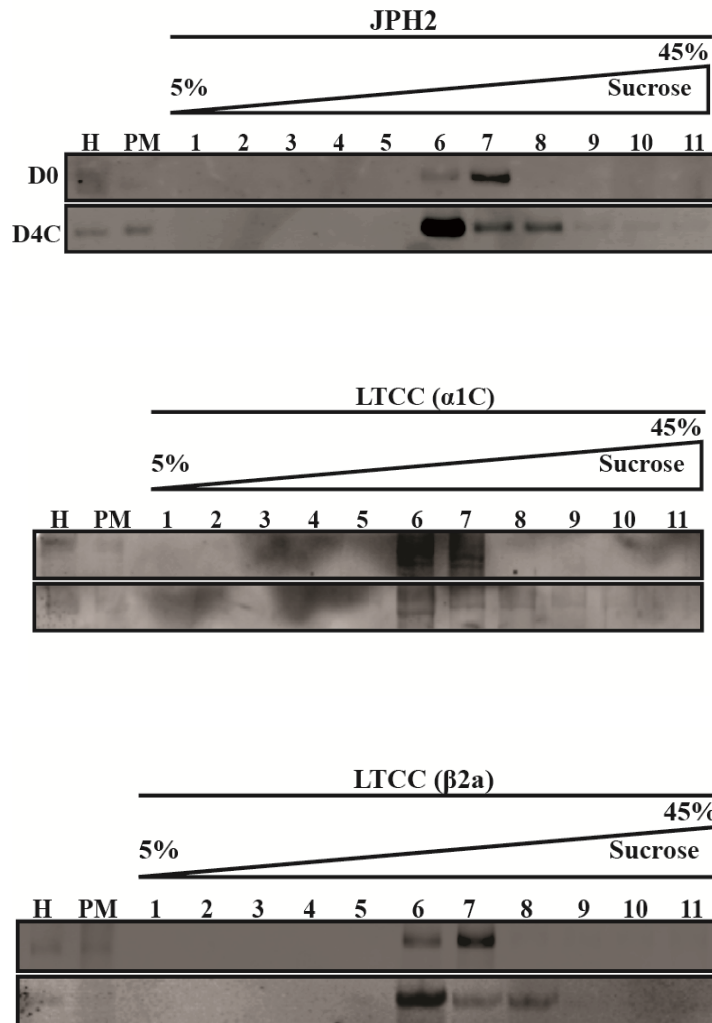


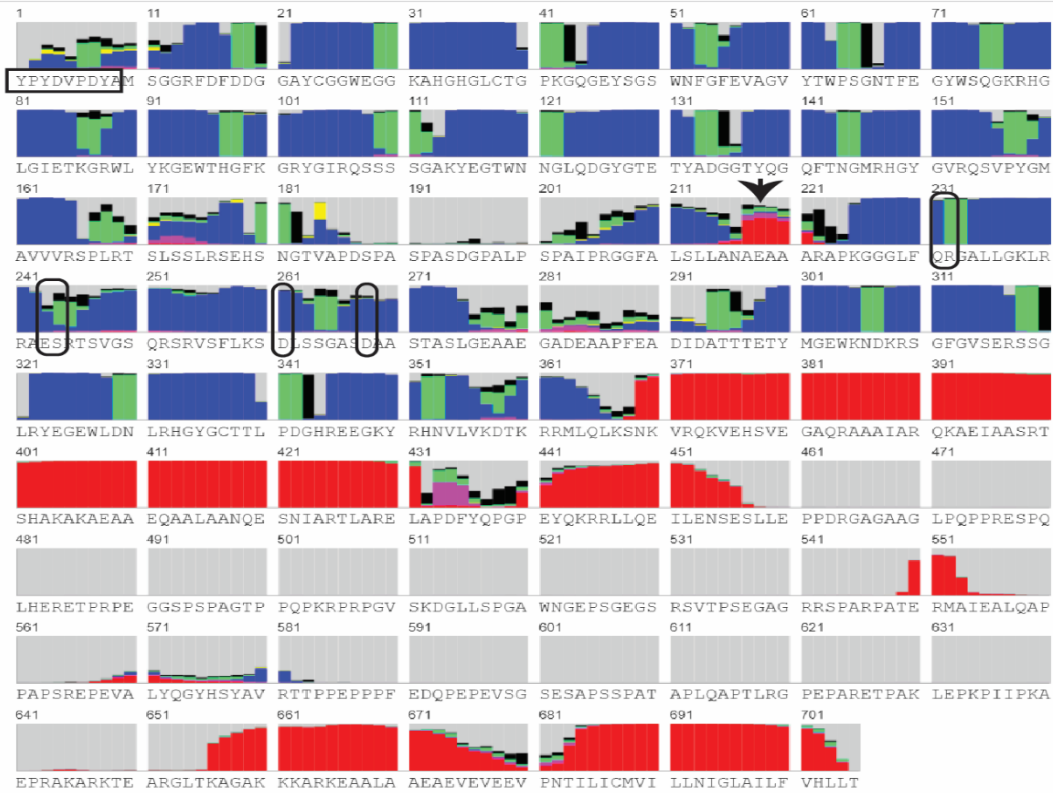
Figure 11. JPH2 and LTCC redistribute across the PM during remodeling in culture.

Representative Western blots of JPH2, LTCC (α 1C) and LTCC (β 2a) across sucrose density gradient fractions (F1–F11) of freshly isolated AFVMs at day 0 (D0) and control AFVMs cultured for 4 days (D4C).

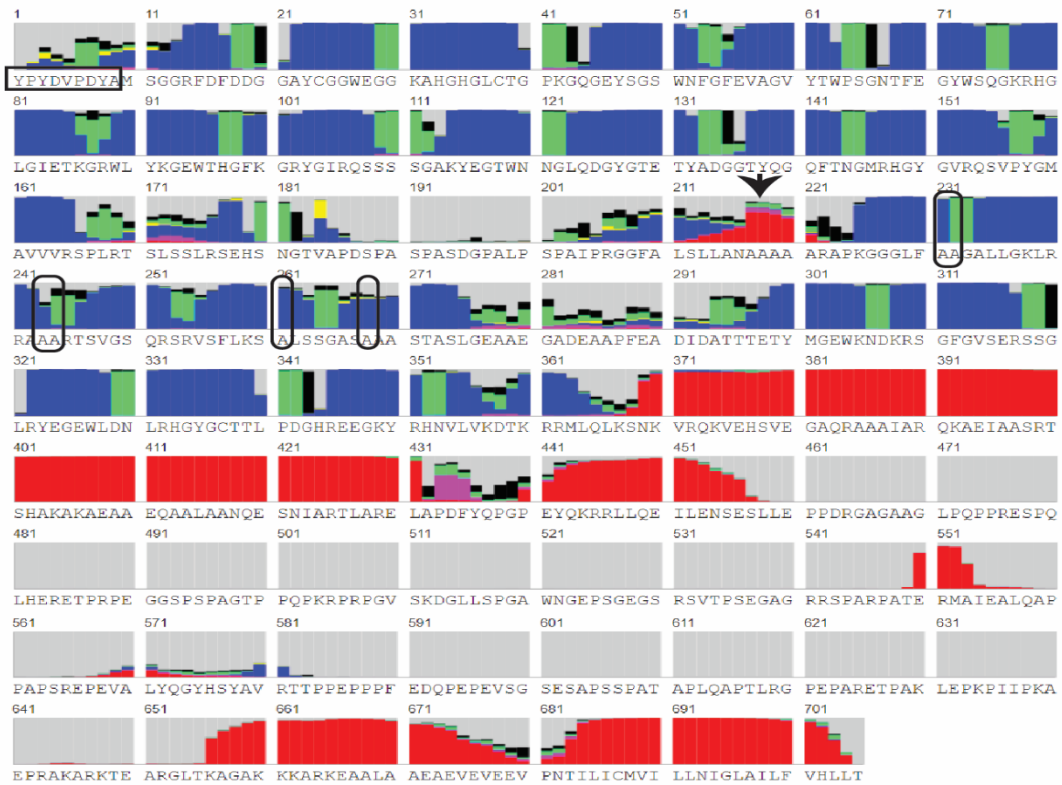
Mutating the Joining region in JPH2 leads to exacerbation of T-tubules remodeling and reduced dyad frequency

The role of JPH2 Joining region was examined. We generated Adenoviral (Ad) vector carrying seven-point mutations in the Joining region of human JPH2 isoform (with the consideration that human JPH2 shares 89% protein identity with *Felis catus* JPH2). The mutant JPH2 reagent (Ad-mut^{PG1}JPH2) was tagged with the HA peptide on the JPH2 N-terminus to detect transduction efficiency in AFVMs, which was 85%, 46 hours post-transduction. Ad-WT (human) JPH2 with HA tag was also tested (Figures 9A and 9B). We modeled the putative protein secondary and tertiary structures[129, 130] of HA-WT-JPH2 and HA-mut^{PG1}JPH2 to explore the steric structure of JPH2. Overall, WT-JPH2 3D model (P-value 1.37×10^{-05}) showed a similar structure to the 3D model of mut^{PG1}JPH2 (P-value 2.29×10^{-05}) (Figure 9C). Mapping of the secondary protein structure detected that mutation E209A mildly increased the probability of α -helix structure (55.7% in WT-JPH2 vs. 64.5% in mut^{PG1}JPH2), while the rest of the mutations did not introduce any critical alterations (Figure 12). Seven-point mutations in mut^{PG1}JPH2 caused tertiary conformational changes in the Joining region solely without affecting MORN motifs, α -helical domain, divergent and TM domains in mut^{PG1}JPH2 (Table 1).

A



B

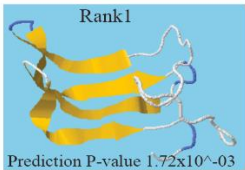
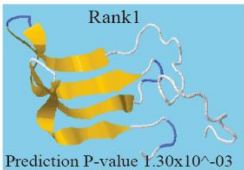
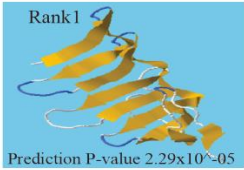
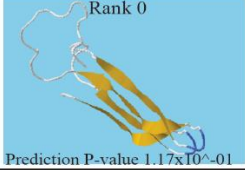
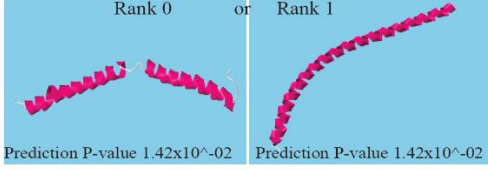
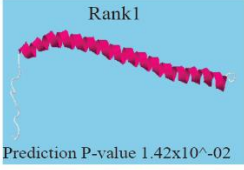
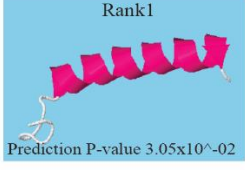


Legend:



Figure 12. Secondary protein structure predictions for (A) WT-JPH2 with HA tag and (B) mut^{PG1}JPH2 with HA tag via RaptorX. The HA peptide sequence is indicated in horizontal box (9 amino acids on the N terminus). The arrow points out to mutation E209A (here E218A because of HA tag insertion) with higher preference for α -helix structure. The vertical frames indicate the point mutations that did not alter the predicted probabilities for protein secondary structure.

Table 1. Comparison of tertiary structure modeling of JPH2 constructs

	HA _{tag} - WT JPH2	HA _{tag} - mut ^{PG1} JPH2
Domain prediction	1. Domain 1: [369-438aa] P-value 1.42×10^{-02} 2. Domain 2: [68-167aa] P-value 1.37×10^{-05} 3. Domain 3: [1-67aa] P-value 1.72×10^{-03} 4. Domain 4: [227-368aa] P-value 1.36×10^{-04} 5. Domain 5: [168-226aa] P-value 1.17×10^{-01} 6. Domain 6: [675-705aa] P-value 3.05×10^{-02} Overall model P-value 1.37×10^{-05}	1. Domain 1: [369-441aa] P-value 1.42×10^{-02} 2. Domain 2: [68-167aa] P-value 2.29×10^{-05} 3. Domain 3: [1-67aa] p-value 1.30×10^{-03} 4. Domain 4: [227-368aa] P-value 1.78×10^{-04} 5. Domain 5: [168-264aa] P-value 1.12×10^{-02} 6. Domain 6: [675-705aa] P-value 2.97×10^{-02} Overall model P-value 2.29×10^{-05}
Domain 3: HA peptide and MORN I motif	 <p>Prediction P-value 1.72×10^{-03}</p>	 <p>Prediction P-value 1.30×10^{-03}</p>
Domain 2: MORN I motif and beginning of Joining region	 <p>Prediction P-value 1.37×10^{-05}</p>	 <p>Prediction P-value 2.29×10^{-05}</p>
Domain 5: Joining region	 <p>Prediction P-value 1.17×10^{-01}</p>	 <p>Prediction P-value 1.12×10^{-02}</p>
Domain 4: Joining region, MORN II motif and beginning of α-Helical region	 <p>Prediction P-value 1.36×10^{-04}</p>	 <p>Prediction P-value 1.78×10^{-04}</p>
Domain 1: α-Helical region and beginning of Divergent region	 <p>Prediction P-value 1.42×10^{-02} Prediction P-value 1.42×10^{-02}</p>	 <p>Prediction P-value 1.42×10^{-02}</p>
Domain 6: C-terminus (TM) transmembrane domain	 <p>Prediction P-value 3.05×10^{-02}</p>	 <p>Prediction P-value 2.97×10^{-02}</p>

JPH2 and HA protein expression were confirmed in AFVMs 4 days after transduction with Ad-WT-JPH2 and Ad-mut^{PG1}JPH2 (Figure 9D). Overexpression of WT-JPH2 in AFVMs restored the occurrence of T-tubules that were degraded in D4C cultured AFVMs (Figure 9F.3). The density of transverse and longitudinal T-tubular elements was increased along with increased T-tubular integrity (Figures 9G-2H). Interestingly, very few T-tubules were detected in AFVMs transduced with mut^{PG1}JPH2 (Figure 9F.4). The density of transverse and longitudinal T-tubular elements and T-tubule integrity were significantly lower than in D4C and WT-JPH2 overexpressing cardiomyocytes (Figure 9G and 9H). JPH2 and HA staining revealed that overexpression of WT-JPH2 restored JPH2 density D4C AFVMs (Figure 9E, Figures 9I.3 and 9J), and increased JPH2 integrity (Figure 9K) without fully reversing the ongoing remodeling. Overexpression of mut^{PG1}JPH2, however, induced JPH2 localization to PM surface (Figure 9E), leaving the mid-section of the cardiomyocyte vacant of JPH2 (Figure 9I.4-I.5 and Figure 10.A), as shown across Z-stack confocal scanning (Figure 10.A). As a result, JPH2 density and integrity (Figure 9J-9K) in mid-section of mut^{PG1}JPH2 cardiomyocytes were significantly reduced compared to D0 and WT-JPH2 overexpressing cardiomyocytes. Notably, T-tubular pattern and morphology differ between species. Small animal models (rodents) exhibit denser, deeper and narrower T-tubular network than large mammals in correspondence to the difference in their heart rates[13, 15]. We tested the effects of Ad-WT-JPH2 and Ad-mut^{PG1}JPH2 on isolated adult rat ventricular myocytes (ARVMs), which showed similar effects on T-tubule and JPH2 expression patterns that were observed in AFVMs (Figure 13). (human JPH2 protein shares 86% similarity with *Rattus norvegicus* JPH2).

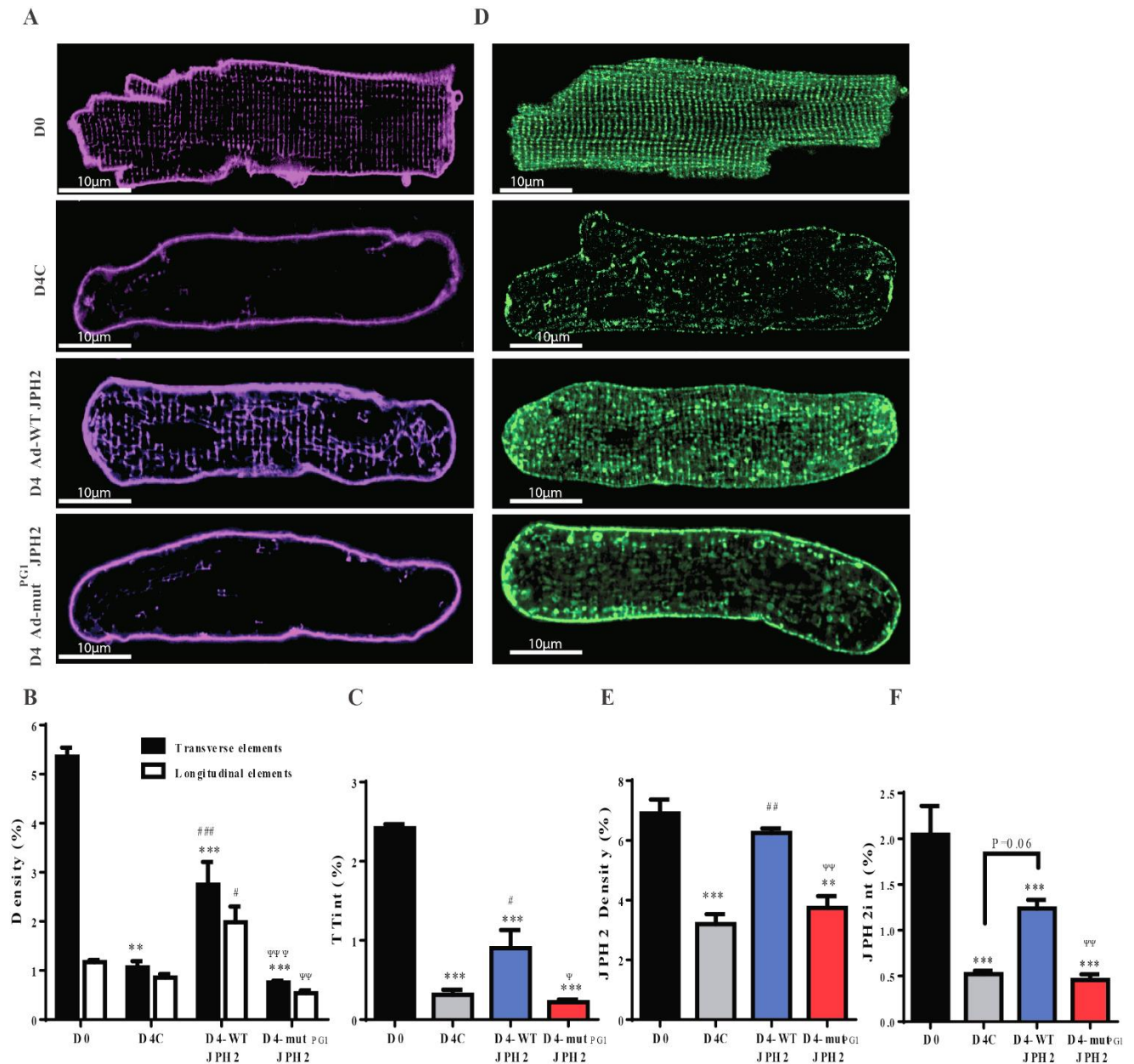


Figure 13. Overexpression of $mut^{PG1}JPH2$ averts the restoration of T-tubules in cultured ARVMs. (A) Distribution of T-tubules detected by Di-8-ANEPPS stain in freshly isolated ARVMs at day 0 (D0), after 4 days of culture in control ARVMs (D4C), in cells overexpressed with Ad-WT-JPH2 (D4-WT-JPH2) and in cells overexpressed with Ad- $mut^{PG1}JPH2$ (D4- $mut^{PG1}JPH2$). The entire area of the cell was selected to measure (B) both T-tubular transverse and longitudinal densities and (C) the global T-tubular integrity. (D)

Representative images of JPH2 staining in ARVMs at D0, control cells at D4, and AFRVMs overexpressed with either Ad-WT-JPH2 or Ad-mut^{PG1}JPH2. (E) Calculated JPH2 global density and (F) JPH2 global integrity. N=3 isolations, n=15 cells. ***/***P<0.05/0.01/0.001 vs. D0, ###/####P<0.05/0.01/0.001 vs. D4C and $\Psi/\Psi\Psi/\Psi\Psi\Psi$ P<0.05/0.01/0.001 vs. D4-wtJPH2.

Since JPH2 is crucial for spanning the junctional complexes between PM and jSR, we evaluated the effect of WT-JPH2 and mut^{PG1}JPH2 overexpression on cardiomyocyte structure, dyad frequency and dyad morphology using Transmission electron microscopy (Figure 9L, Figure 14). Myofilament disorganization and ‘Z line streaming’ [136], apparent in D4C cardiomyocytes, were restored by overexpression of WT-JPH2. However, overexpression of mut^{PG1}JPH2 induced morphological abnormalities and deranged further the myofilament disarray (Figure 10B). WT-JPH2 overexpression in AFVMs increased dyad frequency in reference to myofibrils (Figure 9L.3 and 4M) and organized Z-line alignments. In addition, WT-JPH2 overexpression increased the length of the dyads, which was measured as the length between T-tubule/jSR contacts (Figure 14). On the contrary, mut^{PG1}JPH2 overexpression in AFVMs sharply reduced the dyad frequency in comparison to dyad frequency detected in WT-JPH2 overexpressed cells in D4C cells (Figure 9L.4 and 9M). Despite changes in dyad frequency, the dyad length remained unaffected (Figure 14).

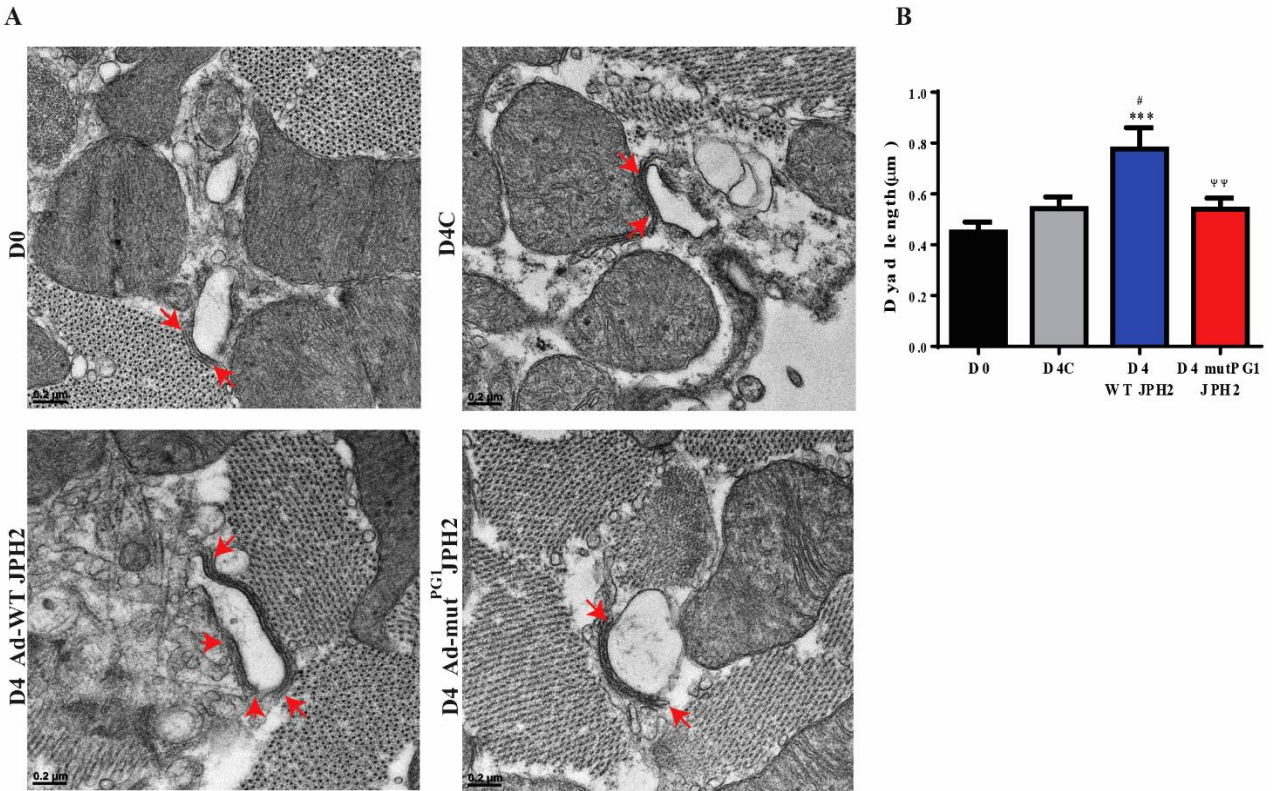


Figure 14. Length analysis profile of dyads. (A) Dyads were identified in locations where flat jSR cisternae were closely juxtaposed to T-tubule (between arrows). Scale 0.2µm. (B) Length of jSR/T-tubule contacts in thin sections. n= 6-7 randomly analyzed cells per group. */**/* P < 0.05/0.01/0.001 relative to D0, ###/###/### P < 0.05/0.01/0.001 relative to D4C, ψ/ψψ/ψψψ P < 0.05/0.01/0.001 relative to 4D WT-JPH2.

The Joining region in JPH2 interacts with LTCC α 1C subunit and elicits LTCC distribution to dyad microdomains where it colocalizes with RyR

Previous studies showed that junctophilin isoforms in skeletal muscle interact with LTCC to ensure adequate muscle contraction[110, 111]. The nature of this interaction in the cardiac muscle remains unclear. The Joining region in JPH2 might be involved in a potential interaction between JPH2 and LTCC in the dyad. To explore this further, we purified PM from AFVMs that were transduced with Ad-WT-JPH2 or with Ad-mut^{PG1}JPH2. Both regents carried the HA peptide tag, which allowed for HA-tag co-immunoprecipitation (Co-IP). Our Co-IP data (Figure 15A) show that LTCC α 1C subunit, but not β 2a subunit, is complexed with JPH2 in the cardiomyocyte PM. The mutated Joining region in JPH2 weakened the protein-protein interactions in PM between the LTCC α 1C pore-forming subunit and JPH2. This was further substantiated using a highly specific and sensitive approach of proximity ligation (PLA) assay in single cells. Overexpression of mut^{PG1}JPH2 in ARVMs strongly reduced the association between JPH2 and LTCC α 1C, in comparison to cardiomyocytes overexpressing WT-JPH2 (Figures 15B and 15C). To assess if the protein-protein interaction between JPH2 and LTCC α 1C elicits the ion channel recruitment to specific domains in the PM, we tested fractionated PM preparations from WT-JPH and mut^{PG1}JPH2 overexpressed AFVMs (Figure 15D). We found that WT-JPH2 overexpression in cultured cardiomyocytes predominantly restored JPH2 and LTCC α 1C distribution back to fractions F6-F7 in the PM (compare Figure 15D to Figure 11). However, mut^{PG1}JPH2 overexpression caused redistribution of JPH2 across the membrane and promoted a profound displacement of LTCC α 1C from its typical residing fractions F6-F7 to fractions F6-F11.

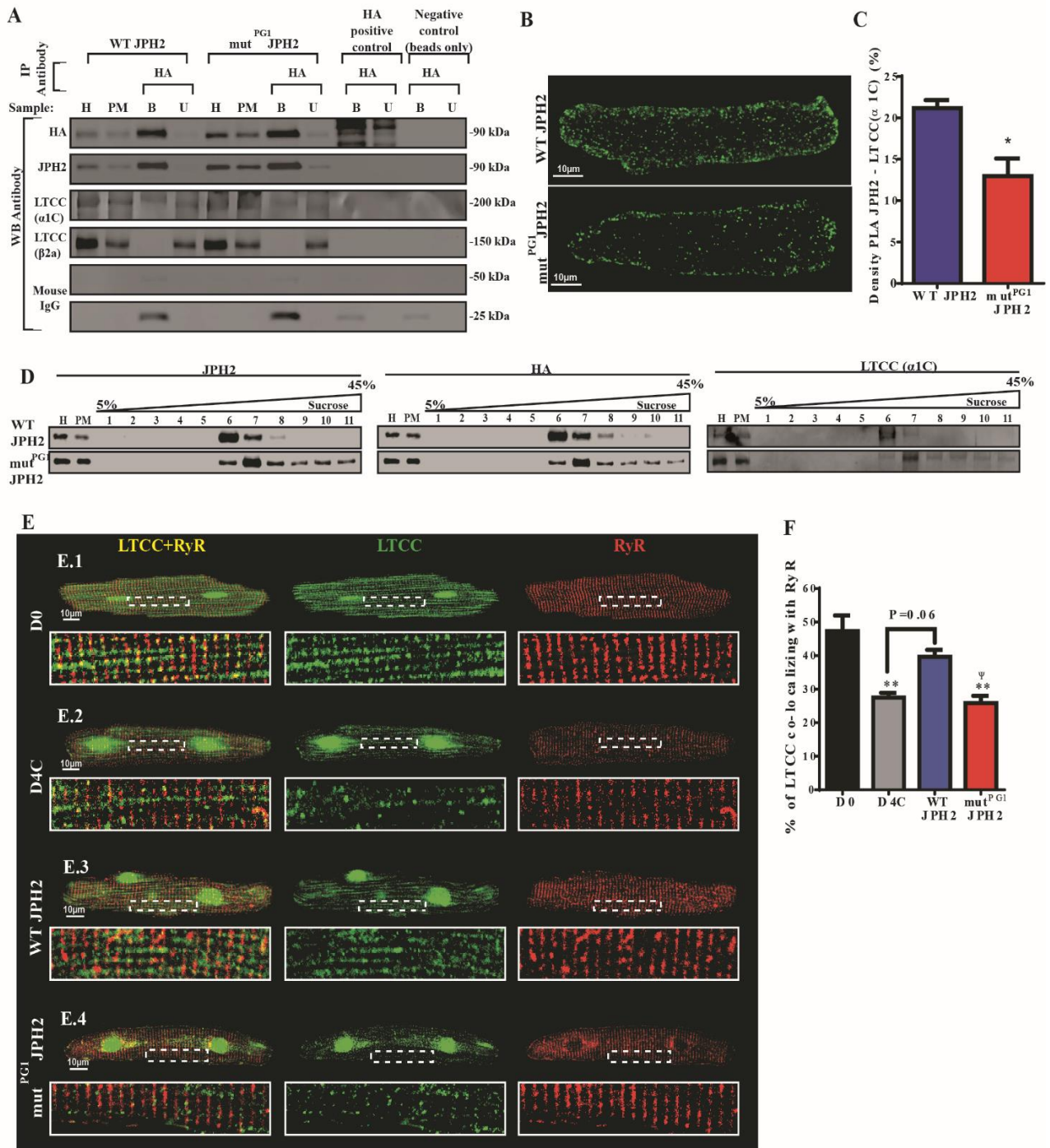
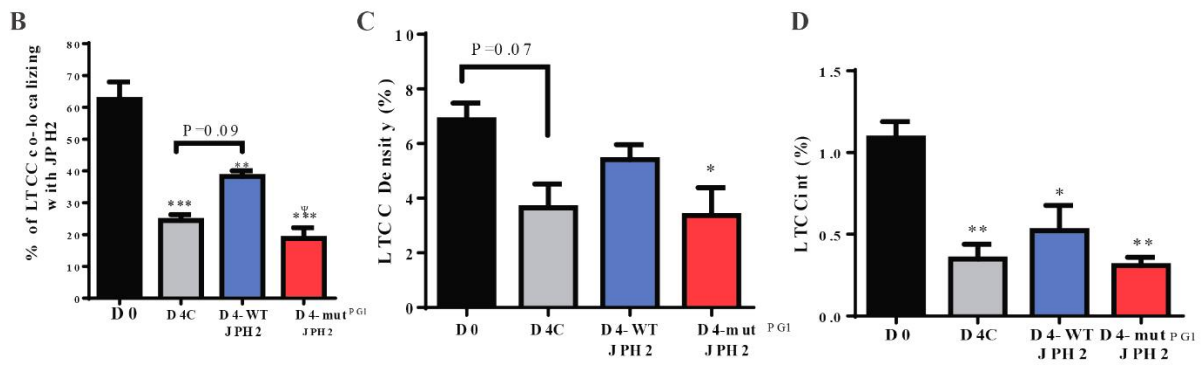
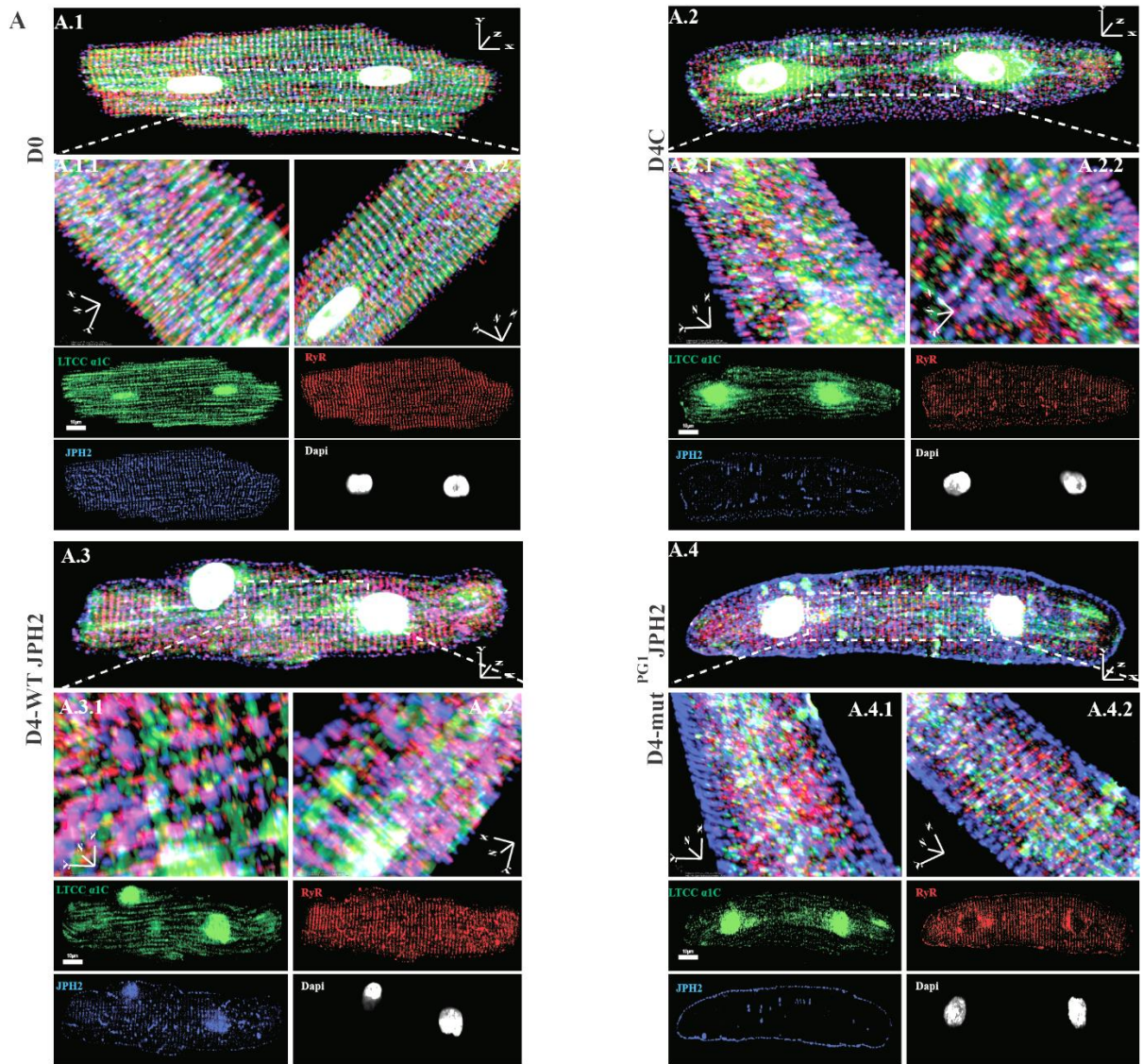


Figure 15. The Joining region in JPH2 interacts with LTCC and regulates membrane microdomain distribution of LTCC. (A) HA-tag co-immunoprecipitation (Co-IP) was performed on purified PM from AFVMs that were overexpressed with either Ad-WT-JPH2 or Ad-mut^{PG1}JPH2. HA, JPH2, LTCC α1C and LTCC β2a were detected in whole cell

homogenate (H), PM, HA bound (B) fraction and unbound (U) fraction. Co-IP was performed using magnetic beads conjugated with HA mouse antibody. Therefore, mouse IgG expression was tested. HA positive control was Escherichia coli extract containing HA tagged GST-PI3K-SH2 domain. **(B)** Proximity ligation (PLA) assay was performed on ARVMs transduced with Ad-WT-JPH2, or with Ad-mut^{PG1}JPH2 to detect protein-protein interaction between JPH2-LTCC α 1C subunit. **(C)** PLA density was measured as the fraction of an area covered by the fluorescence signal. Average values were calculated from at least 5 cells per isolation, N=3 isolations. */**/** P < 0.05/0.01/0.001. **(D)** Representative Western blots of JPH2 and LTCC (α 1C) across sucrose density gradient fractions (F1–F11) of WT-JPH2 and mut^{PG1}JPH2 overexpressed AFVMs. **(E)** AFVMs at D0 (panel E.1), D4C (panel E.2), overexpressed with WT-JPH2 (panel E.3) and overexpressed with mut^{PG1}JPH2 (panel E.4) were immunostained for RyR (red channel – right column) and LTCC α 1C subunit (green channel – middle column). The overlay of green and red channels is depicted in the left column. **(F)** Distance based co-localization percentage of LTCC (α 1C) with RyR. The entire cell surface was analyzed for co-localization excluding the nuclei. N=3 isolations, n=12-15 cells. */**/** P < 0.05/0.01/0.001 vs. D0, ###/### P < 0.05/0.01/0.001 vs. D4C and $\Psi/\Psi\Psi/\Psi\Psi\Psi$ P < 0.05/0.01/0.001 vs. WT-JPH2.

Since co-localization of LTCC with RyR is crucial for CICR and EC coupling, we further examined qualitatively and quantitatively the direct relationship between LTCC-JPH2-RyR dyadic complexes in our AFVMs system. We immunolabeled LTCC, JPH2 and RyR and performed co-localization profiling using a distance-based approach (see methods). Freshly isolated AFVMs (D0) showed clear co-localization patterns of immunostained LTCC-JPH2-RyR (Figure 16A.1) and LTCC-RyR (Figure 15E.1) dyadic complexes. These patterns were decreased in D4C AFVMs (Figure 16A.2 and Figure 15E.2). In WT-JPH2 overexpressing cardiomyocytes, co-localization of LTCC-JPH2-RyR and LTCC-RyR was preserved (Figure 16A.3 and Figure 15E.3), even though, these cardiomyocytes still exhibited structural remodeling (in comparison to D0 cardiomyocytes). In mut^{PG1}JPH2 overexpressing cardiomyocytes, immunostaining showed JPH2 localization to the surface sarcolemma with robustly reduced co-localization patterns of LTCC-JPH2-RyR (Figure 16A.4) and LTCC-RyR complexes (Figure 15E.4). Quantitative analysis of LTCC-RyR co-localization (Figure 15F and Figure 16F) and LTCC-JPH2 co-localization (Figures 16B and 16E) verified our qualitative findings. To survey if WT or mutated JPH2 constructs had any effect on LTCC expression, we measured stained LTCC density and integrity in the same set of images (Figure 16C and 16D). We found that in all cultured AFVMs (baseline and transduced cells), LTCC integrity was reduced in comparison to D0 AFVMs. The density of LTCC was reduced in mut^{PG1}JPH2 transduced cells in comparison to D0 cells but not relatively to WT-JPH2 transduced cells. These changes are attributed to the cell remodeling in culture rather than to the mutated Joining region in JPH2.



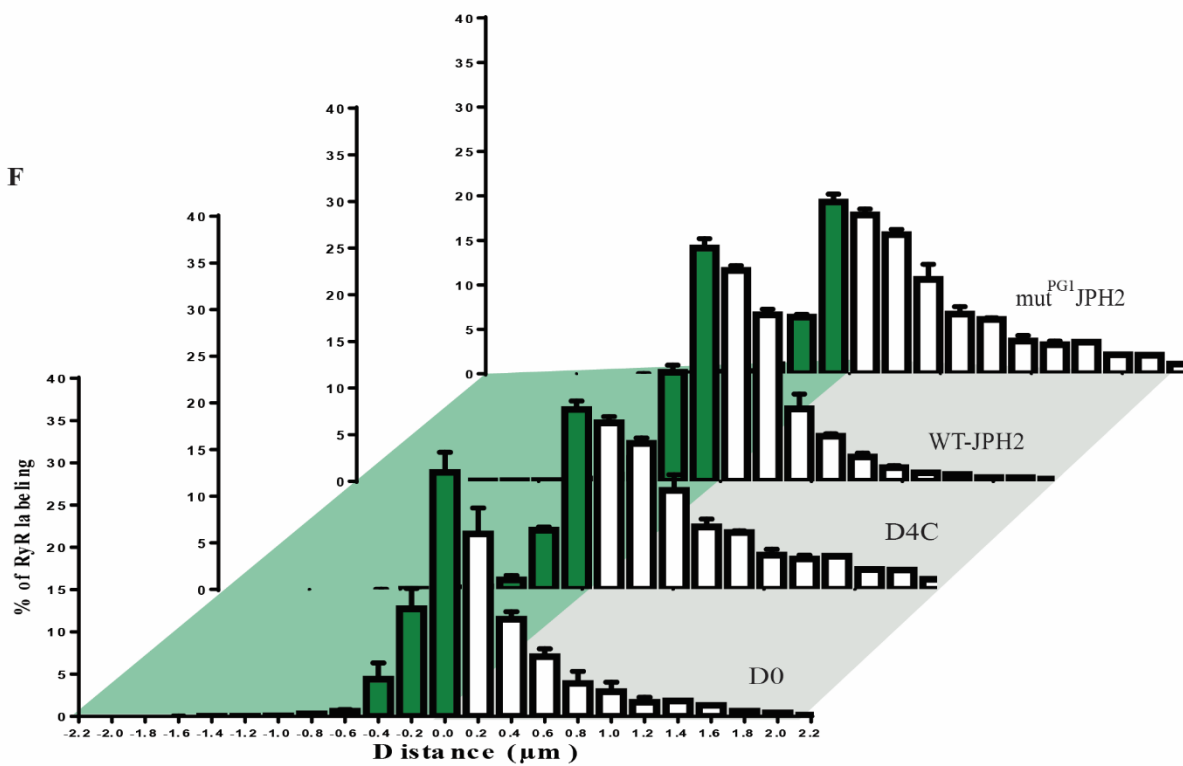
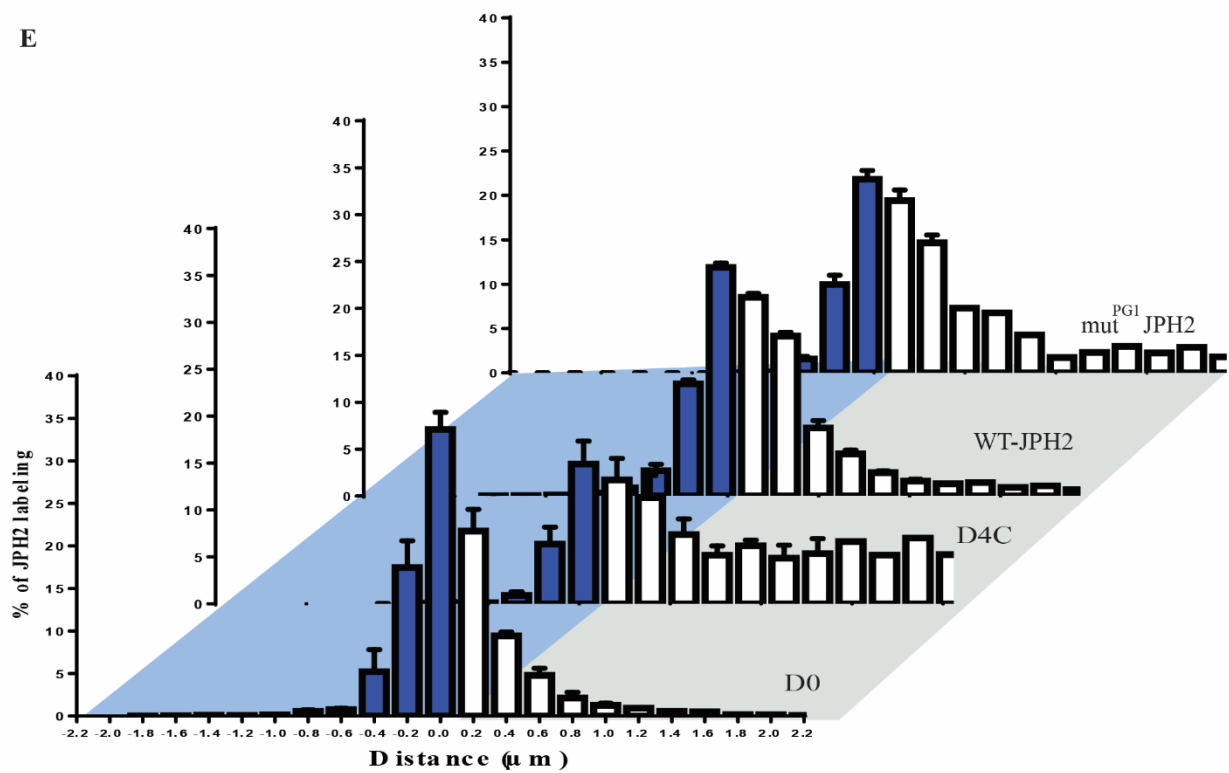


Figure 16. Co-localization of LTCC(α 1C)-JPH2-RyR molecular complex. (A) 3D reconstruction of Z-stack confocal images consisted of 4 channels: green – LTCC α 1C

staining, red – RyR staining, blue – JPH2 staining and white – Dapi staining. **(A.1)** Freshly isolated cardiomyocyte (D0). Calibration scale x:0.15 μ m, y:0.15 μ m, z:0.65 μ m. **(A.2)** Non-transduced cardiomyocyte 4 days in culture (D4C). Calibration scale x:0.12 μ m, y:0.12 μ m, z:0.65 μ m. **(A.3)** Cardiomyocyte transduced with Ad-WT-JPH2. Calibration scale x:0.12 μ m, y:0.12 μ m, z:0.65 μ m. **(A.4)** Cardiomyocyte transduced with Ad-mut^{PG1}JPH2. Calibration scale x:0.14 μ m, y:0.14 μ m, z:0.50 μ m. In every tested subgroup, the two upper panels represent 3D reconstruction of cardiomyocyte stained for LTCC(α 1C)-JPH2-RyR. The two lower panels represent 2D channels breakdown. **(B)** Distance based co-localization percentage of LTCC α 1C with JPH2. N=3 isolations, n=12-15 cells. **(C)** Calculated LTCC (α 1C) global density and **(D)** LTCC (α 1C) global integrity. N=3 isolations, n=12-15 cells. ***/***P<0.05/0.01/0.001 vs. D0, ###/####P<0.05/0.01/0.001 vs. D4C and $\Psi/\Psi\Psi/\Psi\Psi\Psi$ P<0.05/0.01/0.001 vs. D4-WT-JPH2. **(E)** Co-localization quantification of JPH2 with LTCC (α 1C). The histogram shows the total percentage labeled of JPH2 labeling (excluding nuclei region) as a function of the distance to the edge of the nearest region of LTCC (α 1C). The blue bars correspond to the fraction of JPH2 labeling that was detected within the segmented borders of LTCC (α 1C) staining. Average data is shown from N=3 isolations, n=12-15 cells per group. **(F)** The histogram shows the total percentage labeled of RyR labeling (excluding nuclei region) as a function of the distance to the edge of the nearest region of LTCC (α 1C). The green bars correspond to the fraction of RyR labeling that was detected within the segmented borders of LTCC (α 1C) staining. Average data is shown from N=3 isolations, n=12-15 cells per group.

We next sought to distinguish whether JPH2 overexpression is sufficient to preserve the T-tubular system in cultured AFVMs, or the actual crosstalk between JPH2 and LTCC is crucial for the stabilization of T-tubules. LTCC (α 1C) abundance in AFVMs was reduced by transducing cells with Ad-LTCC (α 1C)-shRNA-V3 (Figure 17). Staining of LTCC α 1C validated reduction in the protein levels (Figure 18A – upper panel). Knocking down LTCC α 1C did not result in further downregulation of JPH2 and T-tubule density and/or integrity, since both were already downregulated in culture as shown in Ad-scramble shRNA control cells (Figure 18A – middle and lower panel, Figure 18B-E). Overexpression of both Ad-LTCC (α 1C)-shRNA-V3 and Ad-WT-JPH2, induced increased JPH2 levels with a tendency to localize to PM surface (Figure 18A – middle panel). JPH2 density and integrity were indeed restored in these cells (Figure 18B-C). However, the T-tubular network was not reestablished, as T-tubule density and integrity remained decreased (Figure 18D-E). Thus, it is likely that overexpression of JPH2 alone, without establishing LTCC-JPH2 interaction, is not sufficient to restore and stabilize T-tubules.

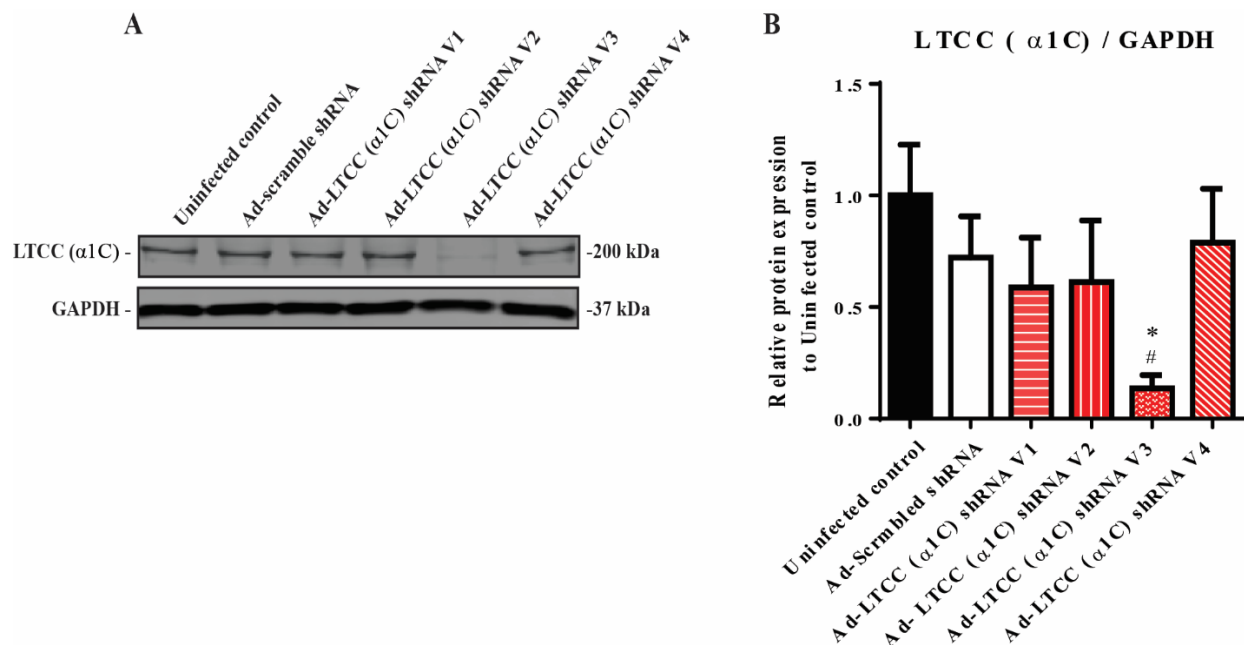


Figure 17. LTCC ($\alpha 1C$) knockdown in AFVMs. (A) AFVMs were transduced in culture with four Adenoviral shRNA vectors (V1-V4) targeting LTCC ($\alpha 1C$). Vectors were tagged with RFP to verify transduction efficiency in culture. Protein expression was tested by Western blot, which identified that Ad- LTCC ($\alpha 1C$) shRNA V3 successfully knocked down LTCC expression. (B) Corresponding quantifications showing significant knockdown of LTCC in AFVMs by Ad- LTCC ($\alpha 1C$) shRNA V3. N=3, *P<0.05 vs. uninfected control, #P<0.05 vs. Ad-scrambled shRNA.

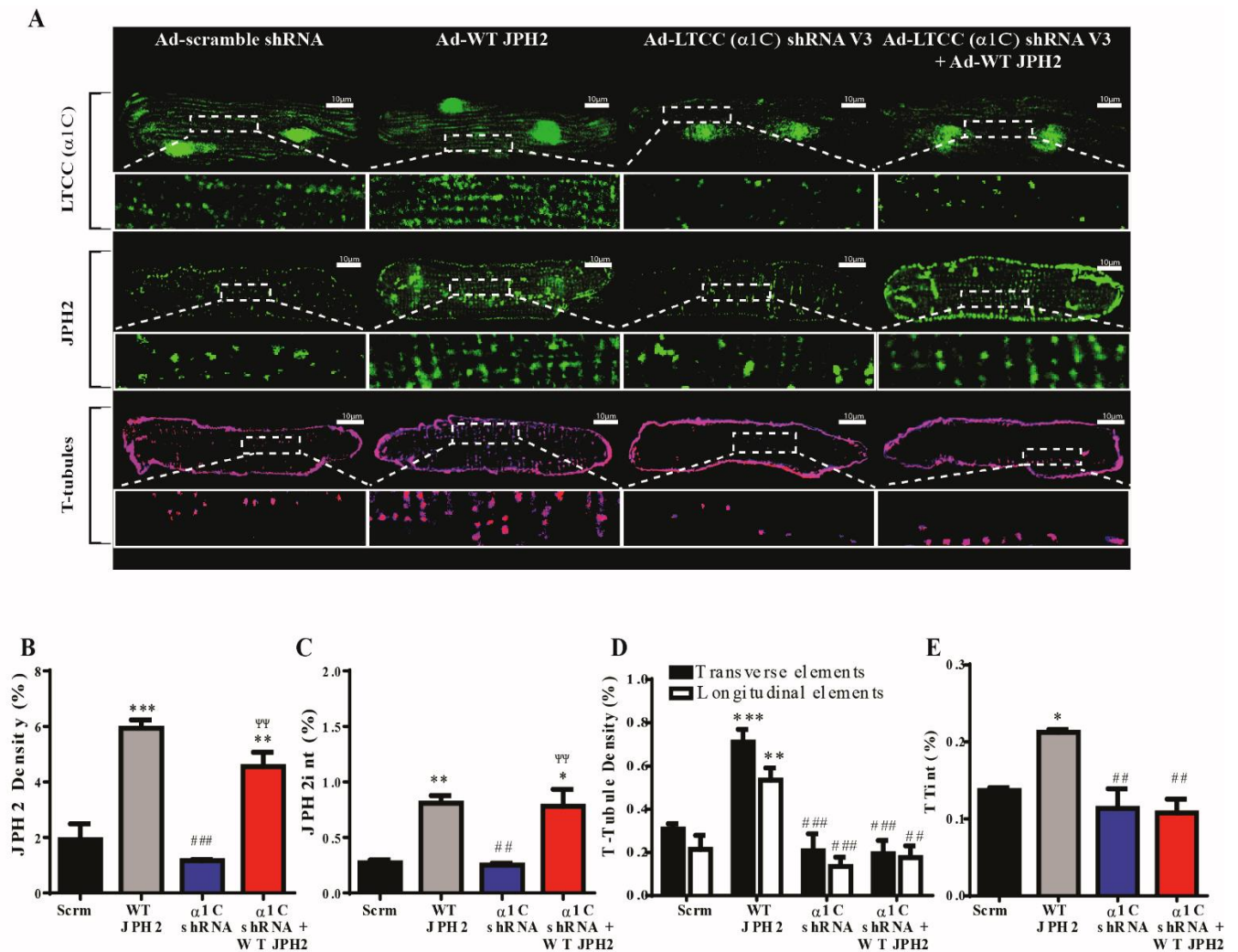


Figure 18. LTCC and JPH2 jointly stabilize T-tubules. (A) AFVMs were transduced with Ad-scrambled shRNA, Ad-WT-JPH2, Ad-LTCC ($\alpha 1C$) shRNA-V3 and combination of

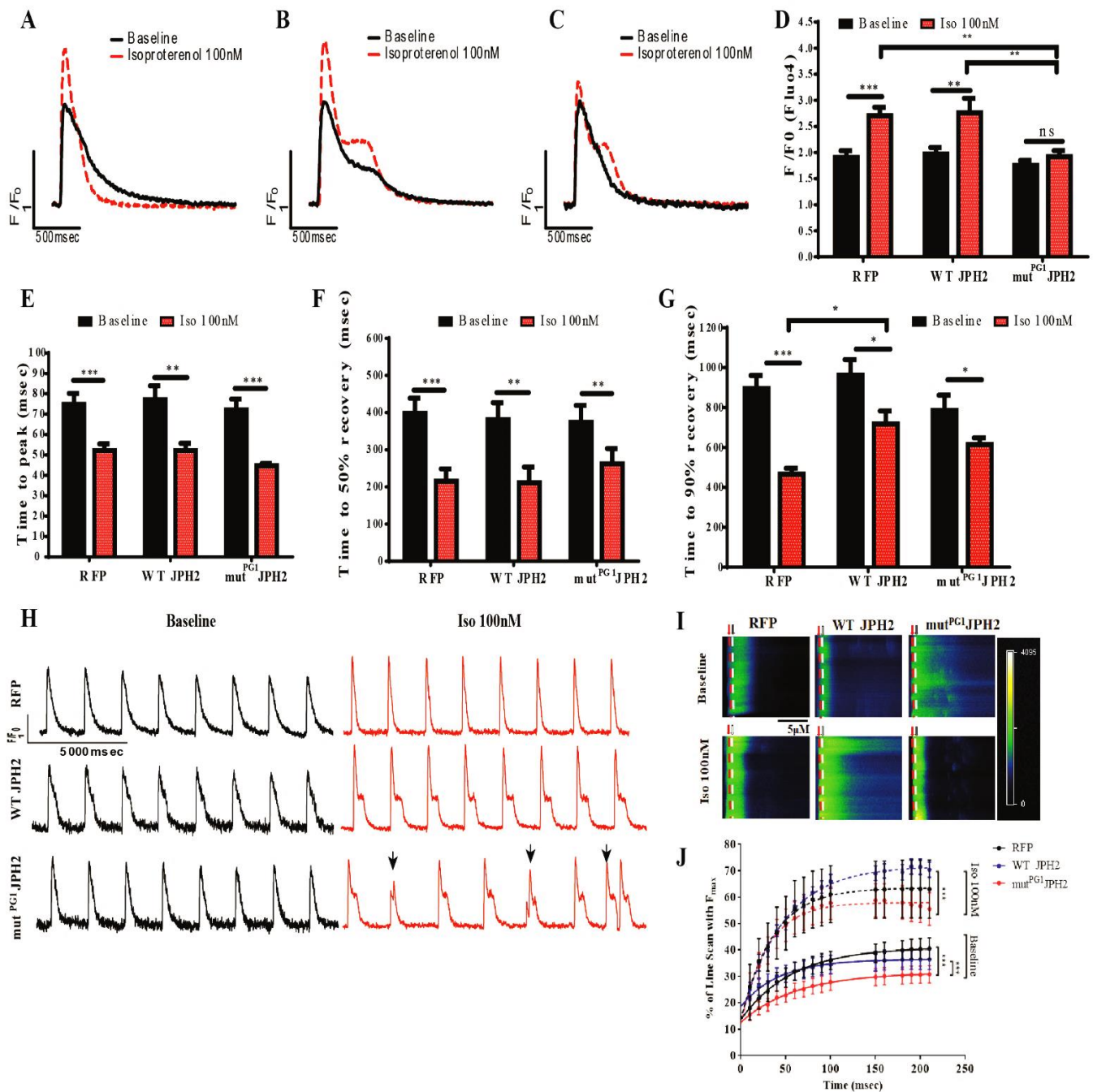
AD WT-JPH2 + Ad-WT-JPH2, Ad-LTCC ($\alpha 1C$) shRNA-V3. Immunostaining for LTCC $\alpha 1C$ is shown in the upper panel, confirming knock down of LTCC. JPH2 staining is shown in the middle panel and di-8-ANPPES T-tubular stain is presented in the lower panel. **(B)** Quantification of JPH2 density. **(C)** JPH2 staining integrity analysis. **(D)** T-tubular density analysis and **(E)** T-tubular integrity analysis. N=3 isolations, n=10-11 cells, */**/**P<0.05/0.01/0.001 vs. Ad-scrambled shRNA, #/##/###P<0.05/0.01/0.001 vs. Ad-WT-JPH2, $\Psi/\Psi\Psi/\Psi\Psi\Psi$ P<0.05/0.01/0.001 vs. Ad-LTCC ($\alpha 1C$) shRNA-V3.

Disrupting the interaction between the Joining region in JPH2 and LTCC in cardiomyocytes impairs EC coupling and CICR

The effect of modulating the interaction between the Joining region in JPH2 and the LTCC on cell physiology was explored by measuring cytosolic Ca^{2+} transients in AFVMs overexpressing red fluorescence protein (RFP; control), WT-JPH2 or mut^{PG1} JPH2. Given that β -adrenergic stimulation facilitates intracellular Ca^{2+} release during EC coupling[150, 151], baseline Ca^{2+} transients as well as responses to β -adrenergic agonist Isoproterenol (Iso 100nM) were measured (Figure 19). Baseline Ca^{2+} transients were not different in any of the three groups. Iso induced similar increases in cytosolic Ca^{2+} transients amplitude in RFP and WT-JPH2 overexpressing myocytes. However, Iso did not significantly increase the amplitude of the Ca^{2+} transient in mut^{PG1} JPH2 expressing AFVMs (Figure 19C-D). Iso accelerated the kinetics of Ca^{2+} transient decay in all groups (Figure 19E-G). The time to 90% recovery in WT-JPH2 overexpressed myocytes was longer after Iso (Figure 19G). Iso triggered pro-arrhythmic Ca^{2+} waves in mut^{PG1} JPH2 AFVMs that were paced at 0.5Hz. Spontaneous Ca^{2+} release was observed between paced Ca^{2+} transients in mut^{PG1} JPH2 AFVMs (Figure 19H – indicated by arrows). To better understand the mechanism of pro-

arrhythmic Ca^{2+} transients in $\text{mut}^{\text{PG1}}\text{JPH2}$ AFVMs, the spatial uniformity of SR Ca^{2+} release was examined with confocal line scanning (Figure 19I). At baseline, disordered Ca^{2+} wave propagation ($>210\text{msec}$) was observed in $\text{mut}^{\text{PG1}}\text{JPH2}$ AFVMs. Spatial uniformity was significantly delayed in $\text{mut}^{\text{PG1}}\text{JPH2}$ AFVMs compared to RFP and WT-JPH2 myocytes. Iso decreased the percentage of unresponsive Ca^{2+} release zones (likely couplons) in all groups. With Iso present, the percentage of spatial synchrony of couplons in $\text{mut}^{\text{PG1}}\text{JPH2}$ myocytes still occurred significantly later than in WT-JPH2, or with a relative delay compared to RFP myocytes (Figure 19J). These results indicate that $\text{mut}^{\text{PG1}}\text{JPH2}$ myocytes had fewer Ca^{2+} couplons than other myocytes, which is likely linked to the loss of T-tubules. Spontaneous Ca^{2+} release after slow pacing (Figure 19K) and faster pacing (Figure 20) frequencies was observed in the presence of Iso. RFP and WT-JPH2 overexpressed AFVMs exhibited synchronous Ca^{2+} release during 0.5Hz and 1Hz pacing. A few isolated spontaneous Ca^{2+} release events were shown after pacing, which are typically attributed to pacing induced SR Ca^{2+} overload. $\text{mut}^{\text{PG1}}\text{JPH2}$ overexpressed myocytes exhibited significant asynchronous Ca^{2+} release during pacing protocols. A distinct pattern of spontaneous Ca^{2+} release was observed during the pacing phase in these cells. In these myocytes local Ca^{2+} release was observed at the edges of the cell and there was failure to propagate either inward or along the myocyte (Figure 19K – indicated via black arrows). 3D plotting of the line scan images clearly showed that these spontaneous Ca^{2+} release events arose from the edges of the $\text{mut}^{\text{PG1}}\text{JPH2}$ expressing cell (Figure 19L – indicated via black arrows). Following the pacing phase, $\text{mut}^{\text{PG1}}\text{JPH2}$ myocytes demonstrated multiple Ca^{2+} spontaneous releases, random Ca^{2+} triggered events (Figure 19K – black arrows) and Ca^{2+} alternans (Figure 19K – grey arrows). Using the 3D plotting, we determined that spontaneous Ca^{2+} releases and Ca^{2+} alternans had uniform distribution

across the cells, albeit with distinct intensities (Figure 19L – red arrows vs. grey arrows, respectively). Modified LTCC function and loss of β -adrenergic signaling are common phenomena in diseased cardiomyocytes [152].



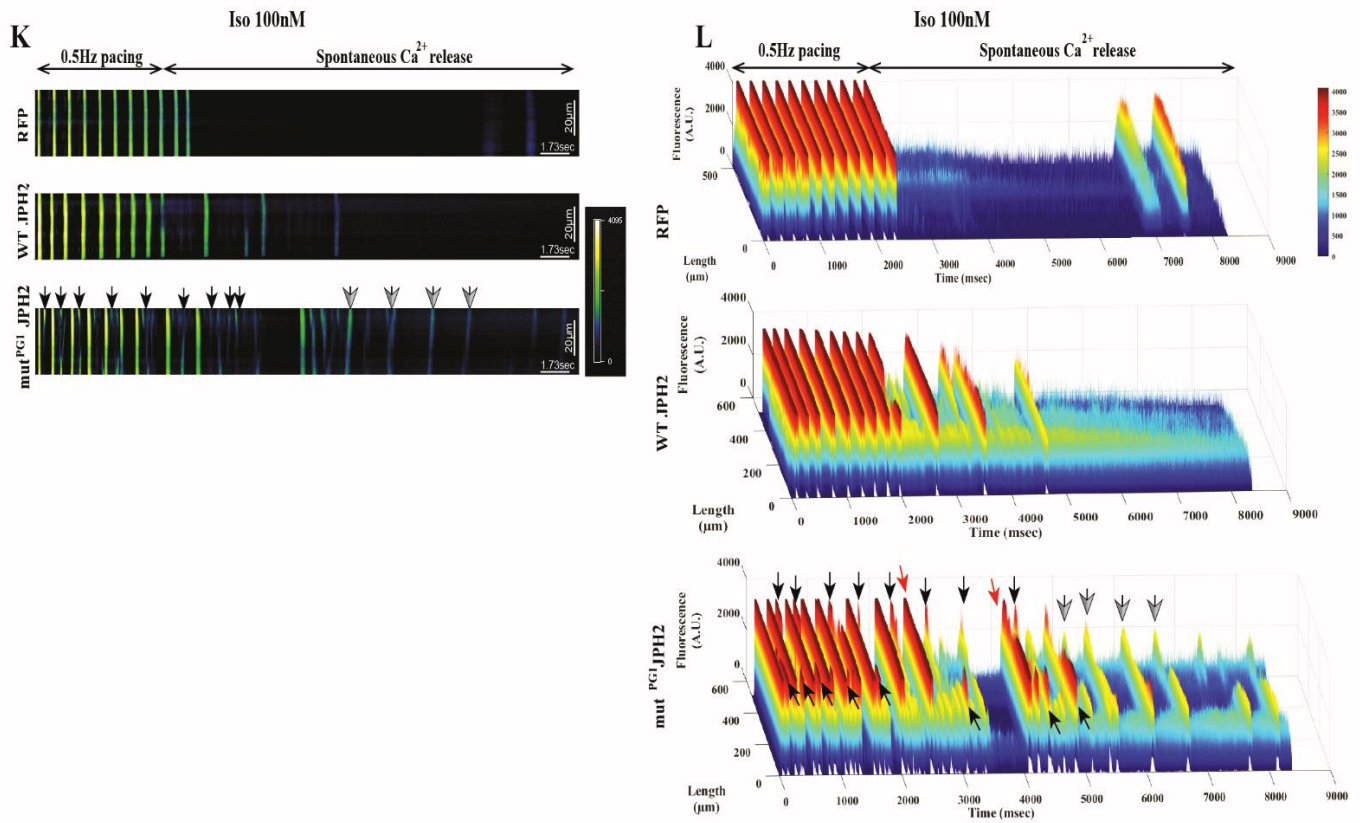


Figure 19. Mutation of the Joining region in JPH2 alters Ca²⁺ signaling in AFVMs after β -adrenergic stimulation. Representative recordings of intracellular Ca²⁺ transients (Fluo-4) in AFVMs overexpressed with [A] Ad-RFP, [B] Ad-WT-JPH2, [C] Ad-mut^{PG1}JPH2 paced at 0.5Hz with or without isoproterenol (Iso 100nM). [D] Ca²⁺ transient peak amplitude. [E] Ca²⁺ time to peak amplitude. [F] Ca²⁺ time to 50% decay. [G] Time to 90% decay. n = 19-24 cells per group. [H] Representative traces of paced AFVMs overexpressed with RFP/WT-JPH2/ mut^{PG1}JPH2 with and without iso 100nM. Cells were paced at 0.5Hz. Spontaneous Ca²⁺ oscillations are indicated via black arrows. [I] Ca²⁺ release synchrony obtained via confocal line scanning of RFP/WT- JPH2/ mut^{PG1}JPH2 AFVMs. Cells were paced at 0.5Hz with or without Iso 100nM. Spatial profiles are highlighted at 10msec (red dotted line) and 40msec (white dotted line). [J] Percentage of line scan with an index of F/F_{max} representing spatial synchrony of Ca²⁺ release. n=10 cells per group.

*/**/*P<0.05 / 0.01/0.001 comparison of fits. **[K]** Representative line scan recordings of AVFMs overexpressed with RFP/WT-JPH2/ mut^{PG1}JPH2, treated with 100nM Iso and paced at 0.5Hz. Asynchronous Ca²⁺ release during pacing is indicated via black arrows. Ca²⁺ alternans are indicated via grey arrows. **[L]** Representative 3D-reconstruction of representative line-scan recordings determine the characteristics of spatial Ca²⁺ waves spreads in correlation to space and time. Red arrows indicate spontaneous Ca²⁺ release. */**/* P<0.05/0.01/0.001.

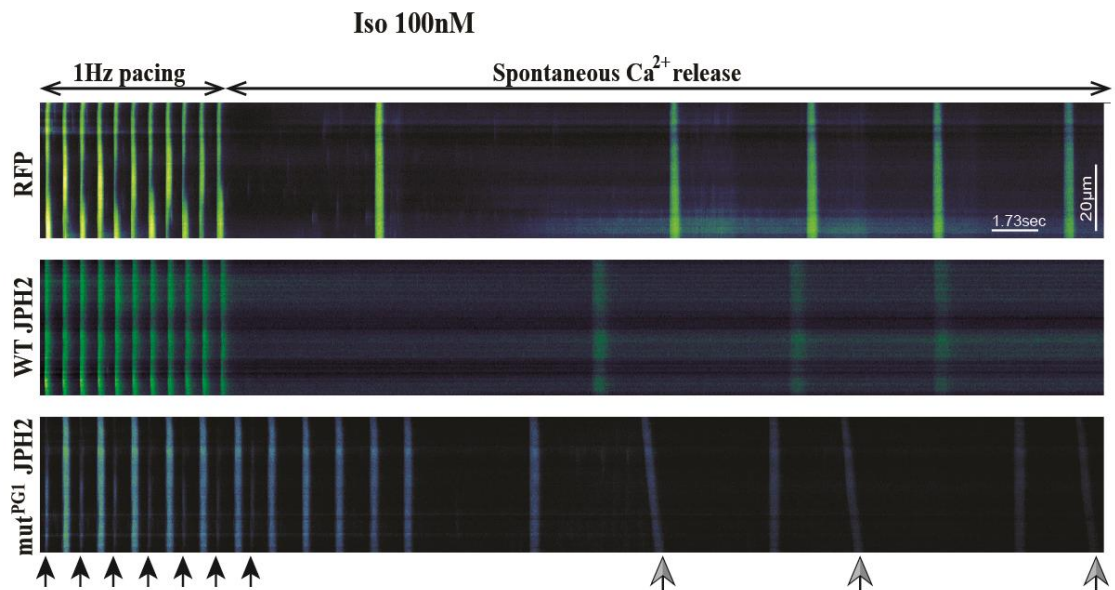
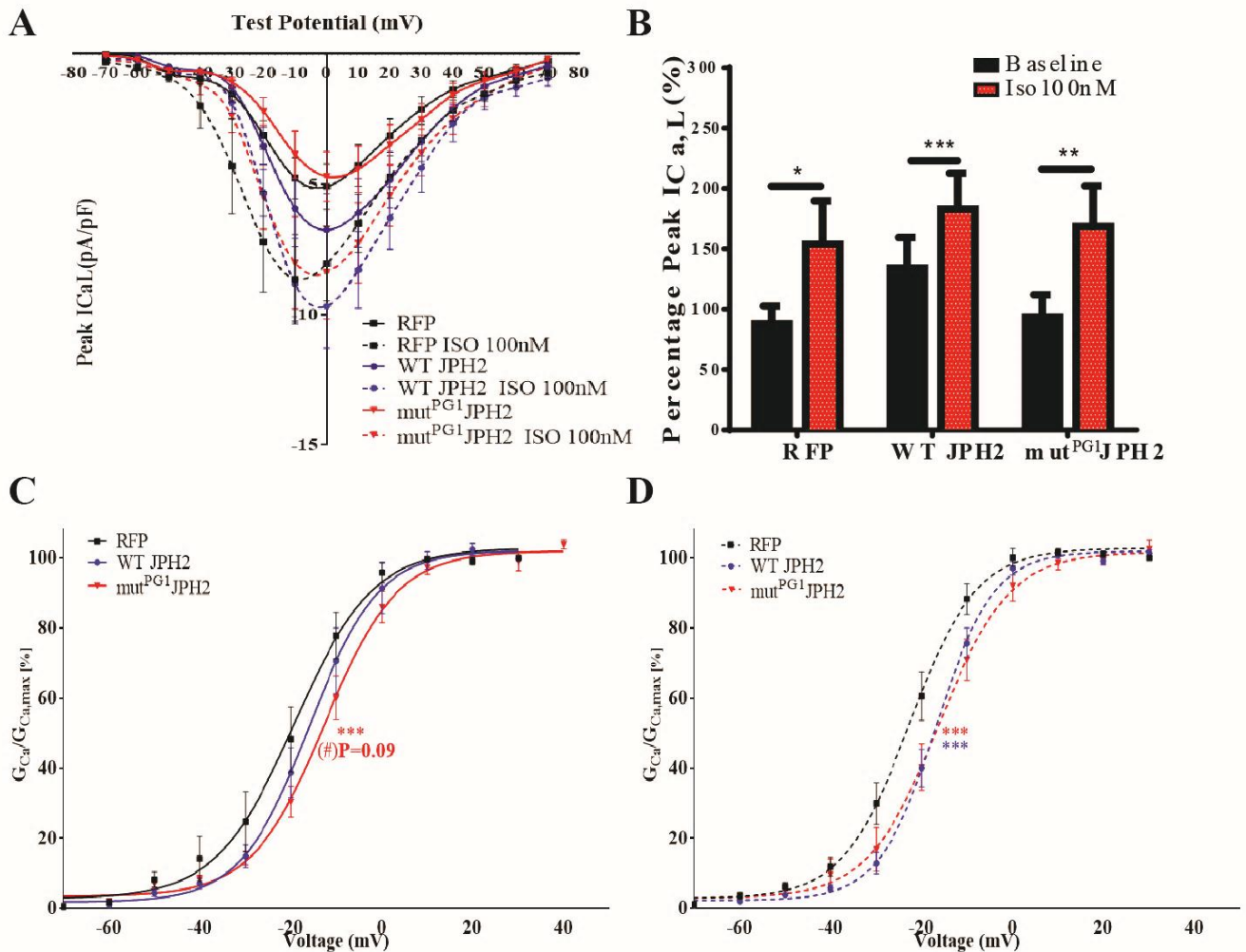


Figure 20. Representative line scan recordings of AVFMs overexpressed with RFP/WT-JPH2/ mut^{PG1}JPH2, treated with 100nM Iso and paced at 1Hz. Asynchronous Ca²⁺ release during pacing is indicated via black arrows. Ca²⁺ alternans are indicated via grey arrows.

To gain insight if mutating the Joining region in JPH2 affected LTCC activity after Iso stimulation, we measured $I_{Ca,L}$ in single isolated AFVM overexpressing RFP, WT-JPH2 or mut^{PG1} JPH2. Basal peak $I_{Ca,L}$ density (Figure 21A) was not significantly different in any of the three tested groups. All groups had substantial increase in $I_{Ca,L}$ after Iso stimulation (Figure 21A-B). There was a significant rightward shift in the voltage dependence of $I_{Ca,L}$ activation in the basal state of mut^{PG1} JPH2 myocytes compared to RFP and WT-JPH2 myocytes (Figure 21C). Iso induced the voltage dependence of $I_{Ca,L}$ activation to shift towards negative potentials in RFP and mut^{PG1} JPH2 myocytes without strongly affecting WT-JPH2 myocytes (Figure 22). A left shift in the voltage dependence of $I_{Ca,L}$ activation is typically observed with PKA-mediated phosphorylation of LTCCs with activation of β -adrenergic signaling[84, 150]. However, WT-JPH2 and mut^{PG1} JPH2 overexpressed myocytes still showed a shift of ~ 10 mV towards more positive potentials relative to RFP control myocytes under Iso stimulation (Figure 21D), indicating aberrant regulation of the voltage in LTCC. Super-resolution patch-clamp[141] was then used to determine LTCC function in specific PM microdomains in ARVMs overexpressed with Ad-WT-JPH2 or Ad- mut^{PG1} JPH2 (Figure 21E-G). Freshly isolated ARVMs exhibited a higher number of functional LTCCs per μm^2 in the T-tubules regions versus membrane surface (crest) (T-tubules>crest) (Figure 21F). This ratio was reversed after 4 days in primary culture in control cells (T-tubules<crest). Overexpression of WT-JPH2 in ARVM increased the density of functional LTCCs and restored the ratio of T-tubules>crest. Our measurements did not detect functional LTCCs in T-tubules of mut^{PG1} JPH2 overexpressing ARVMs. These results indicate that functional LTCCs were localized ultimately in the crest of mut^{PG1} JPH2 cells (Figure 21F). The LTCC open probability was also measured in the presence of LTCC agonist BayK8644 to ensure the maximal open probability of LTCCs

(Figure 21G). The open probability of LTCCs was similar in all groups under these conditions, including LTCCs in the crest of $\text{mut}^{\text{PG1}}\text{JPH2}$ overexpressed cells.

To measure SR Ca^{2+} content, AFVMs were paced to a steady state and SR Ca^{2+} release was induced by a rapid application of caffeine. Similar amplitudes of caffeine-induced SR Ca^{2+} release was seen in the RFP, WT-JPH2 and $\text{mut}^{\text{PG1}}\text{JPH2}$ overexpressing AFVMs. Perfusing myocytes with Iso induced increase in SR Ca^{2+} release in RFP control and WT-JPH2 myocytes. However, an increase in the caffeine-induced SR Ca^{2+} release was not seen in $\text{mut}^{\text{PG1}}\text{JPH2}$ myocytes (Figure 21H-I).



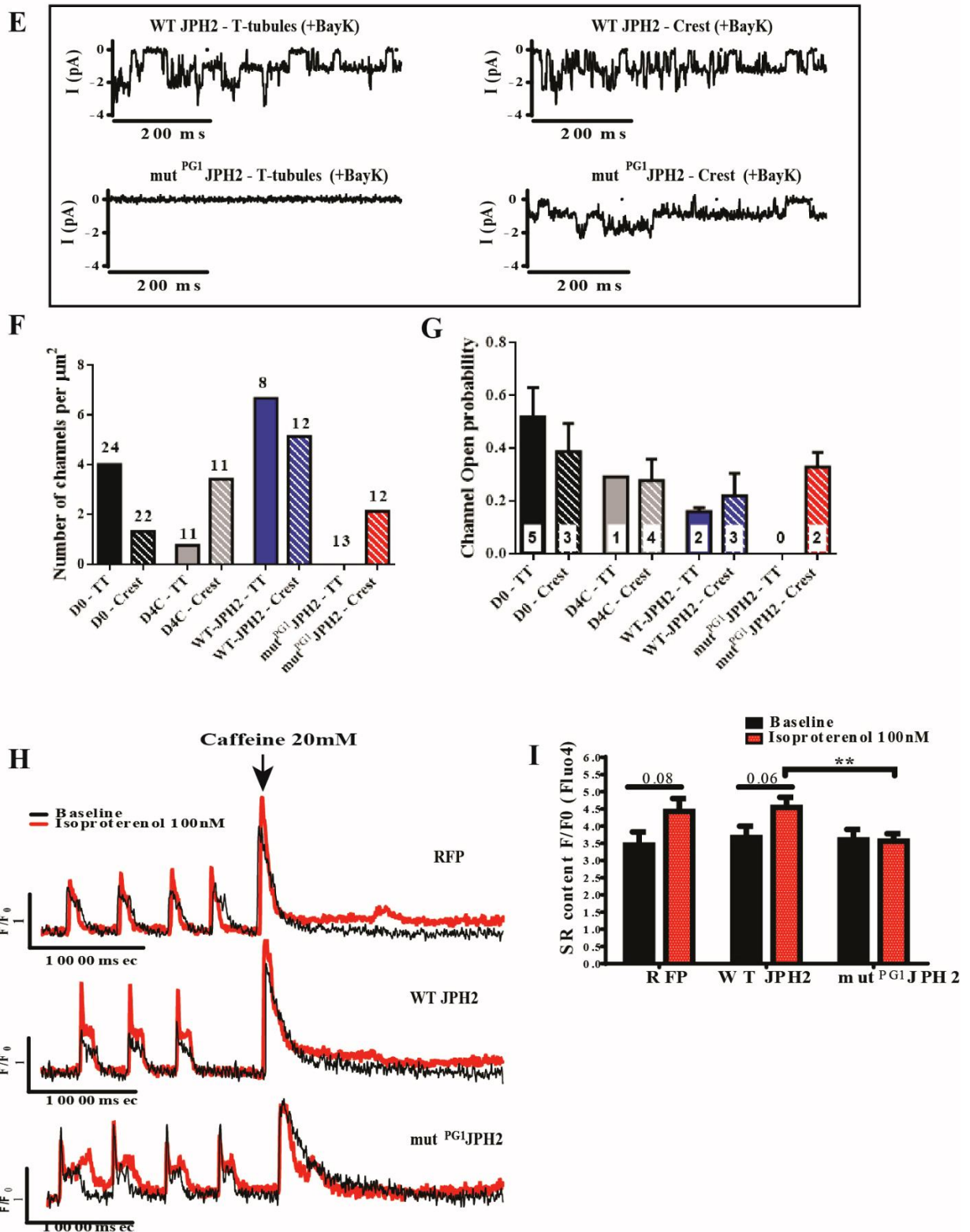


Figure 21. Abnormal LTCC localization to the crest with modified voltage dependence activation and reduced CICR in *mut^{PG1}JPH2* AFVMs. [A] $I_{Ca,L}$ -voltage relationships in

RFP/WT-JPH2/ mut^{PG1}JPH2 overexpressed AFVMs with or without Iso 100nM. N=3 isolations, n=11-14 cells per group. **[B]** Peak amplitude of Ca²⁺ current through LTCC. N=3 isolations, n=11-14 cells per group. ***/***P<0.05 / 0.01/0.001. Voltage dependence of I_{Ca,L} activation in RFP/WT-JPH2/ mut^{PG1}JPH2 overexpressed AFVMs were fit with Boltzmann Equation $G/G_{max}=1/[1+\exp(V_{0.5}-V)/k]$ in baseline **[C]** and in response to Iso 100nM **[D]**. N=3 isolations, n=11-14 cells per group. ***/***P<0.05 / 0.01/0.001 vs. RFP, ###/### P<0.05/0.01/0.001 vs. WT-JPH2 using Boltzmann sigmoidal fitting. **[E]** Single LTCC activity was recorded in T-tubules or non-tubular areas of the surface membrane (Crest) using super-resolution scanning patch clamp in the presence of the LTCC agonist BayK8644 (5μM in the pipette). Examples of original recordings indicate with a holding potential of -96.7mV, channels were activated by a step to -6.7mV. **[F]** Channel density calculated per μm². The number indicated for each column is the total number of patches. **[G]** Channel open probability at -6.7 mV. The number indicated for each column is number of patches with one or more Ca²⁺ channel(s). **[H]** Representative traces of Ca²⁺ transients amplitudes and total SR content indicated by the amplitude of caffeine induced SR Ca²⁺ release in paced AFVMs and. **[I]** Bar graph showing SR Ca²⁺ release peak amplitude. **[J]** Fractional release indicating the ratio between global Ca²⁺ transient to SR Ca²⁺ release. Data are presented as mean ± SEM. N=3 isolations, n= 10-25 cells per group. ***/***P<0.05 / 0.01/0.001.

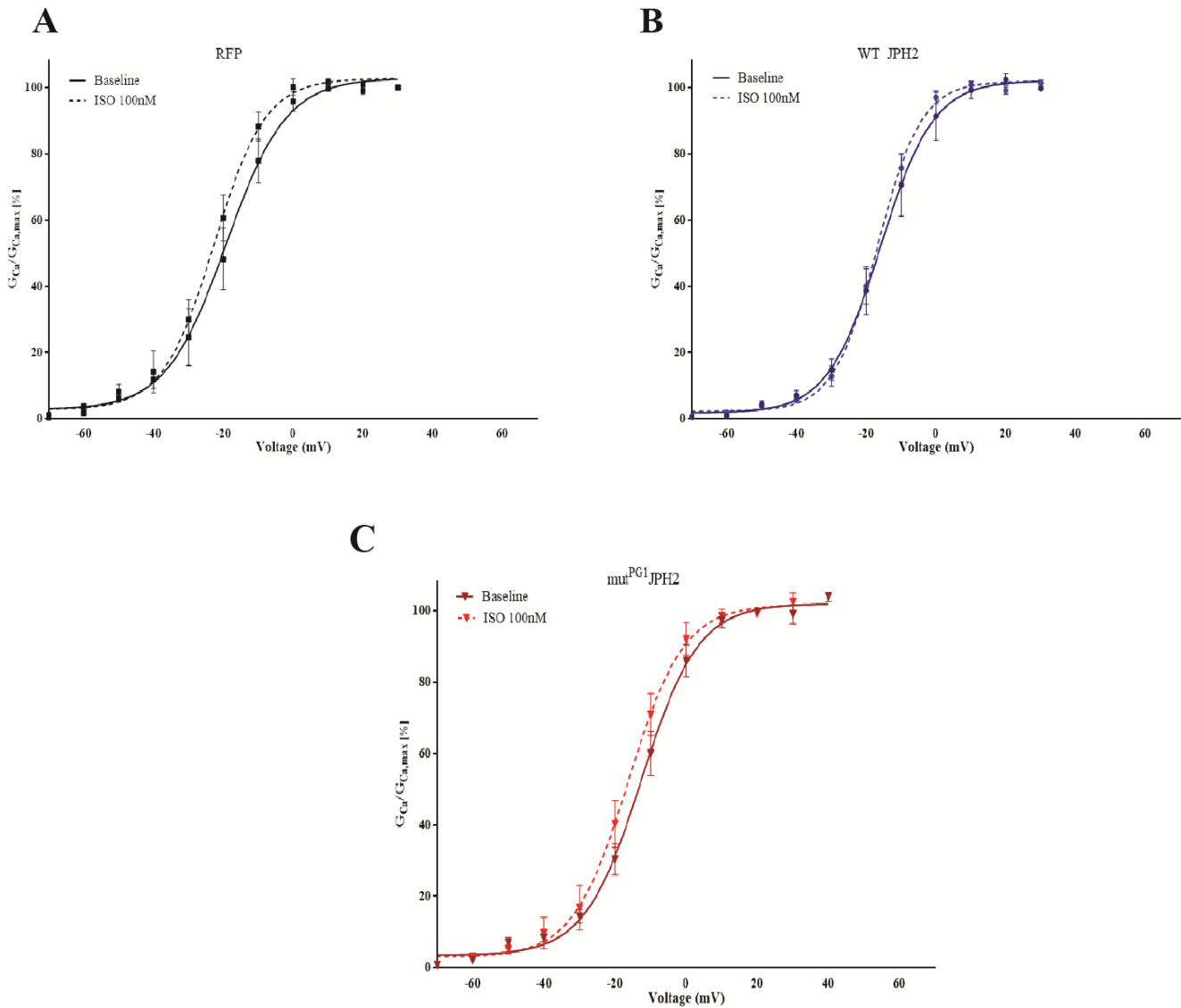


Figure 22. Voltage dependence of $I_{Ca,L}$ activation in [A] RFP,[B] WT-JPH2 and [C] mut^{PG1}JPH2 overexpressed AFVMs with or without Iso 100nM. A negative shift in voltage dependence of $I_{Ca,L}$ activation (Boltzmann Equation $G/G_{max}=1/[1+\exp(V_{0.5}-V)/k]$) was observed in RFP and mut^{PG1}JPH2 overexpressed cells in response to Iso 100nM. WT-JPH2 overexpressed cells remained unchanged. N=3 isolations, n=11-14 cells per group.

The effect of mut^{PG1}JPH2 overexpression on EC coupling proteins and Ca²⁺ handling proteins in cardiomyocytes

JPH2 is an essential structural regulator of the dyadic cleft. Mutation of JPH2 resulted in changes in the dyad density and alteration of EC coupling. Overexpression of mut^{PG1}JPH2 in cardiomyocytes did not induce changes in the abundance levels of the EC coupling proteins residing in the cardiac dyads (Figure 23A-I and Figure 24A-D). No significant differences in the expression levels of total RyR, LTCC (α 1C), SERCA2a or PLB were observed. BIN1, which has been previously shown to localize to T-tubules and regulate LTCC trafficking to the T-tubules[35, 153], also did not differ in WT-JPH2 or mut^{PG1}JPH2 overexpressed AFVMs in comparison to D0 and D4C AFVMs. However, CaMKII activation in D4C and WT-JPH2 myocytes was altered through autophosphorylation at a known Thr287 site[154]. CaMKII activation was significantly increased in mut^{PG1}JPH2 myocytes in comparison to D0 and WT-JPH2 myocytes (Figure 23E). mut^{PG1}JPH2 induced RyR S2814 and PLB T17 phosphorylation (Figure 23C and 23H), which are known CaMKII phosphorylation sites [71, 155]. Phosphorylation sites of RyR S2808 and PLB S16 that are PKA mediated remained unaffected in WT-JPH2 or mut^{PG1}JPH2 overexpressing myocytes (Figure 23B and 23G). Overall, CaMKII is a necessary modulator of Ca²⁺ balance in the myocytes and its increased activation in mut^{PG1}JPH2 myocytes may indicate unstable intracellular Ca²⁺ mobilization.

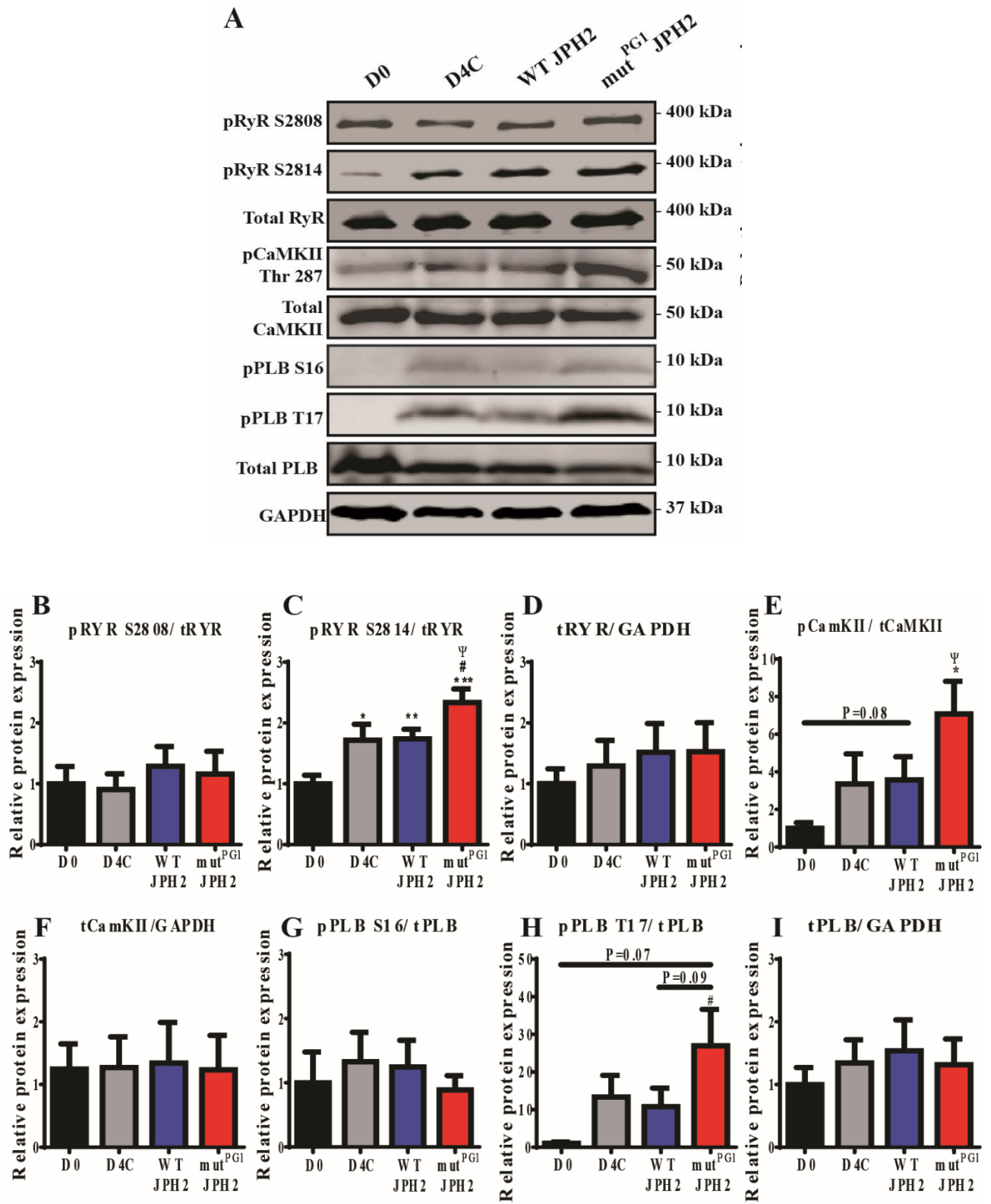


Figure 23. Global effect of WT-JPH2 and mut^{PG1}JPH2 overexpression on Ca²⁺ handling proteins. [A] Representative Western blot of EC coupling and Ca²⁺ handling proteins: RyR

(basal and phosphorylated states), PLB (total and phosphorylated states) and CaMKII (basal and phosphorylated states). Whole-cell lysates from freshly isolated AFVMs (D0), control cultured AFVMs for 4 days (D4C), Ad-WT-JPH2 or Ad-mut^{PG1}JPH2 overexpressed AFVMs 4 days in culture were tested for protein expression levels. **[B-I]** Average quantified values expressed relative to D0 AFVMs. Tested protein levels were normalized to GAPDH loading control. Phosphorylated protein expression was normalized to total protein expression. N=3-5 experiments. ***/****P<0.05/0.01/0.001 vs. D0, ###/#### P<0.05/0.01/0.001 vs. D4C and ^{Ψ/ΨΨ/ΨΨΨ} P<0.05/0.01/0.001 vs. D4-WT-JPH2.

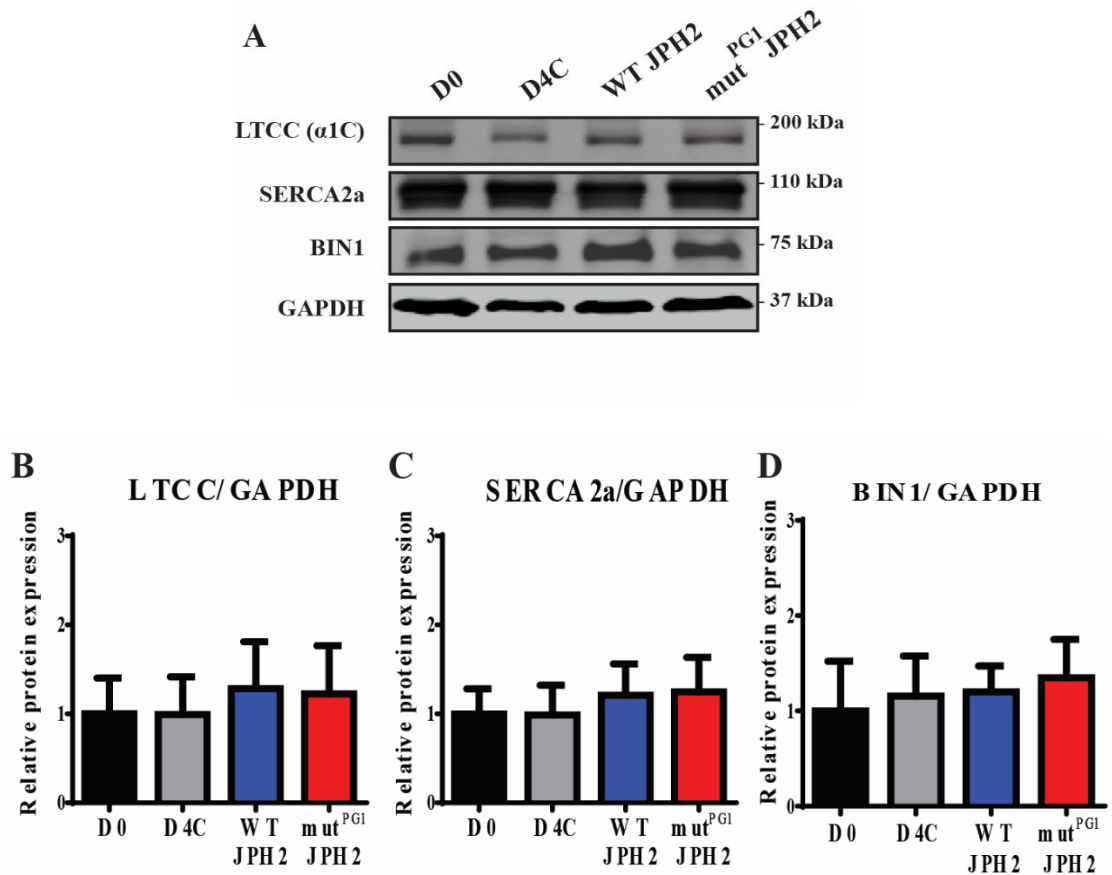


Figure 24. Effect of mut^{PG1}JPH2 on expression of EC coupling proteins. [A]

Representative Western blot of EC coupling and Ca²⁺ handling proteins: LTCC, SERCA2a

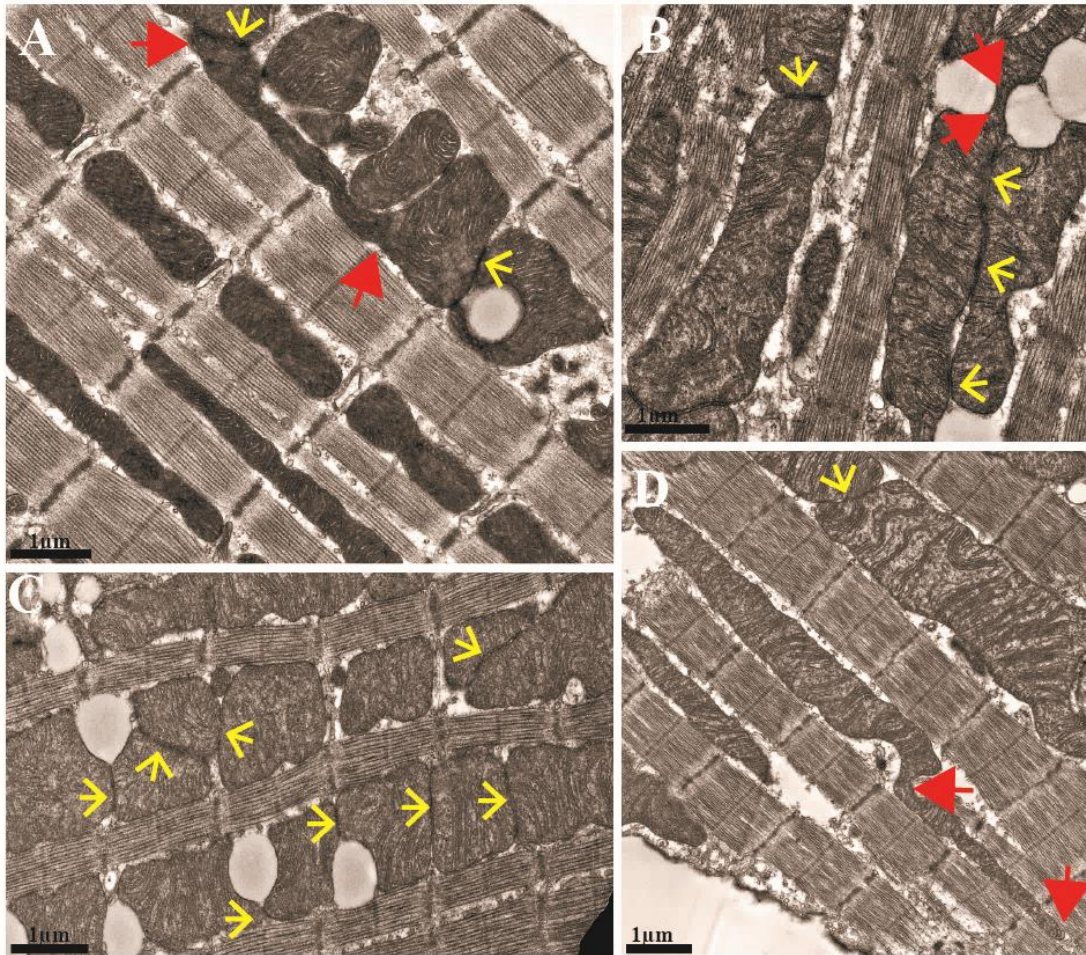
and BIN1. Whole-cell lysates from freshly isolated AFVMs (D0), control cultured AFVMs for 4 days (D4C), Ad-WT-JPH2 or Ad-mut^{PG1}JPH2 overexpressed AFVMs 4 days in culture were tested for protein expression levels. **[B-D]** Average quantified values expressed relative to D0 AFVMs. Tested protein levels were normalized to GAPDH loading control. Phosphorylated protein expression was normalized to total protein expression. N=3-5 experiments.

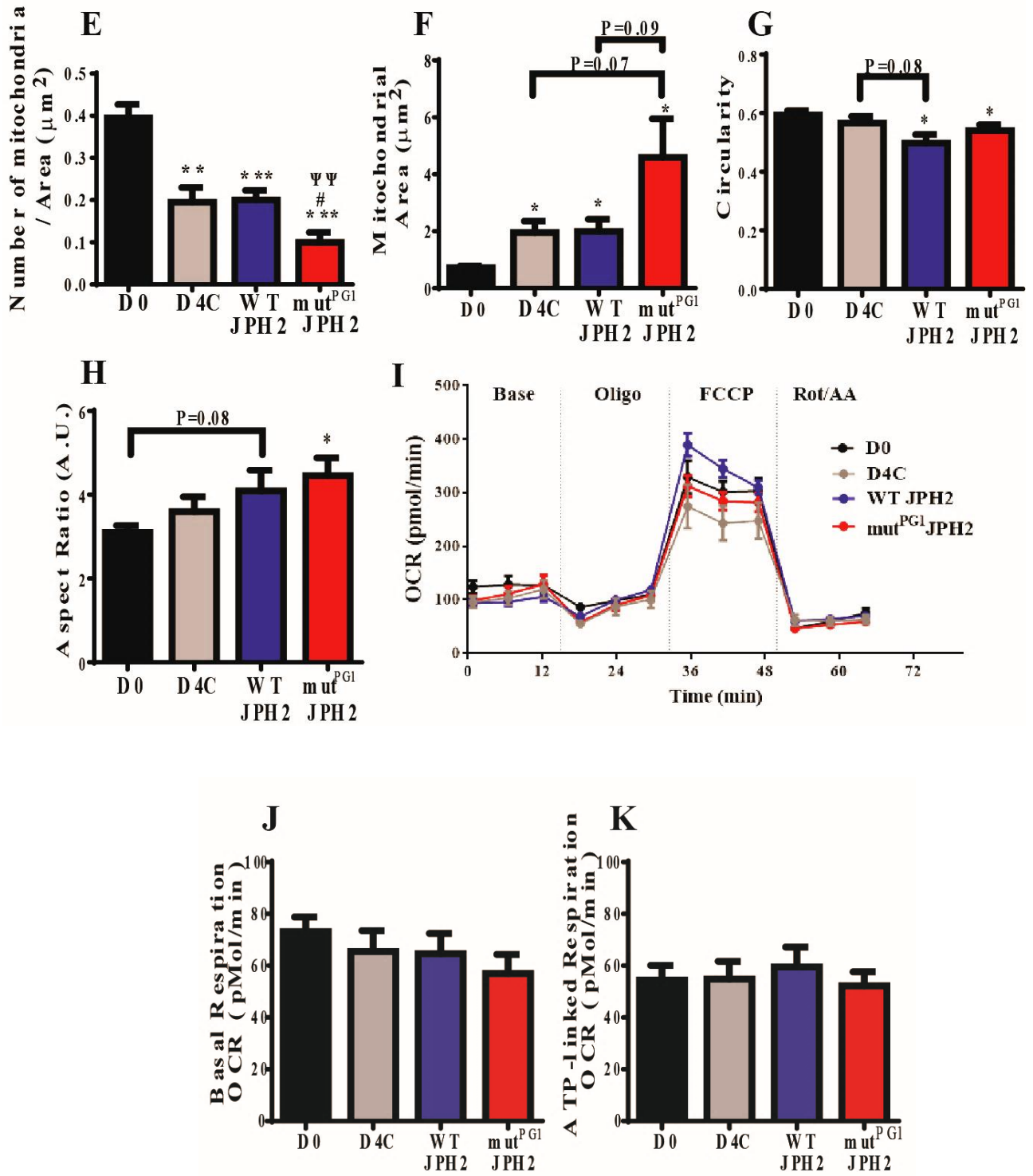
Cardiomyocyte overexpression of WT and mut^{PG1} JPH2 alter mitochondrial morphogenesis and bioenergetics

Disruption of Ca²⁺ homeostasis is a stress trigger that can affect the energetic balance of the cell, primarily through the alteration of mitochondrial structure and function. We observed modified mitochondrial ultrastructure in myocytes overexpressing WT-JPH2 and mut^{PG1}JPH2. Using transmission electron microscopy, healthy D0 myocytes were visualized with cylindrical shaped mitochondria with rounded edges (and few round-shape mitochondria) that were highly organized in longitudinal rows (Figure 25A and Figure 9L.1). Remodeling of cardiomyocytes in cell culture resulted in a significant reduction of mitochondria number, accompanied by enhanced shape variability (Figure 25B, 25E and Figure 9L.2). Overall, the average mitochondrial surface area was increased in D4C myocytes (Figure 25F). These changes occurred inclusively also in WT-JPH2 overexpressing myocytes, with a reduction in mitochondrial circularity and increased aspect ratio (Figure 25C, Figure 9L.3 and Figures 25G-H). mut^{PG1}JPH2 overexpressing myocytes exhibited a significant reduction in mitochondrial number (Figure 25E) compared to all other conditions. In addition, the mitochondria in these cells appeared more tubular and were 2-fold larger than mitochondria in D4C or WT-JPH2 myocytes (Figures

25D, 25F and Figure 9L.4), suggesting that these mitochondria sense intracellular changes occurring in mut^{PG1}JPH2 cells and undergo morphological adaptation. In freshly isolated myocytes, the mitochondrial distribution is mostly spacious with occasional events of physical contacts between two adjacent mitochondria, termed as “kissing” junctions [156, 157], which were also present in D4C and mut^{PG1}JPH2 myocytes. However, WT-JPH2 myocytes demonstrated significantly increased frequency of “kissing” junctions (Table 2 and Figure 25A-D indicated in yellow arrows), indicating coordinated communication through structural associations. Other conserved structures known as mitochondrial nanotunnels [157, 158] were detected in electron microscopy images. Nanotunnels were positively identified if they clearly contained the outer and inner mitochondrial membranes along with a continuation of mitochondrial matrix and cristae. We quantified the frequency of short distance nanotunnels (<1 μ m) and long distance nanotunnels (\geq 1 μ m) (Figure 25B and Figure 25A, respectively – indicated between red arrows), and found that nanotunnels are relatively rare events occurring in D0 myocytes (Table 2). In comparison to D0 myocytes, D4C and WT-JPH2 myocytes showed a higher abundance of nanotunnel structures, with a strong tendency towards short length nanotunnels. Conversely, mut^{PG1}JPH2 myocytes showed significantly increased frequency in long distance nanotunnels and similar frequency in short distance nanotunnels with respect to all other groups (Table 1 and Figure 25D – between red arrows). To address whether these morphological modifications affect mitochondrial bioenergetics, we measured oxygen consumption rate (OCR) via a Seahorse analyzer (Figure 25I). No differences were found in basal respiration, ATP linked respiration and proton leak (Figure 25J, 25K and 25N, respectively). Notably, we found elevated maximal respiration and increased spare capacity in WT-JPH2 overexpressed myocytes (Figures 25L and 25M, respectively),

suggesting that these myocytes could produce more ATP and better sustain stress than D0 and D4C myocytes. Overexpression of mut^{PG1}JPH2 abrogated this mitochondrial capability to preserve bioenergetics achieved by WT JPN2 overexpression in myocytes. Nonetheless, mut^{PG1}JPH2 myocytes could still sustain maximal respiration, and maintain normal mitochondrial spare capacity similarly to freshly isolated myocytes or D4C myocytes (Figure 25L-M).





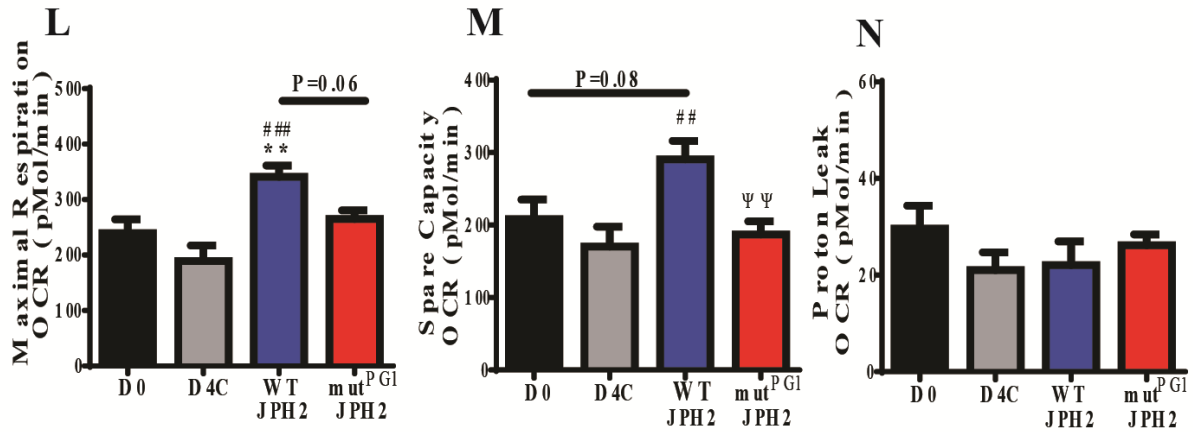


Figure 25. Global effect of WT-JPH2 and mut^{PG1}JPH2 overexpression on mitochondrial

disposition, morphogenesis and bioenergetics in AFVMs. Ultrastructure of cardiac

mitochondria in [A] D0 cardiomyocytes, [B] D4C cardiomyocytes, [C] WT-JPH2

overexpressed cardiomyocytes and [D] mut^{PG1}JPH2 overexpressed cardiomyocytes.

Physical contact between two adjacent mitochondria termed as “kissing events” is

indicated via yellow arrows. Sites of longitudinally oriented nanotunnels are indicated

between the red arrows. Long distance nanotunnel shown in D0 myocyte has length of

2.6µm and diameter of 194nm. Short distance nanotunnel represented in D4C myocyte has

length of 567nm and diameter of 0.121nm. Long distance nanotunnel indicated in

mut^{PG1}JPH2 myocytes has length of 4.05µm and diameter of 306nm. [E] Quantification of

number of mitochondria per cellular area. [F] Measurement of mitochondrial area. [G]

Quantification of mitochondrial shape including circularity and [H] aspect ratio. [I]

Seahorse analysis of mitochondrial oxygen consumption rates (OCR) in AFVMs. [J] Basal

OCR. [K] ATP-linked respiration after addition of ATP synthase inhibitor, oligomycin.

[L] Maximal respiration after addition of protonophore, FCCP. [M] Spare respiratory capacity (max – basal). [N] Proton leak (post-oligomycin OCR – non-mitochondrial OCR).

n = 13–20 per condition. */**/**P<0.05/0.01/0.001 vs. D0, ###/### P<0.05/0.01/0.001

vs. D4C and $\Psi/\Psi\Psi/\Psi\Psi\Psi$ P<0.05/0.01/0.001 vs. WT-JPH2.

Table 2. Frequency of mitochondrial disposition and nanotunnel structure

Samples	Frequency of mitochondrial “kissing” junctions (#events / #mito) (mean ± SEM)	Frequency of short distance (<1µm) nanotunnels (#tunnels / #mito) (mean ± SEM)	Frequency of long distance (≥1µm) nanotunnels (#tunnels / #mito) (mean ± SEM)	Total frequency of nanotunnels (#tunnels / #mito) (mean ± SEM)
D0	0.26 ± 0.07	0.07 ± 0.01	0.020 ± 0.004 ^{¥¥}	0.09 ± 0.02
D4C	0.25 ± 0.06	0.16 ± 0.03 [*]	0.08 ± 0.02 ^{**} , [¥]	0.24 ± 0.03 ^{**}
WT-JPH2	0.52 ± 0.07 ^{*, #}	0.20 ± 0.05 [*]	0.08 ± 0.02 [*] , [¥]	0.29 ± 0.04 ^{**}
Mut ^{PG1} JPH2	0.32 ± 0.04 ^Ψ	0.19 ± 0.04 [*]	0.16 ± 0.02 ^{***} , ^{#, Ψ}	0.36 ± 0.05 ^{**}

*/**/**P<0.05/0.01/0.001 versus D0, Student t test

###/### P<0.05/0.01/0.001 versus D4C, Student t test

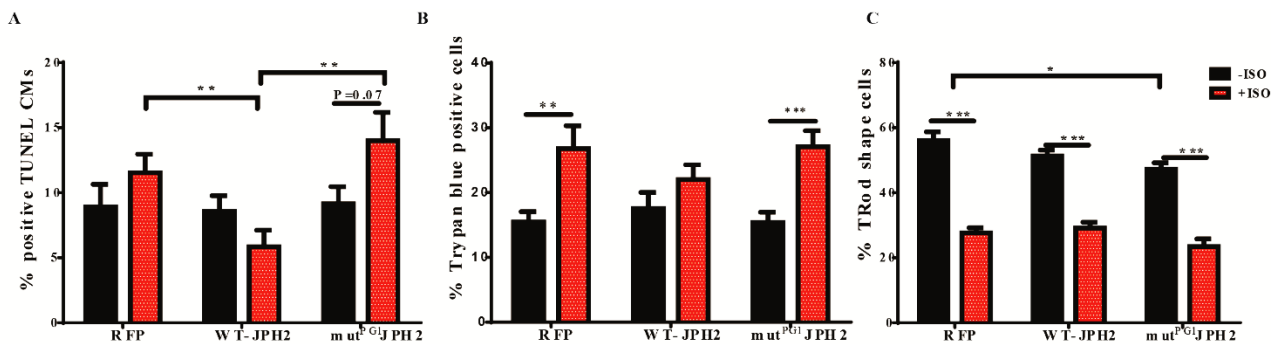
$\Psi/\Psi\Psi/\Psi\Psi\Psi$ P<0.05/0.01/0.001 versus WT-JPH2, Student t test

^{¥/ ¥¥/ ¥¥¥} P<0.05/0.01/0.001 versus short distance nanotunnels in the same tested group, Student t test

n= 5-7 images per group, >280 mitochondria analyzed in each group

Cardiomyocyte overexpression of mut^{PG1} JPH2 does not exacerbate cell death after Iso stimulation

Cell death due to Ca²⁺ overload can occur by either necrosis, apoptosis, or autophagy. We examined the effect of mut^{PG1}JPH2 overexpression on programmed cell death (apoptosis) using terminal deoxynucleotidyl transferase-mediated deoxyuridine triphosphate nick-end labeling (TUNEL) assay. Our data indicated that 10μM Iso for 48 hours did not induce significant apoptosis in RFP control or WT-JPH overexpressing myocytes (Figure 26A). In mut^{PG1}JPH2, we identified an increased trend of apoptosis that was significantly higher than WT-JPH2 overexpressing myocytes, but not different than RFP control myocytes. Evaluation of cell death by necrosis, which was performed by staining myocytes with disrupted membrane (typical after necrosis) via Trypan blue, demonstrated no significant differences in cell death percentage after Iso treatment between the groups (Figure 26B). Quantification of rod shape myocytes, as an indication for myocytes with health structure, showed the Iso treatment reduced the percentage of rod shape cell equally in all groups (Figure 26C). We also quantified percentage of viable myocytes that did not uptake Trypan blue but lost their rod shape morphology. Our data indicate that mut^{PG1}JPH2 significantly induced irregular myocyte shape at baseline, which was exacerbated with 10μM Iso treatment. Overall, mut^{PG1}JPH2 did not promote increase in cell death via apoptosis or necrosis.



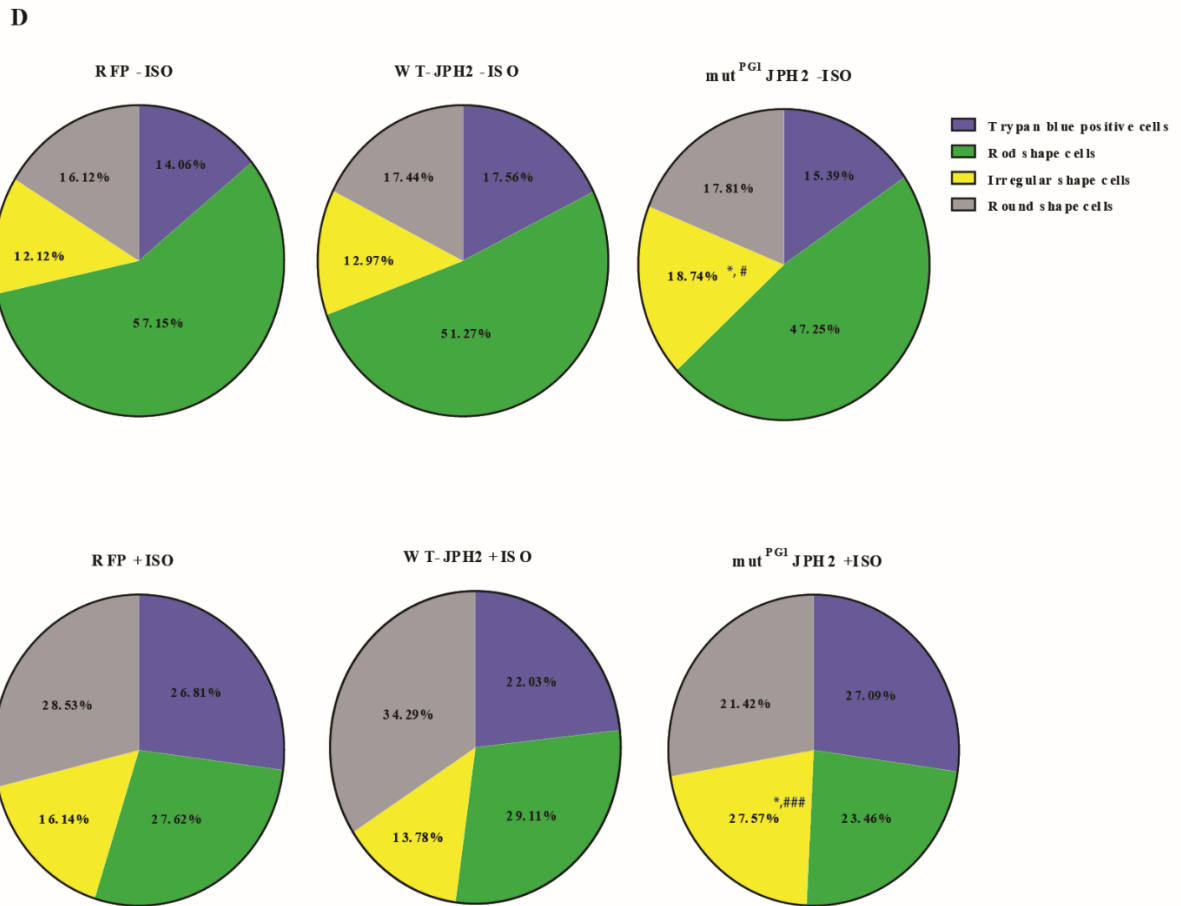


Figure 26. *mutPGL1JPH2* does not exacerbated cell death after Iso. [A] Percentage of TUNEL positive cardiomyocytes. [B] Percentage of Trypan blue positive cardiomyocytes. [C] Percentage of rod shape myocytes. N= 3 isolations. At least 15 images were analyzed for TUNEL and Trypan blue staining analysis. ^{*}/^{**}/^{***}/^{****}P<0.05/0.01/0.001. [D] Segmentation of viable rod shaped myocytes versus viable irregular myocytes, or round shaped myocytes that were compared to dead myocytes with a positive staining for Trypan blue. ^{*}/^{**}/^{***}/^{****}P<0.05/0.01/0.001 vs. RFP control, [#]/^{##}/^{###}/^{####} P<0.05/0.01/0.001 vs. WT-JPH2.

Discussion

JPH2 is a structural protein required for T-tubule maturation and cardiac dyad stabilization [159]. The LTCC has been shown to interact with JPH2 in skeletal muscle[110, 111]. The present work shows that LTCC interacts with the Joining region in JPH2 in cardiomyocytes, and this interaction is crucial for the recruitment of LTCC to T-tubules, assembly of cardiac dyads and regulation of EC coupling.

Alteration of JPH2 abundance elicits LTCC disposition during cardiomyocyte remodeling

Murine and human studies have shown that disturbance in JPH2 expression in the heart contributes to the progression of cardiac pathology[102, 123]. In accordance with these studies, the present experiments showed that in a large mammalian animal model with compensated LVH had reduced abundance of JPH2 in the cardiomyocytes PMs. Usually, compensated cardiac hypertrophy precedes HF and establishes the earliest molecular processes leading to cardiomyocyte remodeling[46, 102]. Our findings indicate that these early pathological changes *in vivo* include redistribution of JPH2 across the cardiomyocyte PM with modification of JPH2 localization and formation of aggregates. The nature of these aggregates remains unclear, yet we speculate that they could be linked to either JPH2 degradation or JPH2 turnover. In parallel, we also detected LTCC $\alpha 1C$ and $\beta 2a$ redistribution across the PM as part of the cardiac hypertrophic remodeling. Interestingly, LVH promoted reduction in the JPH2: LTCC $\alpha 1C$ subunit expression ratio in the PM, suggesting that if JPH2 clusters with LTCC, the incidence of such clustering is downregulated in cardiac hypertrophy. Our *in vitro* model utilized isolated AFVMs after establishing a clear phenotypic link between LVH *in vivo* and cardiomyocyte remodeling

in culture. A strong advantage of using a primary culture of adult cardiomyocytes when studying cellular remodeling of cardiac disease is the similarity in morphology and behavior of cultured myocytes to those myocytes in intact diseased heart, especially in the case of AFVMs that recapitulate human cardiac electrophysiological properties[146, 160]. Similarly to previous observations in intact hypertrophic heart[46], T-tubular network was found to be downregulated and disorganized in D4C AFVMs compared to freshly isolated AFVMs. These findings went hand in hand with reduced JPH2 density and integrity in cultured AFVMs. Considering that a high concentration of LTCCs is in T-tubules[13], our data suggest that T-tubule degradation in cultured AFVMs induced LTCC mobilization out of T-tubules. This idea was validated by isopycnic ultracentrifugation studies that showed LTCC redistribution across the PM in cultured myocytes, which also depicted redistribution of JPH2. Altogether, our findings raised the question whether altered expression of JPH2 and LTCC during cardiac remodeling occurred independently or interdependently due to a direct association between JPH2 and LTCC.

The role of the Joining region in JPH2

Understanding the role of the Joining region in JPH2 was required for our assessment of the potential LTCC-JPH2 interaction in the heart. The Joining region is located between two MORN motifs that are closely associated with the PM membrane of T-tubules, making it an appealing domain that could potentially interact with LTCC. Previously it was described that JPH2 interacted with the C-terminus of LTCC in skeletal muscle[111]. In another study, a region encompassing 216-399 amino acids in JPH2 was truncated, leading to disruption of JPH2-LTCC interaction in the triad[110]. The Joining region in JPH2 coincides in 143-284 amino acids, therefore, we adopted a meticulous approach of

Adenoviral overexpression in AFVMs with mut^{PG1}JPH2, which aimed to preserve the length of JPH2 and all its remaining domains, while mutating several charged/polar amino acids that are presumably involved in protein-protein interaction with LTCC. Comparison of mut^{PG1}JPH2 secondary and tertiary structures against WT-JPH2 validated that any steric shift introduced by the mutagenesis was explicitly taking place in the Joining region. Overexpressing WT-JPH2 and mut^{PG1}JPH2 in cultured myocytes revealed distinct effects on JPH2 spatial localization, density and integrity (Figure 9E-K). While overexpressing WT-JPH2 restored the missing JPH2 across the cultured cardiomyocyte, overexpressing mut^{PG1}JPH2 resulted in strong predilection of JPH2 to localize towards the sarcolemma, renouncing the mid-cardiomyocyte sections absent of JPH2. This manifestation had a robust impact on the composition of T-tubule system, dyad frequency and overall cardiomyocyte architecture. Our qualitative and quantitative characterization of T-tubule structure showed that overexpressing WT-JPH2 in cultured cardiomyocytes restored T-tubules that were degraded in culture conditions. However, overexpressing mut^{PG1}JPH2 exaggerated the remodeling of the gross T-tubule network, raising the concern of the electrical stability in these cardiomyocytes. Data from our study show that WT-JPH2 overexpression in myocytes caused an increase in dyad size and frequency in accordance with previously published work[115]. Nevertheless, the frequency of dyads was profoundly reduced in mut^{PG1}JPH2 overexpressing myocytes (Figure 9L and 14), without altering the expression levels of Ca²⁺ handling proteins (Figure 24 and Figure 23). These findings were quite puzzling because the mut^{PG1}JPH2 construct contained normal MORN motifs on the N-terminus enabling regular interaction with T-tubules, and intact transmembranal domain on the C-terminus, which is responsible for docking JPH2 to the jSR membrane. These domains are essentially responsible for stabilizing the dyad by

bringing closer the junctional complex between T-tubules and jSR. We conclude that the mutating the Joining region solely was sufficient to induce a robust effect on degradation of cardiac dyads and overall myofilament disorganization. This discovery supports the idea that the JPH2 Joining region is necessary for stabilization of T-tubules and assembly of cardiac dyads.

The Joining region in JPH2 interacts with LTCC

In the current study, we explored the hypothesis that LTCC interacts with the Joining region in JPH2. Co-IP and PLA studies indicated that mut^{PG1}JPH2 reduced the protein-protein interaction specifically between LTCC α 1C and JPH2 by ~40% (Figure 15A-C). Overexpressing mut^{PG1}JPH2 decreased the co-localization between JPH2 and LTCC, and between LTCC and RyR that would normally occur in the cardiac dyads. Given that dyads are more abundant in the T-tubules rather than in the sarcolemma (75% vs. 25%, respectively)[33, 81], our results strongly suggest that mut^{PG1}JPH2 blocked JPH2-LTCC interactions in the dyads. PLA substantiated that the remaining unblocked JPH2-LTCC interactions appeared at the periphery of the cardiomyocyte. One possible explanation is that the Joining region in JPH2 recruits LTCC to the T-tubules, but in the absence of T-tubules, JPH2 and LTCCs eventually translocate to the sarcolemma. Sucrose density gradient of purified PM corroborated these data by showing that mut^{PG1}JPH2 overexpression in myocytes induced JPH2 and LTCC redistribution across the PM (Figure 15D). An additional explanation is that LTCC is undergoing turnover that promotes channel reservoirs just underneath the PM. Such reservoirs were previously observed with Connexin-43 channels that could buffer the channel's density in response to stressful conditions[161]. Although mut^{PG1}JPH2 overexpression induced only ~40% reduction in

JPH2-LTCC interaction, we predicted that the subsequent effect on CICR would be actually significant. The reason is that LTCC:RyR ratio in the dyad is ~1:10[54], indicating that LTCC is an “amplifying switch” that initiates CICR. With LTCCs being redistributed across the PM and in the absence of T-tubules, we expected to see reduced efficiency of EC coupling. Indeed, previous studies showed that relocation of $I_{Ca,L}$ away from the t-tubules occurs in HF [87]. Reversing the heart into an immature phenotype is commonly observed in pathological remodeling associated with HF. This usually includes reactivation of fetal gene expression and lack of T-tubules[87, 162]. Just like in HF, the embryonic heart lacks T-tubules, which mature only at the neonatal stage. Interestingly, the heart manages to sustain a contractile force at the expense of inefficient EC coupling[13]. mut^{PG1} JPH2 overexpressing myocytes reversed into an immature cardiac phenotype similarly to immature and failing cardiomyocytes. Previously, it was established that JPH2 has a central role in the formation and stabilization of T-tubule[114, 159]. Since the mutagenesis of the Joining region in JPH2 disrupted the interaction with LTCC and induced downregulation of T-tubules, we examined if overexpression of only WT-JPH2 was sufficient to preserve the T-tubule network. The present experiments showed that when myocytes were treated with shRNA to silence LTCC ($\alpha 1C$) expression in combination with WT-JPH2 overexpression (Figure 18), there was no sustained preservation of T-tubules. These studies strongly suggest that a direct association between LTCC and the Joining region in JPH2 is necessary for LTCC recruitment to the T-tubules to enable T-tubular stabilization and assembly of cardiac dyads.

Interaction between The Joining region in JPH2 and LTCC is important for efficient EC coupling

Remodeling of T-tubules is a pivotal determinant of inefficient EC coupling in cardiomyocytes. Despite exhibiting structural abnormalities, mut^{PG1}JPH2 overexpressing myocytes had normal basal cytosolic Ca²⁺ transients. However, these cells developed abnormal pro-arrhythmic Ca²⁺ waves after exposure to β -adrenergic stimulation (Figure 19). These behaviors are similar to those in a clinical syndrome of catecholaminergic polymorphic ventricular tachycardia (CPVT), where patients develop arrhythmias in response to physical activity or emotional stress[163]. Interestingly, human studies identified two mutations in the JPH2 Joining region: E169K leading to atrial fibrillation[121] and S165F leading to hypertrophic cardiomyopathy[123]. Collectively, these reports and our data accentuate that the Joining region is an important domain involved JPH2 tight regulation of CICR. Our current work proposes a novel mechanism by which mutations in the Joining region disrupt the interaction between LTCC and JPH2, leading to the displacement of LTCC away from the T-tubules.

The amplitude of average Ca²⁺ transient in mut^{PG1}JPH2 myocytes had smaller responses to Iso (Figure 19C), indicating either lack of I_{Ca} trigger, or unresponsive SR Ca²⁺ load in response to Iso[150]. Poorly organized dyads and loss of T-tubules in mut^{PG1}JPH2 myocytes, promote physical loss of Ca²⁺ release units (couplons)[39, 127]. This explains our observation of reduced synchrony of Ca²⁺ release from couplons at baseline and after Iso stimulation. Our data also illustrated that mut^{PG1}JPH2 overexpressing myocytes had non-linear Ca²⁺ cycling dynamics with spontaneous Ca²⁺ releases and alternans, which are known precursors of lethal arrhythmia[164]. Based on our observations (Figure 19H, K-L),

we classified two types of alternans in mut^{PG1}JPH2 myocytes after Iso exposure. The first was delayed afterdepolarization-induced triggered activity (DAD), involving “leaky” RyR, which usually becomes deleterious during catecholamine stimulation[97]. DADs occurred in mut^{PG1}JPH2 myocytes as asynchronous Ca²⁺ release appearing right after normal Ca²⁺ wave. The underlying mechanism involves spontaneous Ca²⁺ release from an SR overloaded with Ca²⁺. The second type of alternans was early afterdepolarization (EAD), which is typically developed due to I_{Ca,L} during the late plateau phase of action-potential[97]. EADs induced Ca²⁺ release at the edges of mut^{PG1}JPH2 cell without being able to propagate to the center of the cell. This commonly occurs in myocytes lacking T-tubules. We conclude that lack of T-tubules in mut^{PG1}JPH2 myocytes increased the risk to develop Ca²⁺ alternans. DADs and EAD reflect defective EC coupling with obvious disruption of Ca²⁺ homeostasis. We distinguished between the effect mut^{PG1}JPH2 had during Iso stimulation on I_{Ca} trigger and SR Ca²⁺ release. Clearly, Iso caused a significant increase in I_{Ca,L} (Figure 21A-B), suggesting that dispositioning LTCC away from the T-tubules did not alter their responsiveness to PKA-mediated phosphorylation. However, a positive shift in the voltage dependence of I_{Ca,L} activation in mut^{PG1}JPH2 myocytes was detected at baseline and after Iso stimulation (Figure 21C-D), which may indicate abnormal voltage regulation in LTCC. Using super-resolution patch-clamp, we found compelling evidence that LTCCs in mut^{PG1}JPH2 myocytes translocate from T-tubules to the crest, where they remain functional (Figure 21E-G). Changes in LTCC microdomain location were previously observed in HF[87] and in triggered ventricular arrhythmia[47]. The mechanism that drives LTCCs redistribution in pathological remodeling is not fully understood. We show that this process can be associated with disruption of LTCC-JPH2 interaction. Altogether, lack of T-tubules, reduced the frequency of dyads and relocation

of LTCC to the crest in $\text{mut}^{\text{PG1}}\text{JPH2}$ myocytes produce inefficient LTCC coupling to RyR, resulting in “orphaned” RyRs[64] and reduced SR content release (Figure 27). Indeed, SR Ca^{2+} release in $\text{mut}^{\text{PG1}}\text{JPH2}$ myocytes was not elevated in response to Iso (Figure 21H-I), indicating defective Ca^{2+} regulation by the SR.

JPH2 Joining region contributes to intracellular Ca^{2+} stability and energy balance in cardiomyocyte

Cardiac dyads are compartmentalized Ca^{2+} microsignaling domains in which EC coupling controls the amount of Ca^{2+} triggering CICR. In addition to activation of the contractile machinery, Ca^{2+} also regulates many signaling processes in the cardiomyocyte, including cell bioenergetics and stress response. Our data showed that $\text{mut}^{\text{PG1}}\text{JPH2}$ overexpressing AFVMs had irregular Ca^{2+} dynamics, affecting cellular Ca^{2+} -dependent regulation through activation of CaMKII – a known major Ca^{2+} dependent mediator in cardiomyocytes (Figure 23A, E). Enhanced CaMKII activation is usually linked to many cardiac pathologies including EADs and DADs arrhythmias, cardiomyopathy and HF[47, 62, 165]. We also found enhanced phosphorylation of RYR S2814 (Figure 23A, C), which is a known downstream CaMKII target reportedly linked to “leaky” RyR and spontaneous SR Ca^{2+} release [62, 73].

Our study also identified a link between overexpression of WT-JPH2 and $\text{mut}^{\text{PG1}}\text{JPH2}$ in AFVMs and cardiomyocyte bioenergetics. The link between mitochondrial function and beat-to-beat cytosolic Ca^{2+} is established by the mitochondrial capacity to buffer cytosolic Ca^{2+} , to sense energetic cellular demand, and to activate Ca^{2+} dependent mitochondrial key enzymes participating in oxidative phosphorylation and ATP synthesis[53, 58]. Regardless of the mechanism by which mitochondria responds within to

overexpression of WT-JPH2 or mut^{PG1}JPH2, if by changing mitochondrial Ca²⁺ uptake or by altering mitochondrial enzymes, the differences we observed in mitochondrial morphogenesis and function are most likely linked to mitochondrial ability to sense global cytosolic Ca²⁺ cycling. We observed a high frequency of tight junctions between mitochondria in WT-JPH2 overexpressing myocytes, followed by increased spare capacity and increased maximal respiration (Figures 25C, L, M). This communication form between adjacent mitochondria has been previously described to enable mitochondrial content exchange [156, 158]. Assuming that cell remodeling in culture is an energetically costly process, this type of mitochondrial communication may be bioenergetically protective because mitochondria in WT-JPH2 myocytes *in vitro* store excessive energy on demand. Parallel *in vivo* studies also showed that cardiac overexpression of JPH2 provided protective effect after pressure overload[115], although the mitochondrial function in these hearts was not explored. In mut^{PG1}JPH2 overexpressing AFVMs, we found a different form of mitochondrial communication network – through long-distance nanotunnels. Similarly, it was found that RyR2A4860G^{+/-} cardiomyocytes had increased incidence of long-distance nanotunnels, and surprisingly, the intermitochondrial matrix exchange rate via these nanotunnels was much slower[157]. It is considered that such mitochondrial communicating structures are ‘reaching out for help’[158]. Indeed, we observed an exclusive stressful cellular environment in mut^{PG1}JPH2 myocytes linked to the imbalance of Ca²⁺, myofilament disorganization and loss of T-tubules. A possible explanation is that mitochondria sense these abnormal cellular conditions and form contact with distant mitochondria to keep the ATP production. This can also explain the increase in mitochondria size and shape change (Figure 25F-H), and the possible reason for not detecting increased cell death rate via apoptosis or necrosis (Figure 26). Therefore, we

postulate that the basal respiration, ATP-linked respiration, maximal respiration and spare capacity are preserved in mut^{PG1}JPH2 myocytes, despite of remarkable reduction in mitochondria number (Figure 25E). We cannot entirely exclude mitochondrial fission/fusion processes, which are not the focus of this study but can be an interest for future studies.

In summary, this study demonstrates that LTCC α 1C subunit interacts with the Joining region in JPH2 in cardiomyocyte PM. Disruption of this interaction by mutagenesis in the Joining region led to significant structural alterations of the cardiac dyads and loss of T-tubules, followed by reduced EC coupling and imbalance of Ca²⁺-dependent cellular processes (Figure 27).

Future directions

While the current thesis theme sets extensive experimental data on *in vitro* effects of mut^{PG1}JPH2 in cultured adult ventricular cardiomyocytes, a detailed examination of mut^{PG1}JPH2 in *in vivo* model may aid to evaluate further the mechanism of LTCC and JPH2 interaction in the heart. Specifically, we propose sets of experiments, in which mut^{PG1}JPH2 will be delivered to a mouse heart using Adeno-associated virus. The cardiac function will be assessed to determine the induced effects of LTCC-JPH2 interaction disruption in a healthy heart. Alternatively, we propose a generation of cardiac-specific transgenic mouse model carrying the mut^{PG1}JPH2 transgene to evaluate if this protein-protein interaction is essential for T-tubule formation during cardiac development. It will be important to assess if the mutations at the Joining region of JPH2 predispose the mouse model to cardiomyopathies. Lastly, we would consider applying CRISPR-Cas9 technology to rescue any developing phenotype of mut^{PG1}JPH2 *in vivo* model. We hope that our future

experiments will aid to identify the pathogenesis and potential translational therapeutic approaches for patients developing arrhythmias and cardiomyopathies due to mutations in the joining region of JPH2.

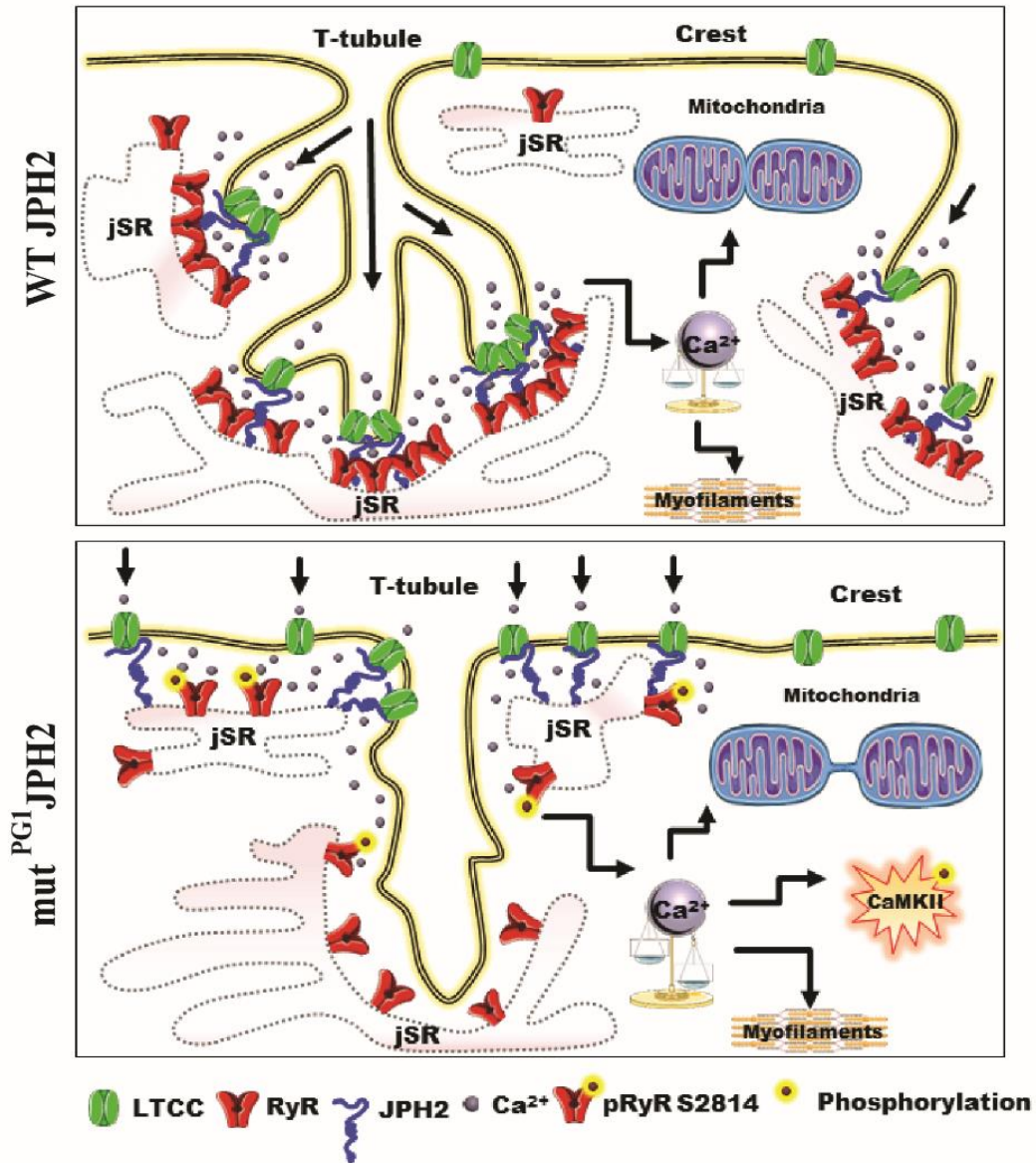


Figure 27. Representative illustration of the LTCC-JPH2 interaction via the Joining region in cardiomyocyte. [Top] In WT-JPH2 overexpressing cardiomyocytes, LTCCs are recruited to the T-tubules and interact with the Joining region in JPH2. LTCCs are localized in spatial proximity to the juxtaposed RyRs forming a dyad complex an enabling efficient

EC coupling. These myocytes exhibit balanced Ca^{2+} dynamics and tight junctions between mitochondria. **[Bottom]** In $\text{mut}^{\text{PG1}}\text{JPH2}$ overexpressing cardiomyocytes, there are degraded T-tubular network and fewer dyads. LTCCs translocate to the crest, leaving “orphaned” RyRs at the jSR. LTCCs have reduced interaction with JPH2, whereas the remaining LTCC-JPH2 interactions take place at the crest. Ca^{2+} dynamics in these myocytes is imbalanced and mitochondria seem to communicate through long-distance tunnels.

REFERENCES CITED

1. Braunwald E: **Heart failure**. *JACC Heart failure* 2013, **1**(1):1-20.
2. Benjamin EJ, Muntner P, Alonso A, Bittencourt MS, Callaway CW, Carson AP, Chamberlain AM, Chang AR, Cheng S, Das SR *et al*: **Heart Disease and Stroke Statistics-2019 Update: A Report From the American Heart Association**. *Circulation* 2019, **139**(10):e56-e528.
3. Lips DJ, deWindt LJ, van Kraaij DJ, Doevendans PA: **Molecular determinants of myocardial hypertrophy and failure: alternative pathways for beneficial and maladaptive hypertrophy**. *European heart journal* 2003, **24**(10):883-896.
4. Heineke J, Molkentin JD: **Regulation of cardiac hypertrophy by intracellular signalling pathways**. *Nature reviews Molecular cell biology* 2006, **7**(8):589-600.
5. Maillet M, van Berlo JH, Molkentin JD: **Molecular basis of physiological heart growth: fundamental concepts and new players**. *Nature reviews Molecular cell biology* 2013, **14**(1):38-48.
6. Berenji K, Drazner MH, Rothermel BA, Hill JA: **Does load-induced ventricular hypertrophy progress to systolic heart failure?** *American journal of physiology Heart and circulatory physiology* 2005, **289**(1):H8-H16.
7. Bui AL, Horwich TB, Fonarow GC: **Epidemiology and risk profile of heart failure**. *Nature reviews Cardiology* 2011, **8**(1):30-41.
8. Azevedo PS, Polegato BF, Minicucci MF, Paiva SA, Zornoff LA: **Cardiac Remodeling: Concepts, Clinical Impact, Pathophysiological Mechanisms and Pharmacologic Treatment**. *Arquivos brasileiros de cardiologia* 2016, **106**(1):62-69.

9. Kaye DM, Krum H: **Drug discovery for heart failure: a new era or the end of the pipeline?** *Nature reviews Drug discovery* 2007, **6**(2):127-139.
10. Klein L, O'Connor CM, Gattis WA, Zampino M, de Luca L, Vitarelli A, Fedele F, Gheorghiade M: **Pharmacologic therapy for patients with chronic heart failure and reduced systolic function: review of trials and practical considerations.** *The American journal of cardiology* 2003, **91**(9A):18F-40F.
11. Huxley AF: **The activation of striated muscle and its mechanical response.** *Proceedings of the Royal Society of London Series B, Biological sciences* 1971, **178**(1050):1-27.
12. Huxley AF, Taylor RE: **Function of Krause's membrane.** *Nature* 1955, **176**(4492):1068.
13. Hong T, Shaw RM: **Cardiac T-Tubule Microanatomy and Function.** *Physiological reviews* 2017, **97**(1):227-252.
14. Pinali C, Malik N, Davenport JB, Allan LJ, Murfitt L, Iqbal MM, Boyett MR, Wright EJ, Walker R, Zhang Y *et al*: **Post-Myocardial Infarction T-tubules Form Enlarged Branched Structures With Dysregulation of Junctophilin-2 and Bridging Integrator 1 (BIN-1).** *Journal of the American Heart Association* 2017, **6**(5).
15. Brette F, Orchard C: **T-tubule function in mammalian cardiac myocytes.** *Circulation research* 2003, **92**(11):1182-1192.
16. Katz AM: **Physiology of the Heart.** Philadelphia: Lippincott Williams and Wilkins; 2011.

17. Soeller C, Cannell MB: **Examination of the transverse tubular system in living cardiac rat myocytes by 2-photon microscopy and digital image-processing techniques.** *Circulation research* 1999, **84**(3):266-275.
18. Kohl T, Lehnart SE: **Imaging T-tubules: dynamic membrane structures for deep functions.** *Cardiovascular research* 2013, **98**(2):162-164.
19. Haddock PS, Coetzee WA, Cho E, Porter L, Katoh H, Bers DM, Jafri MS, Artman M: **Subcellular [Ca²⁺]_i gradients during excitation-contraction coupling in newborn rabbit ventricular myocytes.** *Circulation research* 1999, **85**(5):415-427.
20. Seki S, Nagashima M, Yamada Y, Tsutsuura M, Kobayashi T, Namiki A, Tohse N: **Fetal and postnatal development of Ca²⁺ transients and Ca²⁺ sparks in rat cardiomyocytes.** *Cardiovascular research* 2003, **58**(3):535-548.
21. Ziman AP, Gomez-Viquez NL, Bloch RJ, Lederer WJ: **Excitation-contraction coupling changes during postnatal cardiac development.** *Journal of molecular and cellular cardiology* 2010, **48**(2):379-386.
22. Di Maio A, Karko K, Snopko RM, Mejia-Alvarez R, Franzini-Armstrong C: **T-tubule formation in cardiacmyocytes: two possible mechanisms?** *Journal of muscle research and cell motility* 2007, **28**(4-5):231-241.
23. Lee E, Marcucci M, Daniell L, Pypaert M, Weisz OA, Ochoa GC, Farsad K, Wenk MR, De Camilli P: **Amphiphysin 2 (Bin1) and T-tubule biogenesis in muscle.** *Science* 2002, **297**(5584):1193-1196.
24. Nicot AS, Toussaint A, Tosch V, Kretz C, Wallgren-Pettersson C, Iwarsson E, Kingston H, Garnier JM, Biancalana V, Oldfors A *et al*: **Mutations in amphiphysin 2 (BIN1) disrupt interaction with dynamin 2 and cause**

- autosomal recessive centronuclear myopathy.** *Nature genetics* 2007, **39**(9):1134-1139.
25. Razzaq A, Robinson IM, McMahon HT, Skepper JN, Su Y, Zelhof AC, Jackson AP, Gay NJ, O'Kane CJ: **Amphiphysin is necessary for organization of the excitation-contraction coupling machinery of muscles, but not for synaptic vesicle endocytosis in Drosophila.** *Genes & development* 2001, **15**(22):2967-2979.
26. Vlahovich N, Kee AJ, Van der Poel C, Kettle E, Hernandez-Deviez D, Lucas C, Lynch GS, Parton RG, Gunning PW, Hardeman EC: **Cytoskeletal tropomyosin Tm5NM1 is required for normal excitation-contraction coupling in skeletal muscle.** *Molecular biology of the cell* 2009, **20**(1):400-409.
27. van Oort RJ, Garbino A, Wang W, Dixit SS, Landstrom AP, Gaur N, De Almeida AC, Skapura DG, Rudy Y, Burns AR *et al*: **Disrupted junctional membrane complexes and hyperactive ryanodine receptors after acute junctophilin knockdown in mice.** *Circulation* 2011, **123**(9):979-988.
28. Komazaki S, Nishi M, Takeshima H: **Abnormal junctional membrane structures in cardiac myocytes expressing ectopic junctophilin type 1.** *FEBS letters* 2003, **542**(1-3):69-73.
29. Komazaki S, Ito K, Takeshima H, Nakamura H: **Deficiency of triad formation in developing skeletal muscle cells lacking junctophilin type 1.** *FEBS letters* 2002, **524**(1-3):225-229.
30. Lyon AR, MacLeod KT, Zhang Y, Garcia E, Kanda GK, Lab MJ, Korchev YE, Harding SE, Gorelik J: **Loss of T-tubules and other changes to surface topography in ventricular myocytes from failing human and rat heart.**

Proceedings of the National Academy of Sciences of the United States of America 2009, **106**(16):6854-6859.

31. Louch WE, Sejersted OM, Swift F: **There goes the neighborhood: pathological alterations in T-tubule morphology and consequences for cardiomyocyte Ca²⁺ handling.** *Journal of biomedicine & biotechnology* 2010, **2010**:503906.
32. Louch WE, Bito V, Heinzel FR, Macianskiene R, Vanhaecke J, Flameng W, Mubagwa K, Sipido KR: **Reduced synchrony of Ca²⁺ release with loss of T-tubules-a comparison to Ca²⁺ release in human failing cardiomyocytes.** *Cardiovascular research* 2004, **62**(1):63-73.
33. Brette F, Salle L, Orchard CH: **Quantification of calcium entry at the T-tubules and surface membrane in rat ventricular myocytes.** *Biophysical journal* 2006, **90**(1):381-389.
34. Orchard C, Brette F: **t-Tubules and sarcoplasmic reticulum function in cardiac ventricular myocytes.** *Cardiovascular research* 2008, **77**(2):237-244.
35. Hong TT, Smyth JW, Gao D, Chu KY, Vogan JM, Fong TS, Jensen BC, Colecraft HM, Shaw RM: **BIN1 localizes the L-type calcium channel to cardiac T-tubules.** *PLoS biology* 2010, **8**(2):e1000312.
36. Gorelik J, Wright PT, Lyon AR, Harding SE: **Spatial control of the betaAR system in heart failure: the transverse tubule and beyond.** *Cardiovascular research* 2013, **98**(2):216-224.
37. Nikolaev VO, Moshkov A, Lyon AR, Miragoli M, Novak P, Paur H, Lohse MJ, Korchev YE, Harding SE, Gorelik J: **Beta2-adrenergic receptor redistribution in heart failure changes cAMP compartmentation.** *Science* 2010, **327**(5973):1653-1657.

38. Ibrahim M, Gorelik J, Yacoub MH, Terracciano CM: **The structure and function of cardiac t-tubules in health and disease.** *Proceedings Biological sciences* 2011, **278**(1719):2714-2723.
39. Heinzel FR, Bito V, Biesmans L, Wu M, Detre E, von Wegner F, Claus P, Dymarkowski S, Maes F, Bogaert J *et al*: **Remodeling of T-tubules and reduced synchrony of Ca²⁺ release in myocytes from chronically ischemic myocardium.** *Circulation research* 2008, **102**(3):338-346.
40. He J, Conklin MW, Foell JD, Wolff MR, Haworth RA, Coronado R, Kamp TJ: **Reduction in density of transverse tubules and L-type Ca(2+) channels in canine tachycardia-induced heart failure.** *Cardiovascular research* 2001, **49**(2):298-307.
41. Page E, McCallister LP: **Quantitative electron microscopic description of heart muscle cells. Application to normal, hypertrophied and thyroxin-stimulated hearts.** *The American journal of cardiology* 1973, **31**(2):172-181.
42. Maron BJ, Ferrans VJ, Roberts WC: **Ultrastructural features of degenerated cardiac muscle cells in patients with cardiac hypertrophy.** *The American journal of pathology* 1975, **79**(3):387-434.
43. Schaper J, Froede R, Hein S, Buck A, Hashizume H, Speiser B, Friedl A, Bleese N: **Impairment of the myocardial ultrastructure and changes of the cytoskeleton in dilated cardiomyopathy.** *Circulation* 1991, **83**(2):504-514.
44. Kaprielian RR, Stevenson S, Rothery SM, Cullen MJ, Severs NJ: **Distinct patterns of dystrophin organization in myocyte sarcolemma and transverse tubules of normal and diseased human myocardium.** *Circulation* 2000, **101**(22):2586-2594.

45. Balijepalli RC, Lokuta AJ, Maertz NA, Buck JM, Haworth RA, Valdivia HH, Kamp TJ: **Depletion of T-tubules and specific subcellular changes in sarcolemmal proteins in tachycardia-induced heart failure.** *Cardiovascular research* 2003, **59**(1):67-77.
46. Wei S, Guo A, Chen B, Kutschke W, Xie YP, Zimmerman K, Weiss RM, Anderson ME, Cheng H, Song LS: **T-tubule remodeling during transition from hypertrophy to heart failure.** *Circulation research* 2010, **107**(4):520-531.
47. Sanchez-Alonso JL, Bhargava A, O'Hara T, Glukhov AV, Schobesberger S, Bhogal N, Sikkell MB, Mansfield C, Korchev YE, Lyon AR *et al*: **Microdomain-Specific Modulation of L-Type Calcium Channels Leads to Triggered Ventricular Arrhythmia in Heart Failure.** *Circulation research* 2016, **119**(8):944-955.
48. Crossman DJ, Ruygrok PN, Soeller C, Cannell MB: **Changes in the organization of excitation-contraction coupling structures in failing human heart.** *PloS one* 2011, **6**(3):e17901.
49. Cannell MB, Crossman DJ, Soeller C: **Effect of changes in action potential spike configuration, junctional sarcoplasmic reticulum micro-architecture and altered t-tubule structure in human heart failure.** *Journal of muscle research and cell motility* 2006, **27**(5-7):297-306.
50. Louch WE, Mork HK, Sexton J, Stromme TA, Laake P, Sjaastad I, Sejersted OM: **T-tubule disorganization and reduced synchrony of Ca²⁺ release in murine cardiomyocytes following myocardial infarction.** *The Journal of physiology* 2006, **574**(Pt 2):519-533.
51. Kirk MM, Izu LT, Chen-Izu Y, McCulle SL, Wier WG, Balke CW, Shorofsky SR: **Role of the transverse-axial tubule system in generating calcium sparks and**

- calcium transients in rat atrial myocytes.** *The Journal of physiology* 2003, **547**(Pt 2):441-451.
52. Lipp P, Huser J, Pott L, Niggli E: **Spatially non-uniform Ca²⁺ signals induced by the reduction of transverse tubules in citrate-loaded guinea-pig ventricular myocytes in culture.** *The Journal of physiology* 1996, **497** (Pt 3):589-597.
53. Bers DM: **Calcium cycling and signaling in cardiac myocytes.** *Annual review of physiology* 2008, **70**:23-49.
54. Bers DM: **Cardiac excitation-contraction coupling.** *Nature* 2002, **415**(6868):198-205.
55. Scriven DR, Dan P, Moore ED: **Distribution of proteins implicated in excitation-contraction coupling in rat ventricular myocytes.** *Biophysical journal* 2000, **79**(5):2682-2691.
56. Guo A, Zhang C, Wei S, Chen B, Song LS: **Emerging mechanisms of T-tubule remodelling in heart failure.** *Cardiovascular research* 2013, **98**(2):204-215.
57. Takeshima H, Hoshijima M, Song LS: **Ca(2)(+) microdomains organized by junctophilins.** *Cell calcium* 2015, **58**(4):349-356.
58. Dedkova EN, Blatter LA: **Calcium signaling in cardiac mitochondria.** *Journal of molecular and cellular cardiology* 2013, **58**:125-133.
59. Gomez AM, Valdivia HH, Cheng H, Lederer MR, Santana LF, Cannell MB, McCune SA, Altschuld RA, Lederer WJ: **Defective excitation-contraction coupling in experimental cardiac hypertrophy and heart failure.** *Science* 1997, **276**(5313):800-806.

60. Hobai IA, O'Rourke B: **Decreased sarcoplasmic reticulum calcium content is responsible for defective excitation-contraction coupling in canine heart failure.** *Circulation* 2001, **103**(11):1577-1584.
61. Beuckelmann DJ: **Contributions of Ca(2+)-influx via the L-type Ca(2+)-current and Ca(2+)-release from the sarcoplasmic reticulum to [Ca²⁺]_i-transients in human myocytes.** *Basic research in cardiology* 1997, **92 Suppl 1**:105-110.
62. Bers DM, Grandi E: **Calcium/calmodulin-dependent kinase II regulation of cardiac ion channels.** *Journal of cardiovascular pharmacology* 2009, **54**(3):180-187.
63. Rosca MG, Tandler B, Hoppel CL: **Mitochondria in cardiac hypertrophy and heart failure.** *Journal of molecular and cellular cardiology* 2013, **55**:31-41.
64. Song LS, Sobie EA, McCulle S, Lederer WJ, Balke CW, Cheng H: **Orphaned ryanodine receptors in the failing heart.** *Proceedings of the National Academy of Sciences of the United States of America* 2006, **103**(11):4305-4310.
65. Jones PP, MacQuaide N, Louch WE: **Dyadic Plasticity in Cardiomyocytes.** *Frontiers in physiology* 2018, **9**:1773.
66. Shannon TR, Ginsburg KS, Bers DM: **Potential of fractional sarcoplasmic reticulum calcium release by total and free intra-sarcoplasmic reticulum calcium concentration.** *Biophysical journal* 2000, **78**(1):334-343.
67. Shannon TR, Ginsburg KS, Bers DM: **Quantitative assessment of the SR Ca²⁺ leak-load relationship.** *Circulation research* 2002, **91**(7):594-600.
68. Cheng H, Lederer WJ, Cannell MB: **Calcium sparks: elementary events underlying excitation-contraction coupling in heart muscle.** *Science* 1993, **262**(5134):740-744.

69. Satoh H, Blatter LA, Bers DM: **Effects of $[Ca^{2+}]_i$, SR Ca^{2+} load, and rest on Ca^{2+} spark frequency in ventricular myocytes.** *The American journal of physiology* 1997, **272**(2 Pt 2):H657-668.
70. Belevych AE, Terentyev D, Terentyeva R, Nishijima Y, Sridhar A, Hamlin RL, Carnes CA, Gyorko S: **The relationship between arrhythmogenesis and impaired contractility in heart failure: role of altered ryanodine receptor function.** *Cardiovascular research* 2011, **90**(3):493-502.
71. Respress JL, van Oort RJ, Li N, Rolim N, Dixit SS, deAlmeida A, Voigt N, Lawrence WS, Skapura DG, Skardal K *et al*: **Role of RyR2 phosphorylation at S2814 during heart failure progression.** *Circulation research* 2012, **110**(11):1474-1483.
72. Zhang H, Makarewich CA, Kubo H, Wang W, Duran JM, Li Y, Berretta RM, Koch WJ, Chen X, Gao E *et al*: **Hyperphosphorylation of the cardiac ryanodine receptor at serine 2808 is not involved in cardiac dysfunction after myocardial infarction.** *Circulation research* 2012, **110**(6):831-840.
73. Makarewich CA, Zhang H, Davis J, Correll RN, Trapanese DM, Hoffman NE, Troupes CD, Berretta RM, Kubo H, Madesh M *et al*: **Transient receptor potential channels contribute to pathological structural and functional remodeling after myocardial infarction.** *Circulation research* 2014, **115**(6):567-580.
74. Chen Y, Escoubet B, Prunier F, Amour J, Simonides WS, Vivien B, Lenoir C, Heimburger M, Choqueux C, Gellen B *et al*: **Constitutive cardiac overexpression of sarcoplasmic/endoplasmic reticulum Ca^{2+} -ATPase delays myocardial failure after myocardial infarction in rats at a cost of increased acute arrhythmias.** *Circulation* 2004, **109**(15):1898-1903.

75. Bodi I, Mikala G, Koch SE, Akhter SA, Schwartz A: **The L-type calcium channel in the heart: the beat goes on.** *The Journal of clinical investigation* 2005, **115**(12):3306-3317.
76. Scriven DR, Asghari P, Schulson MN, Moore ED: **Analysis of Cav1.2 and ryanodine receptor clusters in rat ventricular myocytes.** *Biophysical journal* 2010, **99**(12):3923-3929.
77. Best JM, Kamp TJ: **Different subcellular populations of L-type Ca²⁺ channels exhibit unique regulation and functional roles in cardiomyocytes.** *Journal of molecular and cellular cardiology* 2012, **52**(2):376-387.
78. Orchard CH, Pasek M, Brette F: **The role of mammalian cardiac t-tubules in excitation-contraction coupling: experimental and computational approaches.** *Experimental physiology* 2009, **94**(5):509-519.
79. Kawai M, Hussain M, Orchard CH: **Excitation-contraction coupling in rat ventricular myocytes after formamide-induced detubulation.** *The American journal of physiology* 1999, **277**(2):H603-609.
80. Brette F, Salle L, Orchard CH: **Differential modulation of L-type Ca²⁺ current by SR Ca²⁺ release at the T-tubules and surface membrane of rat ventricular myocytes.** *Circulation research* 2004, **95**(1):e1-7.
81. Brette F, Orchard C: **Resurgence of cardiac t-tubule research.** *Physiology* 2007, **22**:167-173.
82. Mukherjee R, Spinale FG: **L-type calcium channel abundance and function with cardiac hypertrophy and failure: a review.** *Journal of molecular and cellular cardiology* 1998, **30**(10):1899-1916.

83. Houser SR: **Reduced abundance of transverse tubules and L-type calcium channels: another cause of defective contractility in failing ventricular myocytes.** *Cardiovascular research* 2001, **49**(2):253-256.
84. Chen X, Piacentino V, 3rd, Furukawa S, Goldman B, Margulies KB, Houser SR: **L-type Ca²⁺ channel density and regulation are altered in failing human ventricular myocytes and recover after support with mechanical assist devices.** *Circulation research* 2002, **91**(6):517-524.
85. Chien AJ, Zhao X, Shirokov RE, Puri TS, Chang CF, Sun D, Rios E, Hosey MM: **Roles of a membrane-localized beta subunit in the formation and targeting of functional L-type Ca²⁺ channels.** *The Journal of biological chemistry* 1995, **270**(50):30036-30044.
86. Catalucci D, Zhang DH, DeSantiago J, Aimond F, Barbara G, Chemin J, Bonci D, Picht E, Rusconi F, Dalton ND *et al*: **Akt regulates L-type Ca²⁺ channel activity by modulating Cavalpha1 protein stability.** *The Journal of cell biology* 2009, **184**(6):923-933.
87. Bryant SM, Kong CH, Watson J, Cannell MB, James AF, Orchard CH: **Altered distribution of I_{Ca} impairs Ca release at the t-tubules of ventricular myocytes from failing hearts.** *Journal of molecular and cellular cardiology* 2015, **86**:23-31.
88. Yamaguchi H, Hara M, Strobeck M, Fukasawa K, Schwartz A, Varadi G: **Multiple modulation pathways of calcium channel activity by a beta subunit. Direct evidence of beta subunit participation in membrane trafficking of the alpha_{1C} subunit.** *The Journal of biological chemistry* 1998, **273**(30):19348-19356.
89. De Ferrari GM, Tavazzi L: **The role of arrhythmias in the progression of heart failure.** *European journal of heart failure* 1999, **1**(1):35-40.

90. HE H: **Experimentelle studien an Saugertherien**
uber das elektrokardiogramm. *Z Exp Pathol Ther* 1910, **7**:363-378.
91. JD W: **The incidence and prognostic value of the pulsus alternans in myocardial and arterial disease.** *Quart J Med* 1913, **6**:453-462.
92. Kanaporis G, Blatter LA: **Membrane potential determines calcium alternans through modulation of SR Ca(2+) load and L-type Ca(2+) current.** *Journal of molecular and cellular cardiology* 2017, **105**:49-58.
93. Aronson RS: **Afterpotentials and triggered activity in hypertrophied myocardium from rats with renal hypertension.** *Circulation research* 1981, **48**(5):720-727.
94. Vermeulen JT, McGuire MA, Opthof T, Coronel R, de Bakker JM, Klopping C, Janse MJ: **Triggered activity and automaticity in ventricular trabeculae of failing human and rabbit hearts.** *Cardiovascular research* 1994, **28**(10):1547-1554.
95. Priori SG, Napolitano C, Tiso N, Memmi M, Vignati G, Bloise R, Sorrentino V, Danieli GA: **Mutations in the cardiac ryanodine receptor gene (hRyR2) underlie catecholaminergic polymorphic ventricular tachycardia.** *Circulation* 2001, **103**(2):196-200.
96. Wehrens XH, Lehnart SE, Reiken SR, Deng SX, Vest JA, Cervantes D, Coromilas J, Landry DW, Marks AR: **Protection from cardiac arrhythmia through ryanodine receptor-stabilizing protein calstabin2.** *Science* 2004, **304**(5668):292-296.
97. Antzelevitch C, Burashnikov A: **Overview of Basic Mechanisms of Cardiac Arrhythmia.** *Cardiac electrophysiology clinics* 2011, **3**(1):23-45.

98. Clusin WT: **Calcium and cardiac arrhythmias: DADs, EADs, and alternans.** *Critical reviews in clinical laboratory sciences* 2003, **40**(3):337-375.
99. Garbino A, Wehrens XH: **Emerging role of junctophilin-2 as a regulator of calcium handling in the heart.** *Acta pharmacologica Sinica* 2010, **31**(9):1019-1021.
100. Nishi M, Mizushima A, Nakagawara K, Takeshima H: **Characterization of human junctophilin subtype genes.** *Biochemical and biophysical research communications* 2000, **273**(3):920-927.
101. Chen B, Guo A, Zhang C, Chen R, Zhu Y, Hong J, Kutschke W, Zimmerman K, Weiss RM, Zingman L *et al*: **Critical roles of junctophilin-2 in T-tubule and excitation-contraction coupling maturation during postnatal development.** *Cardiovascular research* 2013, **100**(1):54-62.
102. Landstrom AP, Beavers DL, Wehrens XH: **The junctophilin family of proteins: from bench to bedside.** *Trends in molecular medicine* 2014, **20**(6):353-362.
103. Garbino A, van Oort RJ, Dixit SS, Landstrom AP, Ackerman MJ, Wehrens XH: **Molecular evolution of the junctophilin gene family.** *Physiological genomics* 2009, **37**(3):175-186.
104. Olsen JV, Blagoev B, Gnäd F, Macek B, Kumar C, Mortensen P, Mann M: **Global, in vivo, and site-specific phosphorylation dynamics in signaling networks.** *Cell* 2006, **127**(3):635-648.
105. Phimister AJ, Lango J, Lee EH, Ernst-Russell MA, Takeshima H, Ma J, Allen PD, Pessah IN: **Conformation-dependent stability of junctophilin 1 (JP1) and ryanodine receptor type 1 (RyR1) channel complex is mediated by their hyper-reactive thiols.** *The Journal of biological chemistry* 2007, **282**(12):8667-8677.

106. Jayasinghe ID, Baddeley D, Kong CH, Wehrens XH, Cannell MB, Soeller C: **Nanoscale organization of junctophilin-2 and ryanodine receptors within peripheral couplings of rat ventricular cardiomyocytes.** *Biophysical journal* 2012, **102**(5):L19-21.
107. Jayasinghe I, Clowsley AH, Lin R, Lutz T, Harrison C, Green E, Baddeley D, Di Michele L, Soeller C: **True Molecular Scale Visualization of Variable Clustering Properties of Ryanodine Receptors.** *Cell reports* 2018, **22**(2):557-567.
108. Minamisawa S, Oshikawa J, Takeshima H, Hoshijima M, Wang Y, Chien KR, Ishikawa Y, Matsuoka R: **Junctophilin type 2 is associated with caveolin-3 and is down-regulated in the hypertrophic and dilated cardiomyopathies.** *Biochemical and biophysical research communications* 2004, **325**(3):852-856.
109. Harvey RD, Calaghan SC: **Caveolae create local signalling domains through their distinct protein content, lipid profile and morphology.** *Journal of molecular and cellular cardiology* 2012, **52**(2):366-375.
110. Golini L, Chouabe C, Berthier C, Cusimano V, Fornaro M, Bonvallet R, Formoso L, Giacomello E, Jacquemond V, Sorrentino V: **Junctophilin 1 and 2 proteins interact with the L-type Ca²⁺ channel dihydropyridine receptors (DHPRs) in skeletal muscle.** *The Journal of biological chemistry* 2011, **286**(51):43717-43725.
111. Nakada T, Kashihara T, Komatsu M, Kojima K, Takeshita T, Yamada M: **Physical interaction of junctophilin and the CaV1.1 C terminus is crucial for skeletal muscle contraction.** *Proceedings of the National Academy of Sciences of the United States of America* 2018, **115**(17):4507-4512.

112. Takeshima H, Komazaki S, Nishi M, Iino M, Kangawa K: **Junctophilins: a novel family of junctional membrane complex proteins.** *Molecular cell* 2000, **6**(1):11-22.
113. Landstrom AP, Kellen CA, Dixit SS, van Oort RJ, Garbino A, Weisleder N, Ma J, Wehrens XH, Ackerman MJ: **Junctophilin-2 expression silencing causes cardiocyte hypertrophy and abnormal intracellular calcium-handling.** *Circulation Heart failure* 2011, **4**(2):214-223.
114. Liang X, Mei Y, Huang X, Shen G, Zhu D, Yu Y, Wang J, Lou Y: **Junctophilin 2 knockdown interfere with mitochondrium status in ESC-CMs and cardiogenesis of ES cells.** *Journal of cellular biochemistry* 2012, **113**(9):2884-2894.
115. Guo A, Zhang X, Iyer VR, Chen B, Zhang C, Kutschke WJ, Weiss RM, Franzini-Armstrong C, Song LS: **Overexpression of junctophilin-2 does not enhance baseline function but attenuates heart failure development after cardiac stress.** *Proceedings of the National Academy of Sciences of the United States of America* 2014, **111**(33):12240-12245.
116. Zhang C, Chen B, Guo A, Zhu Y, Miller JD, Gao S, Yuan C, Kutschke W, Zimmerman K, Weiss RM *et al*: **Microtubule-mediated defects in junctophilin-2 trafficking contribute to myocyte transverse-tubule remodeling and Ca²⁺ handling dysfunction in heart failure.** *Circulation* 2014, **129**(17):1742-1750.
117. Wu CY, Chen B, Jiang YP, Jia Z, Martin DW, Liu S, Entcheva E, Song LS, Lin RZ: **Calpain-dependent cleavage of junctophilin-2 and T-tubule remodeling in a mouse model of reversible heart failure.** *Journal of the American Heart Association* 2014, **3**(3):e000527.

118. Zatz M, Starling A: **Calpains and disease**. *The New England journal of medicine* 2005, **352**(23):2413-2423.
119. Patterson C, Portbury AL, Schisler JC, Willis MS: **Tear me down: role of calpain in the development of cardiac ventricular hypertrophy**. *Circulation research* 2011, **109**(4):453-462.
120. Guo A, Wang Y, Chen B, Wang Y, Yuan J, Zhang L, Hall D, Wu J, Shi Y, Zhu Q *et al*: **E-C coupling structural protein junctophilin-2 encodes a stress-adaptive transcription regulator**. *Science* 2018, **362**(6421).
121. Beavers DL, Wang W, Ather S, Voigt N, Garbino A, Dixit SS, Landstrom AP, Li N, Wang Q, Olivotto I *et al*: **Mutation E169K in junctophilin-2 causes atrial fibrillation due to impaired RyR2 stabilization**. *Journal of the American College of Cardiology* 2013, **62**(21):2010-2019.
122. Matsushita Y, Furukawa T, Kasanuki H, Nishibatake M, Kurihara Y, Ikeda A, Kamatani N, Takeshima H, Matsuoka R: **Mutation of junctophilin type 2 associated with hypertrophic cardiomyopathy**. *Journal of human genetics* 2007, **52**(6):543-548.
123. Landstrom AP, Weisleder N, Batalden KB, Bos JM, Tester DJ, Ommen SR, Wehrens XH, Claycomb WC, Ko JK, Hwang M *et al*: **Mutations in JPH2-encoded junctophilin-2 associated with hypertrophic cardiomyopathy in humans**. *Journal of molecular and cellular cardiology* 2007, **42**(6):1026-1035.
124. Woo JS, Hwang JH, Ko JK, Weisleder N, Kim DH, Ma J, Lee EH: **S165F mutation of junctophilin 2 affects Ca²⁺ signalling in skeletal muscle**. *The Biochemical journal* 2010, **427**(1):125-134.

125. Woo JS, Cho CH, Lee KJ, Kim DH, Ma J, Lee EH: **Hypertrophy in skeletal myotubes induced by junctophilin-2 mutant, Y141H, involves an increase in store-operated Ca²⁺ entry via Orai1.** *The Journal of biological chemistry* 2012, **287**(18):14336-14348.
126. Bailey BA, Houser SR: **Calcium transients in feline left ventricular myocytes with hypertrophy induced by slow progressive pressure overload.** *Journal of molecular and cellular cardiology* 1992, **24**(4):365-373.
127. Harris DM, Mills GD, Chen X, Kubo H, Berretta RM, Votaw VS, Santana LF, Houser SR: **Alterations in early action potential repolarization causes localized failure of sarcoplasmic reticulum Ca²⁺ release.** *Circulation research* 2005, **96**(5):543-550.
128. Wallner M, Eaton DM, Berretta RM, Borghetti G, Wu J, Baker ST, Feldsott EA, Sharp TE, 3rd, Mohsin S, Oyama MA *et al*: **A Feline HFpEF Model with Pulmonary Hypertension and Compromised Pulmonary Function.** *Scientific reports* 2017, **7**(1):16587.
129. Kallberg M, Wang H, Wang S, Peng J, Wang Z, Lu H, Xu J: **Template-based protein structure modeling using the RaptorX web server.** *Nature protocols* 2012, **7**(8):1511-1522.
130. Peng J, Xu J: **RaptorX: exploiting structure information for protein alignment by statistical inference.** *Proteins* 2011, **79 Suppl 10**:161-171.
131. Guo A, Song LS: **AutoTT: automated detection and analysis of T-tubule architecture in cardiomyocytes.** *Biophysical journal* 2014, **106**(12):2729-2736.
132. Duran JM, Taghavi S, Berretta RM, Makarewich CA, Sharp Iii T, Starosta T, Udeshi F, George JC, Kubo H, Houser SR: **A characterization and targeting of**

- the infarct border zone in a swine model of myocardial infarction.** *Clinical and translational science* 2012, **5**(5):416-421.
133. Kubo H, Margulies KB, Piacentino V, 3rd, Gaughan JP, Houser SR: **Patients with end-stage congestive heart failure treated with beta-adrenergic receptor antagonists have improved ventricular myocyte calcium regulatory protein abundance.** *Circulation* 2001, **104**(9):1012-1018.
134. Carlile-Klusacek M, Rizzo V: **Endothelial cytoskeletal reorganization in response to PAR1 stimulation is mediated by membrane rafts but not caveolae.** *American journal of physiology Heart and circulatory physiology* 2007, **293**(1):H366-375.
135. Trappanese DM, Liu Y, McCormick RC, Cannavo A, Nanayakkara G, Baskharoun MM, Jarrett H, Woitek FJ, Tillson DM, Dillon AR *et al*: **Chronic beta1-adrenergic blockade enhances myocardial beta3-adrenergic coupling with nitric oxide-cGMP signaling in a canine model of chronic volume overload: new insight into mechanisms of cardiac benefit with selective beta1-blocker therapy.** *Basic research in cardiology* 2015, **110**(1):456.
136. Lavorato M, Huang TQ, Iyer VR, Perni S, Meissner G, Franzini-Armstrong C: **Dyad content is reduced in cardiac myocytes of mice with impaired calmodulin regulation of RyR2.** *Journal of muscle research and cell motility* 2015, **36**(2):205-214.
137. Jayasinghe ID, Munro M, Baddeley D, Launikonis BS, Soeller C: **Observation of the molecular organization of calcium release sites in fast- and slow-twitch skeletal muscle with nanoscale imaging.** *Journal of the Royal Society, Interface* 2014, **11**(99).

138. Otsu N: **A Threshold Selection Method from Gray-Level Histograms**. In: *IEEE Transactions on Systems, Man, and Cybernetics*. vol. 9; 1979: 62-66.
139. Zhang H, Chen X, Gao E, MacDonnell SM, Wang W, Kolpakov M, Nakayama H, Zhang X, Jaleel N, Harris DM *et al*: **Increasing cardiac contractility after myocardial infarction exacerbates cardiac injury and pump dysfunction**. *Circulation research* 2010, **107**(6):800-809.
140. Chen X, Zhang X, Harris DM, Piacentino V, 3rd, Berretta RM, Margulies KB, Houser SR: **Reduced effects of BAY K 8644 on L-type Ca²⁺ current in failing human cardiac myocytes are related to abnormal adrenergic regulation**. *American journal of physiology Heart and circulatory physiology* 2008, **294**(5):H2257-2267.
141. Bhargava A, Lin X, Novak P, Mehta K, Korchev Y, Delmar M, Gorelik J: **Super-resolution scanning patch clamp reveals clustering of functional ion channels in adult ventricular myocyte**. *Circulation research* 2013, **112**(8):1112-1120.
142. Novak P, Gorelik J, Vivekananda U, Shevchuk AI, Ermolyuk YS, Bailey RJ, Bushby AJ, Moss GW, Rusakov DA, Klenerman D *et al*: **Nanoscale-targeted patch-clamp recordings of functional presynaptic ion channels**. *Neuron* 2013, **79**(6):1067-1077.
143. Ye P, Sheng L, Zhang C, Liu Y: **Atorvastatin attenuating down-regulation of peroxisome proliferator-activated receptor gamma in preventing cardiac hypertrophy of rats in vitro and in vivo**. *Journal of pharmacy & pharmaceutical sciences : a publication of the Canadian Society for Pharmaceutical Sciences, Societe canadienne des sciences pharmaceutiques* 2006, **9**(3):365-375.

144. Gross P, Honnorat N, Varol E, Wallner M, Trappanese DM, Sharp TE, Starosta T, Duran JM, Koller S, Davatzikos C *et al*: **Nuquantus: Machine learning software for the characterization and quantification of cell nuclei in complex immunofluorescent tissue images**. *Scientific reports* 2016, **6**:23431.
145. Bers DM: **Cardiac Na/Ca exchange function in rabbit, mouse and man: what's the difference?** *Journal of molecular and cellular cardiology* 2002, **34**(4):369-373.
146. Pollack PS, Carson NL, Nuss HB, Marino TA, Houser SR: **Mechanical properties of adult feline ventricular myocytes in culture**. *The American journal of physiology* 1991, **260**(1 Pt 2):H234-241.
147. Duthinh V, Houser SR: **Contractile properties of single isolated feline ventriculocytes**. *The American journal of physiology* 1988, **254**(1 Pt 2):H59-66.
148. Silver LH, Hemwall EL, Marino TA, Houser SR: **Isolation and morphology of calcium-tolerant feline ventricular myocytes**. *The American journal of physiology* 1983, **245**(5 Pt 1):H891-896.
149. Wickenden AD, Kaprielian R, Kassiri Z, Tsoporis JN, Tsushima R, Fishman GI, Backx PH: **The role of action potential prolongation and altered intracellular calcium handling in the pathogenesis of heart failure**. *Cardiovascular research* 1998, **37**(2):312-323.
150. Ginsburg KS, Bers DM: **Modulation of excitation-contraction coupling by isoproterenol in cardiomyocytes with controlled SR Ca²⁺ load and Ca²⁺ current trigger**. *The Journal of physiology* 2004, **556**(Pt 2):463-480.
151. Song LS, Wang SQ, Xiao RP, Spurgeon H, Lakatta EG, Cheng H: **beta-Adrenergic stimulation synchronizes intracellular Ca(2+) release during**

- excitation-contraction coupling in cardiac myocytes.** *Circulation research* 2001, **88**(8):794-801.
152. Houser SR, Margulies KB: **Is depressed myocyte contractility centrally involved in heart failure?** *Circulation research* 2003, **92**(4):350-358.
153. Fu Y, Hong T: **BIN1 regulates dynamic t-tubule membrane.** *Biochimica et biophysica acta* 2016, **1863**(7 Pt B):1839-1847.
154. Ishida A, Kitani T, Fujisawa H: **Evidence that autophosphorylation at Thr-286/Thr-287 is required for full activation of calmodulin-dependent protein kinase II.** *Biochimica et biophysica acta* 1996, **1311**(3):211-217.
155. Mills GD, Kubo H, Harris DM, Berretta RM, Piacentino V, 3rd, Houser SR: **Phosphorylation of phospholamban at threonine-17 reduces cardiac adrenergic contractile responsiveness in chronic pressure overload-induced hypertrophy.** *American journal of physiology Heart and circulatory physiology* 2006, **291**(1):H61-70.
156. Huang X, Sun L, Ji S, Zhao T, Zhang W, Xu J, Zhang J, Wang Y, Wang X, Franzini-Armstrong C *et al*: **Kissing and nanotunneling mediate intermitochondrial communication in the heart.** *Proceedings of the National Academy of Sciences of the United States of America* 2013, **110**(8):2846-2851.
157. Lavorato M, Iyer VR, Dewight W, Cupo RR, Debattisti V, Gomez L, De la Fuente S, Zhao YT, Valdivia HH, Hajnoczky G *et al*: **Increased mitochondrial nanotunneling activity, induced by calcium imbalance, affects intermitochondrial matrix exchanges.** *Proceedings of the National Academy of Sciences of the United States of America* 2017, **114**(5):E849-E858.

158. Vincent AE, Turnbull DM, Eisner V, Hajnoczky G, Picard M: **Mitochondrial Nanotunnels**. *Trends in cell biology* 2017, **27**(11):787-799.
159. Reynolds JO, Chiang DY, Wang W, Beavers DL, Dixit SS, Skapura DG, Landstrom AP, Song LS, Ackerman MJ, Wehrens XH: **Junctophilin-2 is necessary for T-tubule maturation during mouse heart development**. *Cardiovascular research* 2013, **100**(1):44-53.
160. Peter AK, Bjerke MA, Leinwand LA: **Biology of the cardiac myocyte in heart disease**. *Molecular biology of the cell* 2016, **27**(14):2149-2160.
161. Shaw RM, Colecraft HM: **L-type calcium channel targeting and local signalling in cardiac myocytes**. *Cardiovascular research* 2013, **98**(2):177-186.
162. Lipsett DB, Frisk M, Aronsen JM, Norden ES, Buonarati OR, Cataliotti A, Hell JW, Sjaastad I, Christensen G, Louch WE: **Cardiomyocyte substructure reverts to an immature phenotype during heart failure**. *The Journal of physiology* 2019, **597**(7):1833-1853.
163. Zhao YT, Valdivia CR, Gurrola GB, Powers PP, Willis BC, Moss RL, Jalife J, Valdivia HH: **Arrhythmogenesis in a catecholaminergic polymorphic ventricular tachycardia mutation that depresses ryanodine receptor function**. *Proceedings of the National Academy of Sciences of the United States of America* 2015, **112**(13):E1669-1677.
164. Rosenbaum DS: **T wave alternans: a mechanism of arrhythmogenesis comes of age after 100 years**. *Journal of cardiovascular electrophysiology* 2001, **12**(2):207-209.

165. Hudmon A, Schulman H, Kim J, Maltez JM, Tsien RW, Pitt GS: **CaMKII tethers to L-type Ca²⁺ channels, establishing a local and dedicated integrator of Ca²⁺ signals for facilitation.** *The Journal of cell biology* 2005, **171**(3):537-547.